

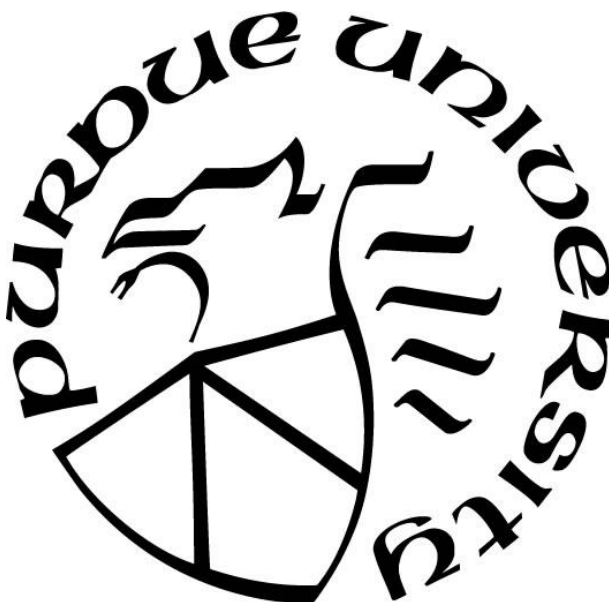
**MODERNIZING DRUG SUBSTANCE MANUFACTURING:
CONTINUOUS CRYSTALLIZATION IN TRADITIONAL AND
INNOVATIVE PLATFORMS**

by
Yiqing Claire Liu

A Dissertation

*Submitted to the Faculty of Purdue University
In Partial Fulfillment of the Requirements for the degree of*

Doctor of Philosophy



Davidson School of Chemical Engineering

West Lafayette, Indiana

December 2019

THE PURDUE UNIVERSITY GRADUATE SCHOOL

STATEMENT OF COMMITTEE APPROVAL

Dr. Zoltan K. Nagy

Davidson School of Chemical Engineering

Dr. Gintaras V. Reklaitis

Davidson School of Chemical Engineering

Dr. Michael T. Harris

Davidson School of Chemical Engineering

Dr. Teresa M. Carvajal

School of Agriculture & Biological Engineering

Approved by:

Dr. Sangtae Kim

Head of the Graduate Program

I dedicate this dissertation to my mom and dad: thank you for your unconditional love and your (mostly mom's) really delicious food.

Now that I look back, I think I was always destined to pursue my Ph.D. When I was little, we did all kinds of experiments together like mixing baking soda with vinegar, dissolving a cold medicine capsule with vinegar (which also explains my love for sour food), and we even wrote a 'paper' together explaining how a computer works with my extremely smooth third-grade writing style of course. Unfortunately, we could not find any ten-year-old peer reviewers.

I love you.

ACKNOWLEDGMENTS

I would like to thank my advisor Prof. Nagy for giving me the opportunity to pursue my Ph.D. under his guidance. I can truly say that this is the single best decision I made in graduate school. I would like to thank him for advising me over the years while allowing me to be creative and independent. He has always been supportive of my decisions whether it is about the direction of my research or about internship choices for my professional development. I have learned so much, scientifically and otherwise. I would also like to thank all the CryPTSys research group members for their help and support, especially my seniors David, Ramon, Yang, and Andy who have been great mentors. Jaron, Ayse, and Wei-lee, the future is yours.

Secondly, I would like to thank my friends for always being there for me. I would especially like to thank Seulgi, Noelia and Laryssa. Without those Zumba afternoons and girls' nights, my graduate school life would have been much less enjoyable. Of course, it would have been better if we had more Brazilian cheese bread, but I suppose we got by (Ahem... Lary, please mail me some). Thank you to Daria and Malak for still being there for me after our departure from Madison. Thank you to Mariana, Sudarshan, Francesco, Omar, Andrew and many other friends for those Friday (Italian) lunches. Thank you to Vu and Sean for all the amazing food both here in Indiana and in D.C. I would also like to acknowledge all the amazing women in the department for being great role models, mentors and friends: thank you Mariana, Sydney, Jenny, Martha, Shankali, Paulami, Yelin, Cara and many others!

Special thanks to the CHE staff: Bev, Nick, Jeff, Jason, Robin, Aimee, etc. They are great at their jobs so that we can do our job. I think every graduate student would agree that we would all be in trouble if we did not have Bev. Thank you! I would also like to thank Jacqueline and Janet for bringing me to SWE conferences.

I would also like to acknowledge David again for introducing me to DPQR at the FDA for my internship. Thank you to everybody there especially Ben, Tom and Celia for giving me advice and guidance during my internship and beyond.

Special thanks to our department head and my mentor Prof. Kim who is the precursor to my amazing Ph.D. journey. My life would be completely different if I did not send that email to ask for advice.

Thank you again Dr. Peña for always making me better.

TABLE OF CONTENTS

LIST OF TABLES	8
LIST OF FIGURES	10
LIST OF ABBREVIATIONS.....	15
ABSTRACT.....	17
1. INTRODUCTION	19
1.1 Background.....	19
1.2 Research Aims	21
1.3 Research Contributions.....	22
1.4 Thesis Structure	23
2. LITERATURE REVIEW	25
2.1 Crystallization Theories	26
2.1.1 Nucleation.....	27
2.1.2 Growth.....	30
2.2 Process Analytical Technology.....	32
2.3 Batch and Continuous Crystallization	44
2.4 Continuous Crystallizers.....	47
2.4.1 Mixed-suspension-mixed-product-removal crystallizers	48
2.4.2 Plug-flow crystallizers.....	56
2.5 Population balance modeling.....	59
2.5.1 Batch.....	60
2.5.2 MSMPR.....	61
2.5.3 PFC	63
2.5.4 Kinetic parameter estimation.....	64
2.6 Integration of continuous crystallization and filtration.....	65
3. POPULATION BALANCE MODEL DEVELOPMENT, VERIFICATION AND VALIDATION OF CARBAMAZEPINE CRYSTALLIZATION IN A TRADITIONAL STIRRED TANK CRYSTALLIZER	68
3.1 Disclaimer.....	68
3.2 Introduction.....	68

3.3	Material and Methods	70
3.3.1	Experimental material and crystallizer setup.....	70
3.3.2	Kinetic expression	71
3.3.3	Experimental methods for kinetic model development	72
3.3.4	Model verification and validation.....	74
3.3.5	Continuous crystallization	77
3.4	Results and Discussion	78
3.4.1	Kinetic model discrimination and parameter estimation	78
3.4.2	Model verification	87
3.4.3	Model validation.....	90
3.4.4	Discussion of model on continuous crystallization	93
3.5	Conclusion	97
4.	SYSTEMATIC PROCESS DEVELOPMENT OF CONTINUOUS CRYSTALLIZATION IN AN INNOVATIVE OSCILLATORY BAFFLE REACTOR: RESIDENCE TIME DISTRIBUTION STUDY	99
4.1	Introduction.....	99
4.2	Experimental Methods and Material.....	100
4.2.1	Oscillatory baffled reactor and stirred tank crystallizer setup.....	100
4.2.2	Liquid and solid residence time distribution measurement	102
4.2.3	Absorbance spectrometry	106
4.2.4	Analysis of liquid and solid residence time distributions	109
4.2.5	Continuous crystallization	111
4.3	Results and Discussion	112
4.3.1	Configurations of the OBR.....	112
4.3.2	Liquid residence time distribution.....	115
4.3.3	Solid residence time distribution	118
4.3.4	Continuous crystallization	120
4.4	Conclusions.....	130
5.	SYSTEMATIC PROCESS DEVELOPMENT OF CONTINUOUS CRYSTALLIZATION IN AN INNOVATIVE OSCILLATORY BAFFLE REACTOR: MODEL AND EXPERIMENT GUIDED START-UP OPTIMIZATION	132

5.1	Introduction.....	132
5.2	Material and Methods	133
5.2.1	Kinetic parameter estimation.....	133
5.2.2	Start-up optimization	135
5.3	Results and Discussion	136
5.3.1	Kinetic parameter estimation.....	136
5.3.2	Model guided batch start-up optimization.....	139
5.3.3	Experimental start-up strategy comparisons.....	140
5.4	Conclusion	146
6.	DEVELOPMENT OF CONTINUOUS FILTRATION IN A NOVEL CONTINUOUS FILTRATION CAROUSEL INTEGRATED WITH CONTINUOUS CRYSTALLIZATION	147
6.1	Introduction.....	147
6.2	Experimental Methods and Material.....	149
6.2.1	Materials	149
6.2.2	System setup	149
6.2.3	Filtration experimental methods.....	151
6.2.4	Integration of crystallization and filtration	152
6.3	Results and Discussion	154
6.3.1	Filtration experiments.....	154
6.3.2	Integration with continuous crystallization	159
6.3.3	Risk considerations of the CFC	163
6.4	Conclusion	167
7.	CONCLUSION AND FUTURE DIRECTIONS.....	168
7.1	Conclusion	168
7.2	Future directions	172
	APPENDIX.....	174
	REFERENCES	176
	VITA.....	201
	PUBLICATIONS.....	202

LIST OF TABLES

Table 2-1 Summary of in-situ PATs.....	41
Table 2-2 Summary of at-line and offline PATs.	44
Table 2-3 Cost analysis of a continuous operation in an OFBC compared to a traditional batch isolation process. Permission obtained from [133] Copyright © 2009, American Chemical Society.	59
Table 3-1 Experimental conditions of dissolution, growth and nucleation experiments.....	73
Table 3-2 Detailed model verification and validation activities entailed in this study and rationale of the level of rigor selected for each activity according to ASME V&V40 [166].	76
Table 3-3 External batch validation experimental conditions.	77
Table 3-4 Single stage and two-stage continuous crystallization experimental conditions.....	78
Table 3-5 Comparison of the mean square error (MSE) in concentration and PSD quantiles of five growth models.....	80
Table 3-6 Simulated product PSD quantiles of GM5 compared to experimental results of growth experiments 1-4.....	81
Table 3-7 Comparison of the MSE in concentration and product PSD quantiles of the five nucleation models.	83
Table 3-8 Simulated product PSD quantiles of BM5 compared to experimental results of nucleation experiments 1-4.	84
Table 3-9 Comparison of the MSE in concentration and product PSD quantiles of the three dissolution models.	85
Table 3-10 Estimated PBM kinetic parameter values and their 95% confidence interval.	86
Table 3-11 Maximum relative difference in dynamic concentration and PSD quantiles with various size discretization.....	88
Table 3-12 Maximum relative changes in concentration and size quantiles with varying ‘ode45’ parameter settings in MATLAB.	89
Table 3-13 Maximum relative changes in concentration and size quantiles with different ODE solvers in MATLAB.	90
Table 3-14 The mean, standard deviation and coefficient of variation of the final concentration and PSD quantiles in the kinetic parameter sensitivity study.....	90
Table 3-15 Simulated product PSD quantiles compared to validation experimental results.....	92
Table 4-1 Three-level-three-factor full factorial design of experiment for RTD studies.	105
Table 4-2 Experimental conditions of comparative liquid and solid RTD studies in the STC. .	106

Table 4-3 Experimental conditions of continuous crystallization studies in the OBR and the STC.	112
Table 4-4 Dimensionless mean residence time t_m and variance σ^2 of liquid RTD in Configurations 1, 2, 3.....	114
Table 4-5 t_m and σ^2 of solid RTDs of small and large particles as well as total particle count in Configurations 1, 2, 3.....	115
Table 4-6 Dimensionless mean residence time (t_m) results of liquid RTD experiments.	116
Table 4-7 Dimensionless variance (σ^2) results of washout experiments.	116
Table 4-8 t_m results of pulse experiments.	119
Table 4-9 σ^2 results of pulse experiments.	120
Table 4-10. The mean and the C.V. of the PSD at various residence times of continuous experiments Exp1-4.	128
Table 5-1 Experimental conditions of batch crystallization experiments in the OBR.	133
Table 5-2 Start-up procedures of continuous crystallization experiments in the OBR	136
Table 5-3 Estimated secondary nucleation and growth kinetic parameter values and 95% their confidence interval.....	137
Table 5-4 Comparison of simulated and experimental batch product size quantiles	138
Table 5-5 Growth kinetic parameters comparison to literature values.	138
Table 5-6 Medium size (D50) and span of samples taken at various residence times (RT) of start- up experiments 1-5.....	145
Table 6-1 Experimental conditions of the stand-alone filtration experiments of PCM and BA systems.....	152
Table 6-2 Start-up and continuous operation conditions of the coupled crystallization and filtration experiment for PCM and BA systems.	154
Table 6-3 D50 and span comparison of the CFC and bench vacuum filtration products for both PCM and BA experiments.	156

LIST OF FIGURES

Figure 2-1 Transitional role of crystallization in a typical manufacturing process of oral solid dosage form drugs.....	25
Figure 2-2 An example of polymorphism: (a) prismatic form I of ortho-amino benzoic acid (OABA), and (b) needle-like form II of OABA. Permission requested from [29] Copyright © 2014 WILEY-VCH Verlag GmbH & Co. KGaA, Weinheim.	26
Figure 2-3 Typical solubility curve and under(super)saturated areas.....	27
Figure 2-4 The schematics of different zones for nucleation, growth and dissolution in a typical phase diagram.	28
Figure 2-5 Metastable zone width (MSZW) of aluminum potassium sulphate in water at different cooling rates reported by Barrett & Glennon[31] (permission obtained). Copyright © 2002 The Institution of Chemical Engineers.	29
Figure 2-6 Microscopic images of paracetamol product of: (a) unseeded versus (b) seeded cooling crystallization. Permission obtained from [48] Copyright © 2007 Elsevier Ltd.....	31
Figure 2-7 Volume equivalent sphere diameter.....	31
Figure 2-8 Animated schematic of (a) agglomeration, (b) breakage, (c) attrition and (d) Ostwald ripening mechanisms.	32
Figure 2-9 Temperature and particle count profile of (a) detailed solution concentration calibration. Permission obtained from [59] Copyright © 2014 WILEY-VCH Verlag GmbH & Co. KGaA, Weinheim; and (b) rapid solution concentration calibration [18].....	35
Figure 2-10 FBRM probe (a) schematics, (b) chord length measurement mechanism and (c) a typical chord length distribution measurement.....	36
Figure 2-11 Typical FBRM profile of nucleation dominated crystallization (top) and growth dominated crystallization (bottom).....	37
Figure 2-12 (a) Control diagram of ADNC, (b) operating profile of an ADNC crystallization process and (c) microscopic images of paracetamol batch crystallization products with and without ADNC. Permission obtained from [63] Copyright © 2012, American Chemical Society.....	37
Figure 2-13 Turbidity meter measurement mechanism.....	38
Figure 2-14 A non-invasive acoustic transducer implemented on a laboratory scale crystallizer and its main characteristic parameters of a typical AE hit. Permission obtained from [72] Copyright © 2012 Elsevier B.V.....	39
Figure 2-15 PVM images of particles during crystallization and dissolution. Permission obtained from [31] Copyright © 2002 The Institution of Chemical Engineers.	40
Figure 2-16 In-situ Raman spectrum of Form I, Form II and mixture of ortho-amino-benzoic acid (OABA). Permission obtained from [79] Copyright © 2014, American Chemical Society.	41

Figure 2-17 At-line concentration monitoring of a crystallization by UPLC. Permission obtained from [81] Copyright © 2016, American Chemical Society.....	42
Figure 2-18 Laser diffraction PSD measurement mechanism.	43
Figure 2-19 Schematic of a typical batch crystallizer with overhead ports for PAT tools and seed addition.	45
Figure 2-20 Typical operating profile of batch, multi-stage continuously stirred tank, and plug flow crystallization in the phase diagram.....	46
Figure 2-21 Equipment set-up of (a) a lab scale (500mL) stirred tank MSMPR [18] and (b) a kilo scale stirred tank MSMPR. Permission obtained from [110] Copyright © 2017, Copyright © 2017 The Authors, some rights reserved; exclusive licensee American Association for the Advancement of Science. No claim to original U.S. Government Works.....	50
Figure 2-22 Animation illustration of MSMPR drawing schemes: skimming (left), submerged (middle), and metal pipe guided bottom drawing (right).....	51
Figure 2-23 A blocked slurry transfer line of a lab scale MSMPR. Permission obtained from [23] Copyright © 2017, ACS.	52
Figure 2-24 (a) Schematic of multistage MSMPR continuous crystallization of cyclosporin with recycle; (b) effect of recycle ratio on product purity and process yield. Permission obtained from [119] Copyright © 2011, American Chemical Society.....	54
Figure 2-25 (a) Schematic of an in-situ wet mill in the MSMPR experimental set-up and (b) volume-based size distribution at different wet mill rpm. Permission obtained from [16] Copyright © 2017, American Chemical Society.	55
Figure 2-26 Volume-based size distribution of particles in crystallizer implemented with sonication and product vessel at (a) silent conditions and (b) 40% power amplitude sonication. Permission obtained from [123] Copyright © 2010 Elsevier Ltd.....	55
Figure 2-27 Typical RTD of MSMPR versus PFC.....	57
Figure 2-28 Image of an encrusted tube section of a tubular PFC.....	57
Figure 2-29 Schematic of the tubular OFBC and a zoomed-in view on a baffled tube segment. Permission obtained from [140] Copyright © 2015, American Chemical Society.	58
Figure 2-30 A custom built stainless steel OFBC unit. Permission obtained from [133] Copyright © 2009, American Chemical Society.	59
Figure 2-31 Population distribution function where shaded area represents the number of particles between size L and $L+dL$ in a unit slurry volume.	60
Figure 2-32 Semilogarithmic population density versus size plot to predict growth rate.	63
Figure 2-33 (a) A picture of CFC manufactured by AWL and (b) schematics of the CFC. Permission obtained from [15] Copyright © 2016 Elsevier B.V.....	66
Figure 2-34 A continuous filtration drying unit developed by AWL. Permission obtained from [147] Copyright © 2019 American Pharmacists Association® Published by Elsevier Inc.....	67

Figure 3-1 Solubility of Carbamazepine Form III in Ethanol and its fitted empirical equation determined in-house.....	71
Figure 3-2 A short overview of risk-based model V&V activity structure according to AMSE V&V 40 standard [166].	75
Figure 3-3 Operating profile of slow cooling growth experiment ‘Growth1’.....	80
Figure 3-4 Fitted concentration result of GM5 compared to experimental concentration results of growth experiments 1-4.	81
Figure 3-5 Operating profile of a fast cooling experiment ‘Nucleation4’.....	83
Figure 3-6 Fitted concentration results of GM5-BM5 compared to experimental concentration results of nucleation experiments 1-4.	84
Figure 3-7 Operating profile of an isothermal dissolution experiment ‘Dissolution1’.....	85
Figure 3-8 Fitted result of DM1 compared to experimental concentration data.....	86
Figure 3-9 Comparison of experimental and simulated dynamic concentration of batch validation experiments.....	92
Figure 3-10 Comparison of experimental and simulated dynamic concentration, and D50 of (a) Single Stage and (b) Two-stage continuous crystallization experiments.	94
Figure 3-11 (a) FBRM total particle count measurement and (b) simulated particle count of the continuous experiments.	95
Figure 4-1 (a) Overall schematic of the OBR, (b) an exploded-view drawing of the baffle shaft, (c) sideview drawing of the baffle shaft, and (d) operating space of the OBR.....	101
Figure 4-2 The continuous operational setup of (a) the OBR and (b) the STC.....	102
Figure 4-3 (a) Sample IR spectrum of 0.1 g/g PCM solution measured by the FTIR and (b) calibration model of PCM EtOH solution of concentrations lower than 0.1 g/g.....	108
Figure 4-4 Operating profile of rapid calibration of (a) the FTIR in the OBR and (b) the UV in the STC.....	108
Figure 4-5 Three possible OBR configurations: inlet at the bottom, outlet at the top (left); outlet at the bottom, inlet at the top (middle); inlet and outlet both at the top (right).	113
Figure 4-6 (a) F-curves of liquid RTD and (b) E-curves of solid RTD in Configuration 1,2 and 3.	114
Figure 4-7 RTD function of small and large particles in Configuration 1 (left), Configuration 2 (middle), and Configuration 3(right).	114
Figure 4-8 Converted liquid RTD E-curves under various conditions in the OBR.....	116
Figure 4-9 Plot of (a) t_m and (b) σ^2 of liquid RTDs against oscillatory Reynolds number Re_o ..	117
Figure 4-10 (a) Comparison of liquid RTD t_m in the OBR and in the STC; (b)comparison of liquid RTD σ^2 in the OBR and in the STC.....	118

Figure 4-11 Measured solid RTD E-curves of various conditions in the OBR.....	119
Figure 4-12 Plot of solid RTD (a) t_m and (b) σ^2 over Re_O	119
Figure 4-13 (a) Comparison of solid RTD t_m in the OBR and in the STC; (b) comparison of solid RTD σ^2 in the OBR and in the STC.....	120
Figure 4-14 Solid RTD E-curves of the four continuous crystallization experiment conditions.....	121
Figure 4-15 (a) σ^2 results and (b) t_m results of solid RTD studies in the OBR at $\tau = 45$ min. The circle represents the optimal operating conditions chosen (2.5 Hz frequency of oscillations and 10 mm amplitude).....	121
Figure 4-16 Total particle count, concentration and square weighted mean chord length (SWMCL) profiles over time of continuous experiments: (a) Exp1 OBR 2.5 Hz – 10 mm (b) Exp2 STC 293rpm (c) Exp3 OBR 2.5 Hz – 15 mm and (d) Exp4 STC 439rpm.....	122
Figure 4-17 Volume weighted particle size distribution (PSD) of samples taken at various residence times of continuous experiments; (a) – (d): Exp1 - Exp4.....	125
Figure 4-18 Microscopic images of samples taken at various residence times of continuous experiments; (a) – (d): Exp1 - Exp4.....	125
Figure 4-19 Close-up process profile of Exp4 at 6-9 residence times.....	129
Figure 4-20 The PSD of samples taken at the last residence times in all 4 continuous experiments.....	130
Figure 5-1 Simulated and experimental concentration profile of Exp1 (top left), Exp2 (top right), Exp3 (bottom left), and Exp4 (bottom right).....	137
Figure 5-2 A comparison of growth rates of various absolute supersaturation and temperatures obtained in this work and from literature.....	139
Figure 5-3 Simulated Start-up5 concentration, particle count (μ_0), and D50 profile applying the optimized start-up batch cooling procedure.....	140
Figure 5-4 Concentration, temperature, total particle count and SWMCL profile overtime of Start-up1 (top) and Start-up2(bottom).....	142
Figure 5-5 Zoom in operating profile of 0-2 residence times of Start-up1 (left) and Start-up2(right).....	142
Figure 5-6 Concentration, temperature, total particle count and SWMCL profile overtime of Start-up3 (top), Start-up4 (middle) and Start-up5 (bottom).....	144
Figure 6-1 (a) A picture and (b) schematics of the continuous filtration carousel (CFC) used in this study manufactured by AWL.....	151
Figure 6-2 Coupled continuous crystallization and filtration system set-up.....	153
Figure 6-3 Moisture content of the filter product with various vacuum times and wash times for PCM and BA slurries.....	155

Figure 6-4 Microscopic images of CFC filtered and moisture balance dried PCM crystals (top row) and BA crystals (bottom row).....	157
Figure 6-5 Operating profile of continuous crystallization of PCM in the OBR.....	160
Figure 6-6 Coupled CFC product moisture content, D50 and span of PCM.....	161
Figure 6-7 Operating profile of continuous anti-solvent crystallization of BA in the OBR.....	162
Figure 6-8 Coupled CFC product moisture content, D50 and span of BA.....	162
Figure 6-9 Ishikawa diagram showing potential risks of continuous filtration that may lead to process failure.	164

LIST OF ABBREVIATIONS

AFC	Anti-fouling control
API	Active pharmaceutical ingredient
ASME	American Society of Mechanical Engineers
ATR-FTIR	Attenuated total reflectance – Fourier transform infrared
ATR-NIR	Attenuated total reflectance – near infrared
ATR-UV/Vis	Attenuated total reflectance – ultraviolet/visible
BA	Benzoic acid
CBZ	Carbamazepine
CFC	Continuous filtration carousel
CFD	Computational fluid dynamics
CI	Confidence interval
CIP	Cleaning-in-place
COBC	Continuous oscillatory baffled crystallizer, also known as OFBC
COU	Context of use
CSD	Crystal size distribution
CV	Coefficient of variation
DBC	Dynamic baffle crystallizer, also known as OBR
DoE	Design of experiment
EtOH	Ethanol
FBRM	Focused beam reflectance measurement
GC	Gas chromatography
HPLC	High-performance liquid chromatography
HRFV	High-resolution finite volume
MOM	Method of moment
MS	Mass spectrometry
MSE	Mean square error
MSMPR	Mixed-suspension-mixed-product-removal

MSZW	Metastable zone width
NCV	Numerical code verification
NMR	Nuclear magnetic resonance
OABA	Ortho-aminobenzoic acid
OBC	Oscillatory baffled crystallizer
OBR	Oscillatory baffle reactor, also known as DBC
ODE	Ordinary differential equation
OFBC	Oscillatory flow baffled crystallizer, also known as COBC
PAT	Process analytical technology
PBM	Population balance model
PCM	Paracetamol
PFC	Plug flow crystallizer
PSD	Particle size distribution
PVM	Particle vision measurement
QbD	Quality-by-design
RTD	Residence time distribution
SASR	Solvent-to-antisolvent ratio
SEM	Scanning electron microscopy
SQA	Software quality assurance
STC	Stirred tank crystallizer
SWMCL	Square weighted mean chord length
UPLC	Ultra-performance liquid chromatography
V&V	Verification and validation
XRD	X-ray diffraction

ABSTRACT

Crystallization, the final isolation and purification step in many drug substance manufacturing processes, has substantial impact on downstream efficiency and possibly final drug product qualities. Currently, crystallization is largely carried out in batch which may suffer from batch-to-batch variations. Continuous crystallization is the missing key to end-to-end continuous manufacturing of oral solid dosage form pharmaceuticals. It is estimated that shifting from batch to continuous operations may help the pharmaceutical industry (1) reduce plant footprint, (2) decrease energy consumption and (3) spawn faster response to drug shortages. The overall aim of this thesis is to study and design continuous crystallization processes in both a traditional stirred tank crystallizer (STC) and a novel oscillatory baffle reactor (OBR). In the STC, the thesis aims to establish a systematic framework to model crystallization via a risk-based approach. This methodology considers the highly regulated nature of the pharmaceutical industry where an impactful model must be verified and validated carefully. The OBR on the other hand is a novel commercial platform in which continuous operations have never been established. Its performance was compared to the STC in terms of residence time distribution where OBR showed more uniform and consistent operation. A start-up study was then carried out to study different start-up strategies to examine their effects on process dynamics and steady state products. The last piece is to study the integration of continuous crystallization with continuous filtration which is not well studied in the current literature. A novel commercial continuous filtration unit, the continuous filtration carousel (CFC) was studied to construct a truly continuous drug substance separation step. The operating conditions were optimized based on filter capacity and filter efficiency studies with particles of different shapes. Continuous coupling of crystallization and CFC was successfully

carried out based on the optimized conditions and a risk consideration discussion was given for process safety assessments.

1. INTRODUCTION

1.1 Background

Historically, pharmaceutical companies saw manufacturing cost as a small enough expense compared to the overall expense that major cost reduction was not needed. However, in recent years, due to expiring patents, high energy cost and potential price regulations, many pharmaceutical companies began investing in improving manufacturing efficiency [1], [2]. Meanwhile regulatory bodies are also changing emphasis from rigid regulations on operating conditions towards encouragement of process understanding and systematic risk-based developments. Traditionally the pharmaceutical industry applies ‘quality by testing (QbT)’ framework for process development where tightly defined material properties are tested at each step including raw material, fixed intermediate, drug substance and drug product to ensure consistent end product quality [3], [4]. Such stringent specification at each testing step may result in large manufacturing waste, post-market recalls and even drug shortages [5]. The manufacturers are not permitted to make changes without filing supplements to the U.S. Food and Drug Administration (for U.S. markets, FDA) regardless of potential improvement of the process safety and efficiency [6]–[9]. To address these challenges, quality by design (QbD) regulatory framework is being adopted which is a systematic, scientific, risk-based, holistic and proactive approach to pharmaceutical process development [3], [4]. QbD requires the identification and definition of critical quality attributes (CQAs) that influence drug product performance and emphasizes on the understanding and control of manufacturing processes to achieve them. The application of process analytical technology (PAT) has been given strong incentives to assist process development for monitoring and control. Based on the understanding of the processes and predefined CQAs, design

space can be established and validated where all products are guaranteed to be ‘on-spec’ regardless of small discrepancies in raw material, operating conditions or intermediates [4], [10], [11].

Continuous manufacturing (CM) have gained industry and regulatory attention for its online monitoring capabilities and steady state, or more accurately state-of-control, operation [3], [10]–[18]. It can be a major movement forward in the pharmaceutical manufacturing sector because of its potential to lower cost while improving product quality [19], [20], inherently promoted by QbD [10]–[12], [21]–[24]. The shift from batch to CM will have significant impact on solid dosage form manufacturing by improving flexibility, agility and sustainability of the process. It is estimated that shifting to CM may result in plant footprint reduction, operating cost decrease, energy requirement decrease and inherent process safety improvement [25].

There are many research and development efforts in developing continuous manufacturing and much progress has been made. Crystallization is one of last missing links in end-to-end continuous pharmaceutical manufacturing development because of its complex two-phase and stochastic nature. Crystallization is a widely used separation and purification step usually as the last drug substance manufacturing step. The product quality attributes of crystallization, such as particle size distribution (PSD), particle shape, particle polymorphism and solution concentration heavily influence the efficiency of downstream processes and may even affect the bioavailability of the final drug product [10], [11], [23], [26], [27]. Typically carried out in batch, there has been, as of late, increasing interest in continuous crystallization development to emulate the progress made in developing continuous reaction chemistry and drug product operations in hopes to enable end-to-end continuous pharmaceutical manufacturing.

1.2 Research Aims

The overall aim of this thesis is to understand and innovate continuous crystallization process development in traditional and innovative platforms. Naturally, traditional platforms are more developed than innovative ones where even proof-of-concept operations are sparingly demonstrated in the current literature. Differently focused studies are carried out to establish systematic and fundamental understandings of each system. The aims are examined through a combination of experimental and computational analysis which are summarized as follows:

- Crystallization modeling development, verification and validation via a risk-based approach in the traditional stirred tank crystallizer (STC).
- Investigation of kinetic transferability from batch to continuous operation in the traditional STC.
- Installation and application of PAT tools in the innovative oscillatory baffle reactor (OBR).
- OBR configuration selection based on liquid and solid residence time distribution (RTD) studies
- Reactor study of OBR: liquid and solid RTD studies and comparison against the traditional STC.
- Preliminary continuous crystallization performance comparison between the OBR and the STC.
- Batch kinetic parameter estimation in the OBR.
- Start-up procedure optimization of continuous crystallization in the OBR.
- Preliminary investigation and risk assessment of a novel continuous filtration unit.

1.3 Research Contributions

The main contribution of this thesis lies in the process development of continuous crystallization which can be summarized as follows:

- Estimation of crystallization kinetics of carbamazepine in a STC which has not been determined in the current literature. Kinetic parameters are essential in developing crystallization models and are useful for future design space exploration.
- Identification of model risk and applicability limitations via systematic model verification and validation activities answering the QbD paradigm shift.
- Establishing continuous operation for the first time in the OBR with PAT capabilities and demonstrated successful continuous crystallization operations promoting further research effort in continuous oscillatory systems.
- Examination of mixing dynamics in the OBR compared to the STC via RTD studies and recognize appropriate oscillation intensity ranges for efficient particle suspension and entrainment.
- Estimation of kinetic parameters of paracetamol in the OBR in comparison with the STC to obtain a batch start-up procedure of continuous crystallization.
- Experimental comparison of different start-up strategies on the process dynamics and steady state product quality attributes of continuous crystallization in the OBR.
- Demonstration of a systematic, model-assisted process development practice from system assembly, mixing dynamics examination, kinetic understanding to computation-aided optimization of operating conditions.
- Establishing a true continuous drug substance separation process by understanding and coupling a continuous filtration unit with a continuous crystallization process.

- Discussion of risk considerations of continuous filtration operations by listing and organizing potential risk factors for safety assessment.

1.4 Thesis Structure

Chapter 2 is a literature review of current progress in the field of continuous crystallization development in the pharmaceutical industry with a focus on reviewing different crystallization equipment. An overview of crystallization fundamentals is given first followed by process analytical technology applications in crystallization processes. Specific studies and findings in different crystallization systems are then reviewed followed by a discussion of modeling efforts of crystallization.

Chapter 3 describes the risk-based model development of carbamazepine crystallization in a traditional stirred tank crystallizer (STC). Sequential experiments separated nucleation, growth and dissolution to increase the efficiency of kinetic parameter estimation process. Low-to-medium credibility goal was reached by performing risk-based, systematic model verification and validation activities outlined by the American Society of Mechanical Engineers (ASME). A short discussion is provided on the transferability of batch crystallization to continuous operation.

Chapter 4 initiates the development of an innovative oscillatory baffle reactor (OBR) for continuous crystallization. Liquid and solid residence time distribution (RTD) studies are discussed as an evaluation of the mixing dynamics in the OBR. Then two sets of continuous crystallization experiments are demonstrated to compare the performance of the OBR with the STC on the continuous crystallization of paracetamol where the OBR produced more consistent and less aggregated products.

Chapter 5 further investigates the OBR to gain a deeper understanding of continuous crystallization process dynamics by studying start-up methods. Five common start-up strategies

are tested: two batch start-ups and three direct continuous operation start-ups. One of the batch start-ups applied an optimized cooling profile obtained using a PBM developed with batch crystallization experiments. A detailed discussion is given to understand the start-up strategies (or lack-there-of) effects on process dynamics as well as steady state products.

Chapter 6 extends the development of continuous drug substance manufacturing to continuous filtration which is at its early development stage in the literature. A novel continuous filtration carousel is described and utilized to develop continuous filtration processes for paracetamol and benzoic acid. An integrated continuous crystallization and filtration process is demonstrated for both compounds applying the operating conditions based on stand-alone filtration experiments which are also discussed in this chapter. In hopes to expedite the application of continuous filtration in the pharmaceutical industry, a risk consideration discussion is given to identify and organize potential risk factors associated with continuous filtration.

Chapter 7 summarizes the findings of the thesis and provide suggestions for future directions in the development of continuous drug substance processes.

2. LITERATURE REVIEW

Crystallization is a process where dissolved solutes transform from their solution phase to crystalline solid phase. It is a key unit operation present in the vast majority of pharmaceutical manufacturing processes to separate and isolate solid drug substance from its mother liquor. In oral solid dosage form production, it is often employed as the final purification step to obtain pure active pharmaceutical ingredient (API), serving the transitional role between drug substance and drug product manufacturing as shown in Figure 2-1. Tailoring the crystal quality attributes such as crystal size distribution (CSD), shape, polymorphic form (multiple crystal structures of the same molecule, Figure 2-2) and purity can have a significant impact on downstream processes as well as the quality of the final drug product [10], [11], [23], [26], [27]. A crystalline particle exhibits regularly arranged molecular structure which is often more stable than amorphous particles which do not have ordered molecular structures [28].

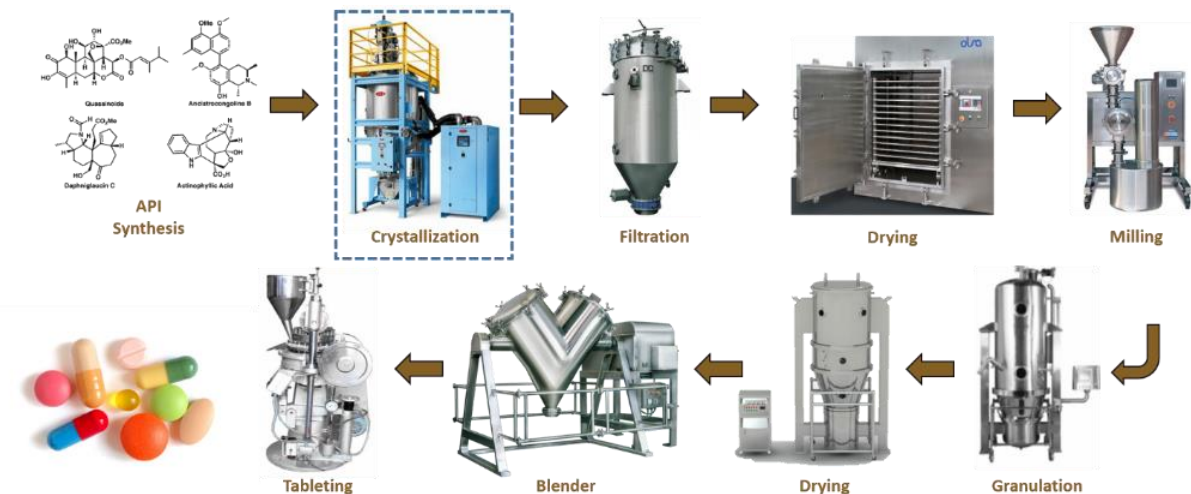


Figure 2-1 Transitional role of crystallization in a typical manufacturing process of oral solid dosage form drugs.

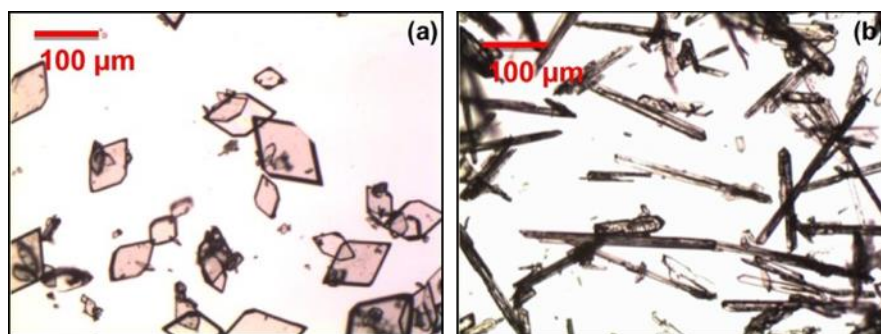


Figure 2-2 An example of polymorphism: (a) prismatic form I of ortho-amino benzoic acid (OABA), and (b) needle-like form II of OABA. Permission requested from [29] Copyright © 2014 WILEY-VCH Verlag GmbH & Co. KGaA, Weinheim.

2.1 Crystallization Theories

A typical solid-solution phase diagram is depicted in Figure 2-3 where the equilibrium solution concentration (solubility curve) as well as the corresponding supersaturated and undersaturated areas are shown. During crystallization, the system starts undersaturated and must move across the solubility curve to become supersaturated. Supersaturated solutions are metastable: the system tends to retrieve back to equilibrium (solubility), but certain amount of supersaturation must be built up to initiate rapid crystal formation. A barely supersaturated system may remain ‘stable’ for days while a system situated deeper into the supersaturation area may become unstable in a matter of minutes resulting in crystallization. It is easy to understand that crystallization is a rate process driven by supersaturation whereas solubility is a thermodynamic property [30]. Supersaturation may be generated by cooling, evaporation, antisolvent addition, reaction, pH manipulation, freezing or a combination of the aforementioned methods and the degree of supersaturation can be expressed as absolute supersaturation ΔC (defined as $C - C_{sat}$), supersaturation ratio S (defined as C/C_{sat}), or relative supersaturation s (defined as $\Delta C/C_{sat}$). Crystallization is generally considered to be a two-step process where sufficient supersaturation must be accumulated to trigger births of

crystals which then grow in size by incorporating solute molecules from the supersaturated solution, or namely, nucleation and growth.

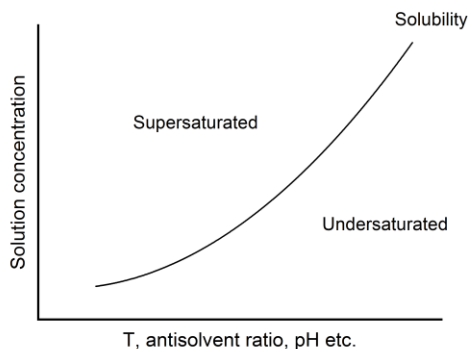


Figure 2-3 Typical solubility curve and under(super)saturated areas.

2.1.1 Nucleation

The birth of a crystal is called nucleation and it consists of two mechanisms: primary nucleation, spontaneous formation of nuclei without the presence of crystal particles, and secondary nucleation, birthing of nuclei triggered by existing crystal particles. As shown in Figure 2-4, primary nucleation occurs near the thermodynamic metastable zone limit. For crystallization process design purposes, the supersaturation required for primary nucleation is often considered to be the metastable zone limit while true thermodynamic metastable zone limit may be elsewhere which is difficult to measure due to the delayed detection of nucleation. The distance between solubility and the metastable zone limit in the phase diagram is called the metastable zone width (MSZW) which is an important guide for crystallization process design. It directly correlates to crystallization kinetics. MSZW is a kinetic property that can be affected by many factors including supersaturation generation rate (i.e. cooling rate or antisolvent addition rate etc.), mixing dynamics, solvent properties, impurities and solution history. Figure 2-5 illustrates the effect of cooling rate on the MSZW of aluminum potassium sulphate crystallization in water [31]. Once primary

nucleation takes place, the generated parent crystal particles will trigger secondary nucleation at a lower supersaturation as shown in Figure 2-4 [32], [33]. Because primary nucleation takes place at the brink of metastability, nuclei are generated in a stochastic, uncontrolled and often undesirable manner. In contrast, secondary nucleation can be controlled by manipulating the parent particles properties such as the size, polymorphic form and load (amount). Therefore, in industrial batch crystallization processes, pre-generated particles are strategically added as ‘seeds’ to bypass primary nucleation, regulate secondary nucleation and promote growth. Sometimes nucleation may be preferred or required, which is often the case in continuous crystallization processes. In such cases, secondary nucleation inducing seeded operation is still preferred to promote secondary nucleation instead of primary nucleation.

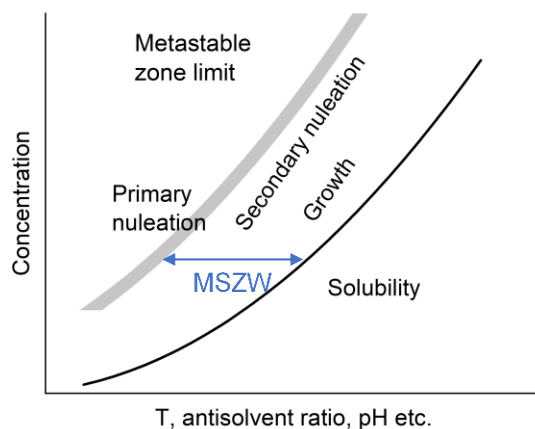


Figure 2-4 The schematics of different zones for nucleation, growth and dissolution in a typical phase diagram.

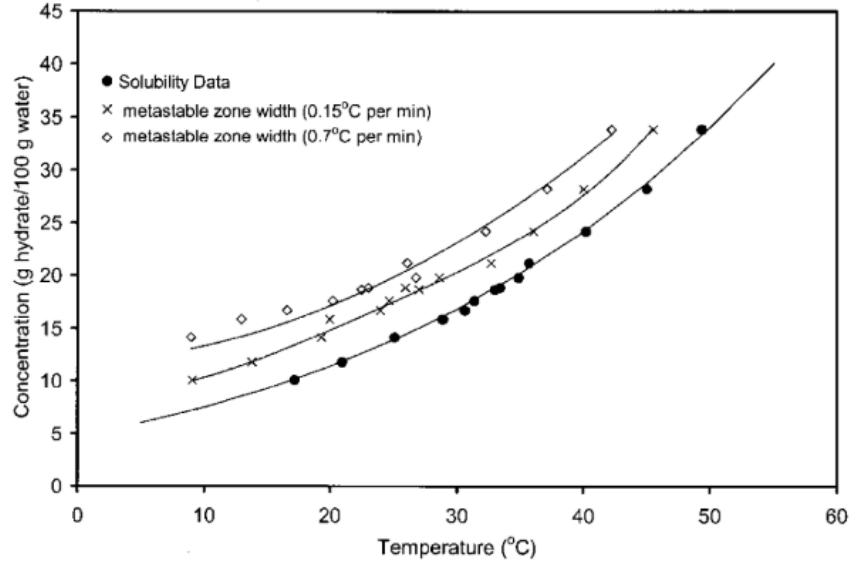


Figure 2-5 Metastable zone width (MSZW) of aluminum potassium sulphate in water at different cooling rates reported by Barrett & Glennon[31] (permission obtained). Copyright © 2002 The Institution of Chemical Engineers.

While there are existing theories [34]–[37] in attempts to explain primary and secondary nucleation mechanisms such as *classical nucleation theory* (Becker & Döring 1935 [38]; Volmer 1939 [39]; Gibbs 1948 [40]), *two-step theory* (Erdemir et al. 2008 [41]; Chakraborty and Patey 2013 [42]; Davey et al. 2013 [43]), *dust breeding* (Ting and McCabe 1934 [44]; Strickland-Constable and Mason 1963 [45]), *needle breeding* (Strickland-Constable 1968 [46]), and *collision breeding* (Strickland-Constable 1968 [46]), the exact mechanisms are not well understood. A general rate expression does not exist for either primary or secondary nucleation. Instead, an empirical Arrhenius-type power law expression is often used to describe nucleation:

$$\text{Primary Nucleation: } J = k_j \exp\left(\frac{j}{T^3 (\ln S)^2}\right) \quad (2.1)$$

$$\text{Secondary Nucleation: } B = k_b S^b \exp\left(-\frac{E_b}{RT}\right) M^m \quad (2.2)$$

where J and B are the primary and secondary nucleation rates respectively with the unit of number of particles per time per slurry volume, S represents supersaturation ratio and can be switched to

absolute supersaturation ΔC , or relative supersaturation s , T is the temperature, M denotes the solid concentration, R is the gas constant, and k_j , j , k_b , b , E_b , m are kinetic parameters that can be estimated from experiments.

2.1.2 Growth

Growth refers to the enlargement of crystals, the rate of which significantly impacts the final CSD. Growth takes place at a lower supersaturation than nucleation in a more controlled manner [28], [32], [47]. It is often preferred to generate larger crystals which can be filtered more efficiently compared to fine particles. In practice, techniques like high seed loading, small seed size, and slow supersaturation generation rate can be applied to promote growth and to suppress nucleation. A comparison of the products of a growth-dominated, seeded batch crystallization experiment against an unseeded experiment is illustrated in Figure 2-6 where seeded products are much larger in size and thus much easier to isolate [48]. The mechanism of crystal growth is complex as crystal structures are complex: it is generally considered as a two-step process involving diffusion followed by the incorporation (equivalent to a reaction) at the surface while other more complex two-dimensional growth theories [49]–[55] have been explored. Different models corresponding to these different theories have been developed mathematically but a generic power law is often used in practice:

$$G = \frac{dL}{dt} = k_g S^g \exp\left(-\frac{E_g}{RT}\right) fn(L) \quad (2.3)$$

where L denotes the characteristic size of the crystal and k_g , g , E_g are kinetic parameters that can be estimated from experiments. Some function of L , $fn(L)$ can be added to express size dependent growth rate. It is important to note here that there are multiple ways to describe crystal size since crystals are three dimensional structures. The characteristic length L is often defined as the volume equivalent sphere diameter (Figure 2-7).

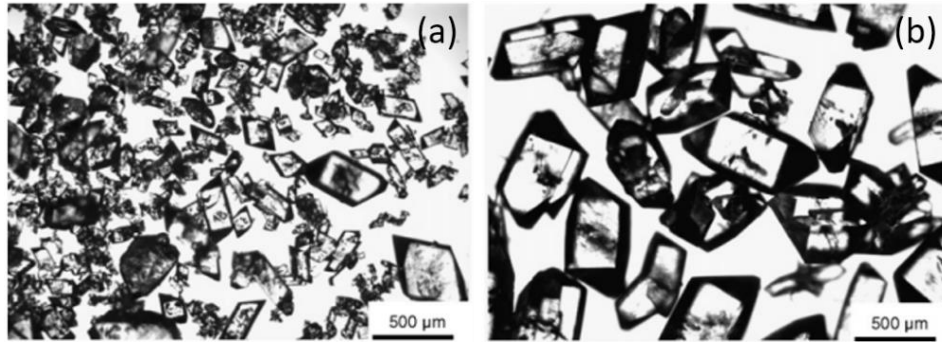


Figure 2-6 Microscopic images of paracetamol product of: (a) unseeded versus (b) seeded cooling crystallization. Permission obtained from [48] Copyright © 2007 Elsevier Ltd.

Even though nucleation rate expressions Eq(2.1), Eq(2.2) and growth rate expressions Eq(2.3) are generalized expressions, they are all not completely empirical. They can be derived from classical nucleation theory and diffusion-reaction growth theory respectively. Thus, the kinetic parameters have some physical meaningfulness to them. In addition to nucleation and growth, other more complex phenomenon are often present during crystallization [36], [56] such as agglomeration (multiple particles clustering together to form one large aggregate, Figure 2-8a), breakage (one particle breaking into two or more particles, Figure 2-8b), attrition (fines ‘chipping off’ from a particle surface as individual particles, Figure 2-8c) and Ostwald ripening (fine particles dissolving despite supersaturation, Figure 2-8d) which may also be important in certain systems.

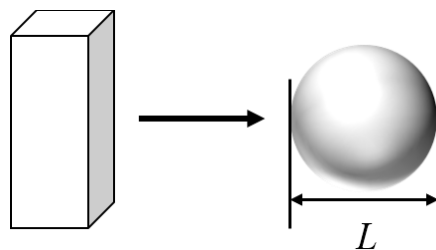


Figure 2-7 Volume equivalent sphere diameter

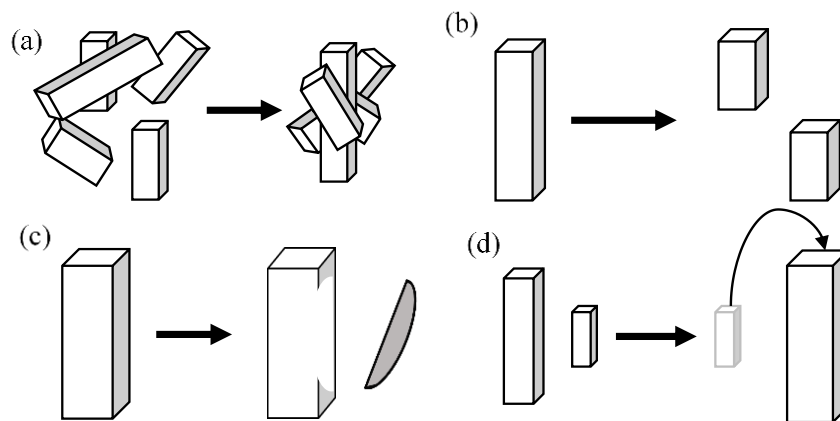


Figure 2-8 Animated schematic of (a) agglomeration, (b) breakage, (c) attrition and (d) Ostwald ripening mechanisms.

2.2 Process Analytical Technology

Process analytical technology (PAT) is essential in the paradigm shift to the QbD regulatory methodology [11]. The incorporation of PAT provides a framework to optimize the process by enhancing the understanding of the process, identifying and diagnosing off-spec processes, and enabling feed-back control strategies. PAT is especially critical to continuous processes to maintain a state-of-control operation. PATs can be in-situ (or online), at-line or offline. In-situ instruments provide real time monitoring of the process quantitatively or qualitatively with almost no delay. In-situ PAT sensors are usually invasive (i.e. must be inserted into the slurry system) and nondestructive (i.e. does not destroy samples). At-line instruments are located at close proximity to the process that poses a short delay but usually give more accurate qualitative and/or quantitative results than in-situ instruments. Offline PATs are usually characterization instruments that provide difficult-to-measure qualitative information. At-line and offline PAT tools are usually destructive.

Concentration is one of the most important quality attributes of a crystallization process. There are many in-situ PAT tools that enable real-time concentration monitoring such as attenuated total reflection ultraviolet/visible (ATR-UV/Vis) spectroscopy, attenuated total reflection Fourier

transform inferred (ATR-FTIR) spectroscopy, attenuated total reflection near infrared (ATR-NIR) spectroscopy and Raman spectroscopy. ATR-UV/Vis is a relatively economical tool that is very useful in tracking single component solution concentration. ATR-UV/vis applies UV/vis light and measures the reflectance. Solution of different concentrations reflects UV light differently. The calibration model is usually quite simple containing temperature and the absorbance of a single significant peak. Thus, the following calibration equation is often used:

$$C = a_1 Abs + a_2 T + a_3 Abs \cdot T + b \quad (2.4)$$

where a_i denotes fitted coefficients, Abs is the absorbance at a certain wavenumber and b is the fitted intercept. ATR-NIR and ATR-FTIR measures reflectance of IR or near IR light. Raman spectroscopy measures the Raman scattering of a laser at different Raman shifts to identify and quantify a compound. IR and Raman spectroscopy usually require a chemometric calibration model. IR spectrum is usually less affected by solid particle presence however, experiments should still be carried out to test that solid concentration that does not significantly affect the reading. In contrast, solid concentration usually has a significant impact on Raman scattering thus certain Raman shifts that are heavily correlated solid concentration changes can be used to track solid concentration in slurry suspensions [57], [58]. IR spectrum sometimes can also be used to track solid concentration if correlated peaks can be identified.

To calibrate quantitative PAT tools such as UV, IR and Raman for solution concentration measurement, a series of experiment should be carried out to reflect the effect of concentration, temperature and sometimes solid concentration on the spectra. In other words, solutions of known concentrations should be measured at different temperatures to construct such calibration models. To do so efficiently, the following experiment is repeated for several concentrations [59]: solution is first heated to ensure complete dissolution and maintained at 10 °C above its solubility

temperature for 30 min. Then the temperature is decreased stepwise until nucleation with 10-30 min hold at each step (Figure 2-9a) until nucleation. Nucleation can be detected by PAT tools such as the FBRM or the human eye which is less accurate. Per experiment, the absorbance is obtained at different temperatures of the same concentration. Once the same experiment is repeated for different concentrations, a calibration model can be developed to calculate concentration at a certain temperature from the spectrum reading. Additional experiments can be carried out to vary solid concentration at fixed concentration to observe the solid concentration effects on the spectrum. A faster but not as accurate method is also commonly used to calibrate concentration measurements [18]. This method requires that the solubility curve against temperature is known. The solution is first held at the lower limit of the temperature range of interest with excess solute material (i.e. the system starts as a slurry). Then the solution is heated stepwise slowly with 30 min hold at each step to ensure equilibrium (Figure 2-9b). Thus, the solution concentration at each temperature step can be assumed as the solubility concentration. This method is commonly known as the rapid calibration method. Its disadvantage is that temperature and concentration effects on the spectrum are not decoupled. If an anti-solvent crystallization process is intended, the solvent to anti-solvent ratio (SASR) should be varied instead of temperature.

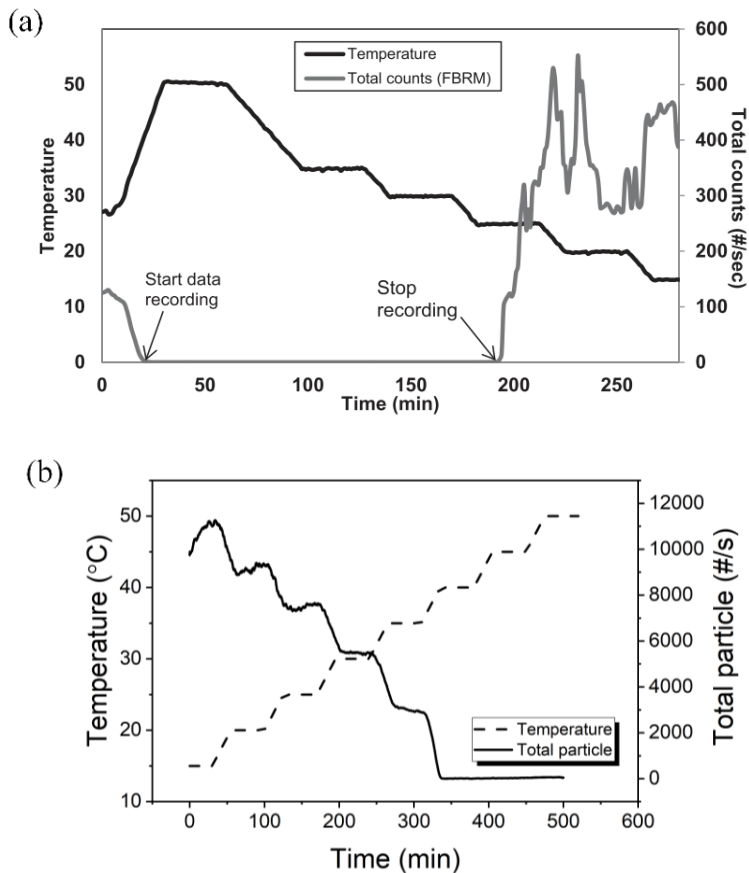


Figure 2-9 Temperature and particle count profile of (a) detailed solution concentration calibration. Permission obtained from [59] Copyright © 2014 WILEY-VCH Verlag GmbH & Co. KGaA, Weinheim; and (b) rapid solution concentration calibration [18].

Solid properties include size, shape and polymorphic form are important for crystallization processes. Focused beam reflectance measurement (FBRM), turbidity meter, ultrasound measurement, acoustic measurement and endoscopes are useful in-situ PAT tools that give quantitative and/or qualitative information about the solid properties.

FBRM is a calibration free tool that measures solid particle count and particle chord length distribution. It has gained popularity over the last decade for its monitoring and control applications [60]–[63]. It consists of a rotating laser optics in a sapphire window (Figure 2-10a) to measure laser back scattering corresponding to the chord length distribution (Figure 2-10b) and the particle count per unit time of its rotation (Figure 2-10c). It is important to notice that FBRM

measurement of particle count and chord length distribution does not quantitatively describe the number of particles in the crystallizer or the solid PSD, but the trend is indicative of the changes in particle population. For example, sudden increase of particle counts accompanied by mean chord length decrease indicates nucleation event (Figure 2-11a); mean chord length increasing overtime suggests possible crystal growth (Figure 2-11b); FBRM coupled with concentration gives great insight into the process that is otherwise difficult to obtain. FBRM can also be used for automated direct nucleation control (ADNC) where particle count is monitored via FBRM and controlled by manipulating supersaturation [63]–[66]. An example of ADNC application in batch crystallization of paracetamol is shown in Figure 2-12. ADNC can also be used to maintain a state-of-control in continuous crystallization processes [67], [68].

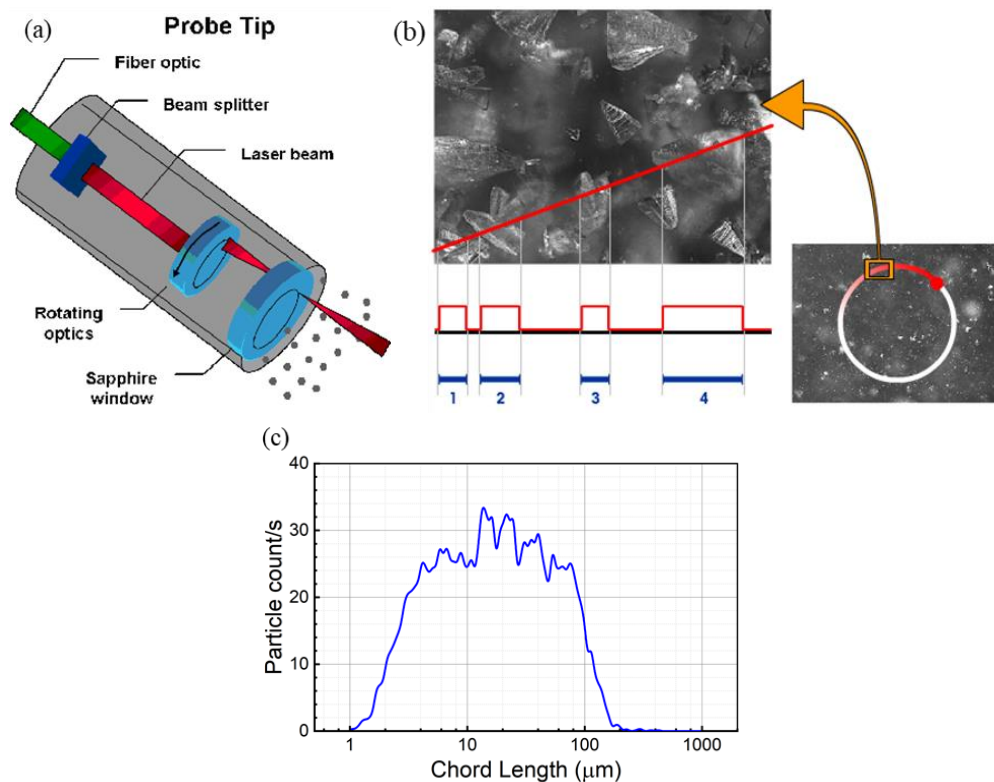


Figure 2-10 FBRM probe (a) schematics, (b) chord length measurement mechanism and (c) a typical chord length distribution measurement.

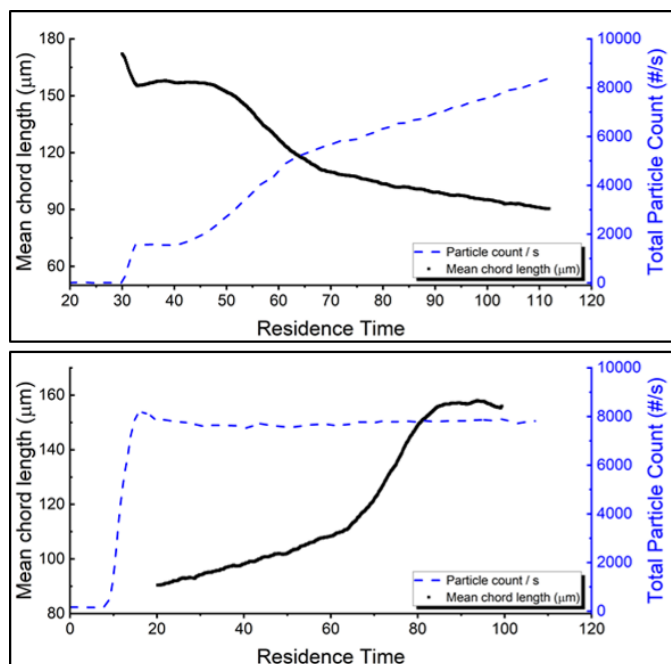


Figure 2-11 Typical FBRM profile of nucleation dominated crystallization (top) and growth dominated crystallization (bottom).

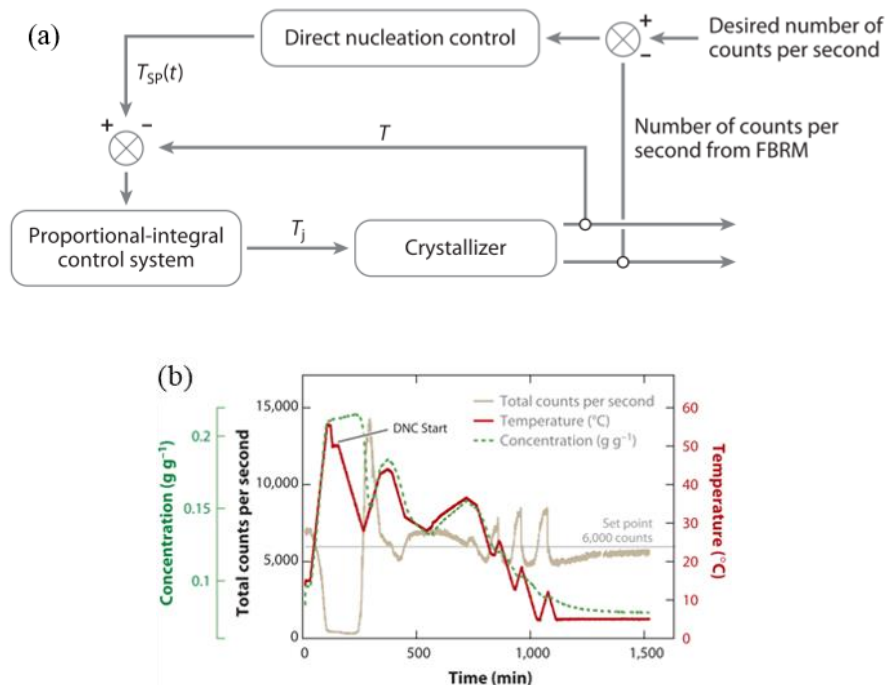
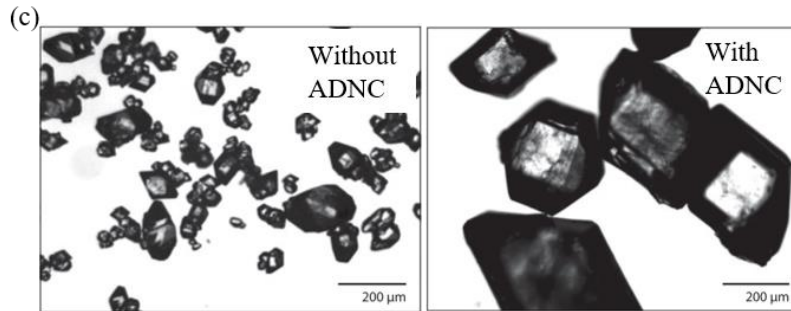


Figure 2-12 (a) Control diagram of ADNC, (b) operating profile of an ADNC crystallization process and (c) microscopic images of paracetamol batch crystallization products with and without ADNC. Permission obtained from [63] Copyright © 2012, American Chemical Society.

Figure 2-12 Continued.



Turbidity meter is another tool that measures solid properties. Turbidity is a phenomenon where a solution loses its transparency due to the presence of solids (Figure 2-13). The turbidity meter does not give detailed particle size distribution (PSD) or chord length information but is often used qualitatively to identify the presence of solids during metastable zone measurement experiments [69]–[71]. There are three types of turbidity measurements: adsorption (fixed sample volume, medium – high solid concentration), forwards scattering (fixed sample volume, low solid concentration) and backward scattering (simple design, open measuring zone).

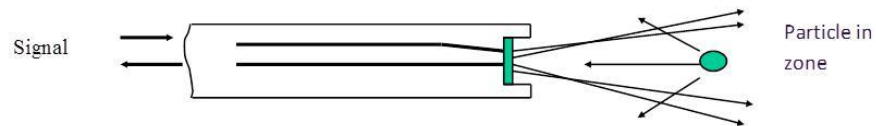


Figure 2-13 Turbidity meter measurement mechanism.

Acoustic emission (AE) measurement is another PAT tool that can monitor solid properties by measuring the elastic energy change of the acoustic wave induced by dynamic changes such as crystallization. In contrast to the other online PATs, AE sensing method is non-invasive as demonstrated in Figure 2-14a. In other words, it does not come into contact with the slurry content because it does not require an observation window. It allows analysis of opaque samples that are difficult to monitor with FBRM or other laser technologies. It is intrinsically safe and relatively

inexpensive, and it can be useful in both MSMPR and PFC operations. However, AE is a less commonly applied technology in the pharmaceutical manufacturing industry mostly due to its largely multivariate measurement data (Figure 2-14b) which requires advanced statistical method to analyze and calibrate.

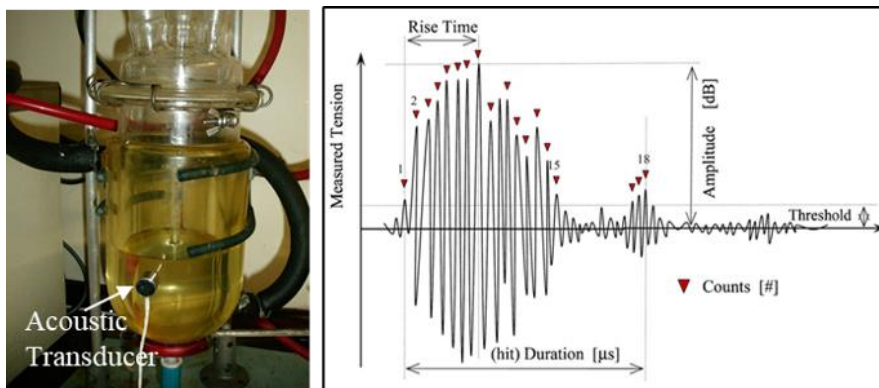


Figure 2-14 A non-invasive acoustic transducer implemented on a laboratory scale crystallizer and its main characteristic parameters of a typical AE hit. Permission obtained from [72] Copyright © 2012 Elsevier B.V.

Endoscopy, or in-situ video monitoring is another useful PAT tool that gives useful visual information of the system. Particle vision measurement (PVM) is a commonly used probe that gives real time microscopic images (examples are shown in Figure 2-15) of the crystals that can be used to visually detect nucleation, growth, agglomeration, and polymorphic transformation amongst other events [31], [61], [73]–[75]. Image analysis can be applied to provide some quantitative information however it is difficult to obtain reliable quantitative information when solid concentration is at medium to high level as the microscopic images become overcrowded and particle images become overlapped [76], [77].

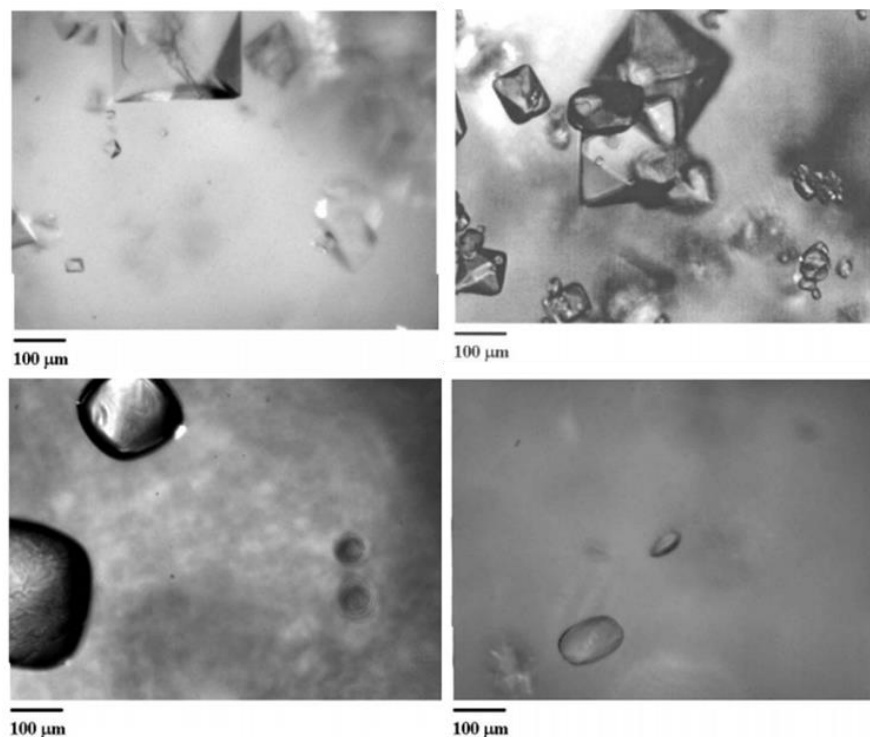


Figure 2-15 PVM images of particles during crystallization and dissolution. Permission obtained from [31] Copyright © 2002 The Institution of Chemical Engineers.

The aforementioned Raman spectroscopy can also be used to monitor solid properties including solid concentration and solid polymorphic form in addition to solution concentration [29], [78], [79]. Different polymorphic forms of crystalline particles yield different Raman readings due to differences in their molecular rotational or vibrational modes which can be picked up by in-situ Raman probes (Figure 2-16) thus useful for polymorph monitoring and control during crystallization. IR spectroscopy can also identify polymorphism of certain compounds. A summary of commonly used in-situ PAT tools for crystallization is listed in Table 2-1.

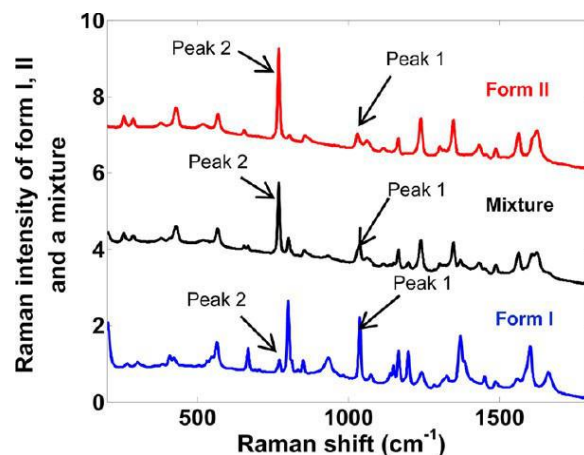


Figure 2-16 In-situ Raman spectrum of Form I, Form II and mixture of ortho-amino-benzoic acid (OABA). Permission obtained from [79] Copyright © 2014, American Chemical Society.

Table 2-1 Summary of in-situ PATs.

PAT	Measurement	Properties Monitored
UV	UV spectrum	Solution concentration
FTIR, NIR	(near) IR spectrum	Solution concentration, solid concentration, polymorphism
Raman	Raman scattering	Solution concentration, solid concentration, polymorphism
FBRM	Laser reflectance	Qualitative particle counts and chord length distribution
Turbidity	Turbidity	Solid concentration
AE	Acoustics	Solid concentration
PVM	Imaging	Particle shape, size, and agglomeration

Relatively complex analytical tools that are unable to fit in the crystallizer yet have a short measurement time (usually in a matter of minutes) are usually placed at-line of the process. These tools may analyze solution concentration, identify impurities and/or measures solid properties. Ultra-performance liquid chromatography (UPLC), mass spectrometry (MS) and gas chromatography (GC) are examples of chemical analytical tools with at-line measurement capabilities. They have been well developed in the field of analytical chemistry and there are many handbooks and literature on their method development. Nevertheless, it is usually difficult to maintain their automatic at-line operations for crystallization processes because they are intricate

instruments and are prone to blockage. Particles and/or gas bubble may get entrained into the instruments from the sampling channel which will likely cause measurement failure and even instrument damage. As a result, they are demonstrated more successful for liquid only upstream reaction process monitoring and are not commonly used for crystallization processes. However, there have been studies that demonstrated the usage of a PATROL UPLC by Waters for at-line concentration monitoring of crystallization processes. Yang et al. [80], [81] studied a UPLC set-up (Figure 2-17) that was equipped with a heated auto sampling line with a filter placed at the inlet to prevent particles from entering the lines. The authors successfully established process monitoring and feedback control strategies with at-line UPLC for crystallization process in two separate studies. Issues with blockage was not discussed in those studies. Manual sampling is also possible which largely prevents particle entrapment in the sampling line by properly treating the sample before measurement but significantly prolongs sampling time while introducing hard-to-monitor human errors.

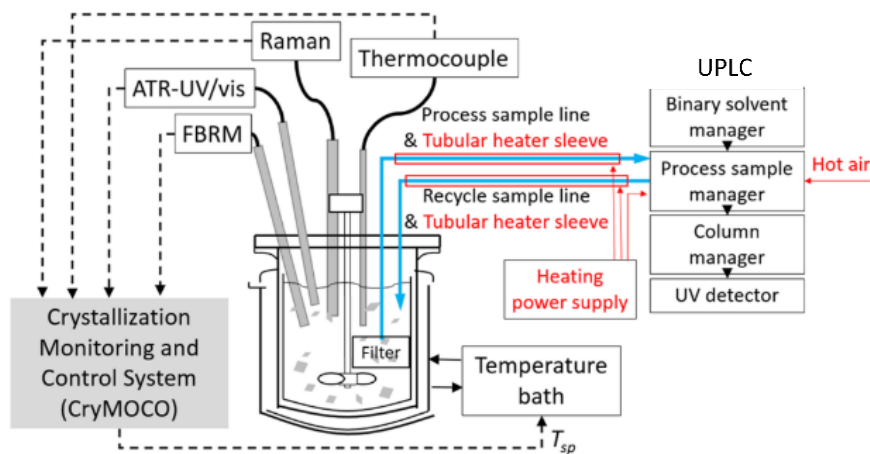


Figure 2-17 At-line concentration monitoring of a crystallization by UPLC. Permission obtained from [81] Copyright © 2016, American Chemical Society.

Laser diffraction wet dispersion sizing technology such as Malvern Mastersizer and Sympatec are also capable of at-line analysis mostly by manual sampling. They are nondestructive instruments that measure volume-based PSD by measuring the laser relative transmission of the dispersed sample in an insoluble liquid as shown in Figure 2-18. Laser diffraction measurement only provides volume-based PSD. Volume-based PSDs can be converted to number-based PSD under certain assumptions, but it is not very accurate in the small/fine particle range. It is also important to note that laser diffraction sizing technology is fundamentally different from FBRM and does not yield comparable results as the FBRM. Some wet dispersion models offer flow-cell capability for automatic at-line or inline monitoring however it is usually difficult to maintain stable sample obscuration for reliable at-line reading.

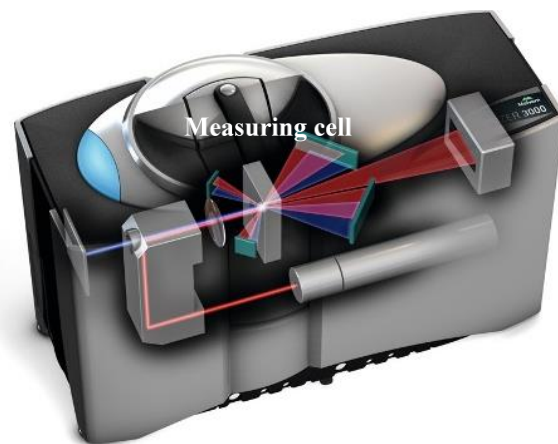


Figure 2-18 Laser diffraction PSD measurement mechanism.

Offline tools are instruments that usually provide comprehensive and accurate information about the system but take longer to process or are very large in size. They are excellent tools to measure properties that are otherwise difficult to measure in-situ or at-line such as multicomponent concentration, molecular structure and thermo stability, whose results can also serve as validation data for in-situ PAT sensors. Offline tools that are helpful for crystallization processes include

high performance liquid chromatography (HPLC) for purities, X-ray diffraction (XRD) for polymorph identification, microscopy (such as scanning electron microscopy SEM) for imaging, nuclear magnetic resonance (NMR) for impurity identification, dry dispersion laser diffraction sizing measurement and image-based sizing technology for PSD and so on. At-line instruments can be used offline as well. A summary of at-line and offline analytical tools is listed in Table 2-2.

Table 2-2 Summary of at-line and offline PATs.

PAT	Measurement	Properties Monitored
HPLC, UPLC	Liquid chromatography	Multicomponent identification and analysis
MS-GC	Gas chromatography	Multicomponent identification and analysis
Malvern Mastersizer	Laser diffraction	Volume-based PSD
Sympatec	Laser diffraction	Volume-based PSD
Malvern Morphologi	Imaging	Number-based PSD, particle morphology
XRD	X-ray diffraction	Solid structure, polymorphism
NMR	Magnetic resonance	Compound identification
SEM	Microscopy	Particle morphology

2.3 Batch and Continuous Crystallization

In order to achieve the desired crystal CQAs, one must design a suitable operating system, supersaturation generation profile, seeding strategy, and operating mode (batch or continuous). If upstream processes allow, a proper solvent should be chosen to avoid high toxicity and increase solvent power so that changing temperature or anti-solvent ratio results in higher changes in solubility. Crystal habits should also be considered when selecting a solvent to avoid difficult shapes (e.x. needle shape), polymorphic impurities and undesirable coloring [82]–[85]. The selection of solvent is also coupled with choosing the type of crystallization such as cooling, antisolvent or reactive crystallization for an optimal design. It is important to obtain the phase diagram and metastable zone limits so that an operating curve can be developed by experimental experience or optimization algorithms. Seeding is commonly practiced in industry to suppress

nucleation and promote growth. Typically for batch crystallizations, 0.5-5 wt% seed loading is used, and added when the system is close to solubility ($\frac{1}{4}$ to $\frac{1}{2}$ into the MSZW) [86], [87]. An empirical design equation can be used to select the seed size based on crystal size and shape [28], [88]:

$$m_s = m_c \left(\frac{d_s}{d_c} \right)^i \quad (2.5)$$

where m_s and d_s stands for mass and size of seed, m_c and d_c denote mass and size of crystals and i is a shape index, 1 for needles, 2 for plates and 3 for cubes/spheres. In addition to operating conditions and seeding techniques, the equipment design is also crucial to implement a well-designed crystallization process. As shown in Figure 2-19, a temperature-controlled vessel equipped with an overhead agitator and various port(s) for material addition and PAT tools installment is often used for crystallization. The material, dimension and mixing scheme of the crystallizer must be properly designed to ensure efficient heat and mass transfer as well as effective suspension of particles.

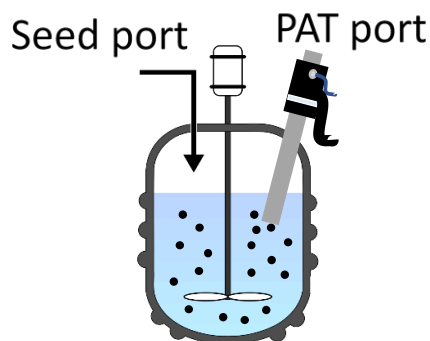


Figure 2-19 Schematic of a typical batch crystallizer with overhead ports for PAT tools and seed addition.

Crystallization of pharmaceuticals have been largely carried out in batch mode [57], [63], [64], [89]–[93]. Batch operations are ‘recipe-based’, simple and relatively low maintenance [14],

[94], [95]. Carefully designed batch crystallization operating curves (black dotted line in Figure 2-20) can achieve relatively uniform CSD and maximum yield; however, it usually requires a very long batch time and consequently batch crystallizers are often very large in size (on the order of several cubic meters). Such large size leads to high capital cost, high operating cost, elaborate scale-up practice, and heavy consequence for failed batches which is a prevailing issue due to batch-to-batch variations [10], [17]. Furthermore, local poorly-mixed spots are often present in large reactors where supersaturation can be exceptionally high triggering primary nucleation despite seeding [96]. Large number of fines are produced as a result leading to possible fouling, filtration failure, excessive agglomeration, and undesired polymorph formation amongst other issues.

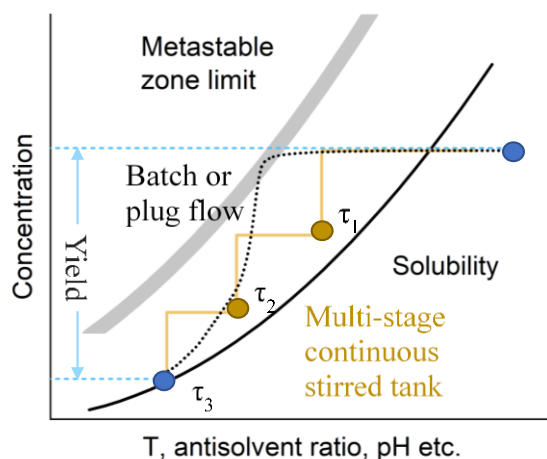


Figure 2-20 Typical operating profile of batch, multi-stage continuously stirred tank, and plug flow crystallization in the phase diagram.

Continuous crystallization on the other hand operates at ‘steady-state’, or more accurately, at a ‘state-of-control’ operation improving process robustness and product consistency [27], [66]. It is crucial to incorporate PAT during continuous crystallization to maintain the consistent state-of-control operation. Continuous operations usually allow smaller-size reactors because of its ability to operate for a long period of time without interruption, enabling on-demand

manufacturing that can be easily relocated and reconfigured between different locations. More importantly, continuous crystallization may be scaled by simply increasing the flow rate with little to no equipment size change which significantly simplifies or potentially eliminates traditional scale-up practices associated with batch crystallization [97]–[99]. However, there are challenges associated with continuous crystallization despite the inherent advantages. These challenges mainly center on the issue of fouling: continuous crystallization inherently requires supersaturation throughout the whole operation which tends to cause encrustation on equipment surfaces and in transfer lines. Coupled with low flow rates required for most pharmaceutical processes, fouling and blockage can easily occur, and the state-of-control operation may subsequently be interrupted [23], [100]. Additionally, the continuous supersaturation present in the crystallizer inevitably leads to lowered yield compared to batch which is another obstacle for shifting to continuous from an economical perspective. Continuous crystallization is by no means a new concept. It has been an established process at large scale production in industries like sugar processing and mineral refining, but it becomes challenging at smaller scales where pharmaceutical industry usually operates. It is often not a trivial decision to operate in batch or continuous mode when developing a crystallization process. Factors like demand, material property, time constraint, budget, and level of technology expertise must be considered during the decision-making process.

2.4 Continuous Crystallizers

There are two general types of continuous crystallizers: mixed-suspension-mixed-product-removal (MSMPR) crystallizers where material is actively fed and removed from a well-mixed vessel producing wide residence time distributions (RTDs), and near plug-flow crystallizers (PFCs) where the material ‘flows’ through a tubular reactor with the RTD being near uniform. MSMPR

operation allows utilization of existing equipment while PFC produces tight RTDs enhancing product consistency. Each type can be the appropriate choice for different crystallization systems.

2.4.1 Mixed-suspension-mixed-product-removal crystallizers

An MSMPR operation consists of one or more well-mixed vessel(s) in series with continuous feed and slurry removal. Successful employment of continuous crystallization in MSMPRs relies on sufficient mixing and proper slurry withdrawal schemes to obtain products in the outlet representative of the bulk slurry. A single MSMPR crystallizer operates at one point in the phase diagram (for example τ_1 on Figure 2-20) but a batch-like operating curve can be replicated by employing a multi-stage MSMPR system (yellow solid line on Figure 2-20). For many APIs, pilot scale crystallizers are enough to meet current demand in continuous mode without further scale-up. The possibility to utilize existing equipment and its simplicity of operation are major advantages of MSMPR systems over other continuous crystallization systems. Another advantage is the ability to operate at long residence times without particle settling issues which is especially beneficial for slow growing compounds [27]. During MSMPR mode operation, some slurry elements immediately exit the crystallizer after entrance, some elements end up never leaving the vessel while most elements are somewhere in between, making up a broad RTD profile. This can be a disadvantage of MSMPR systems because broad RTD may lead to broad CSD [101].

a. Equipment and scale

The most commonly used MSMPR crystallizer is a stirred tank crystallizer (STC) as it is readily available in most labs and pilot plants and it is simple and inexpensive to build. Similar to a batch crystallizer, an overhead stirrer is often used to provide mixing. The agitator type, position and agitational speed are all important design factors to consider for a well-mixed STC. Axial-flow impellers such as pitched blade or retreat curve impellers are often used in crystallization. The

material of the impeller must be durable and chemically compatible. Particles present in pharmaceutical crystallization processes tend to be heavier than its solvent thus the impeller is often positioned closer to the bottom. Sufficient agitation speed is also needed to keep crystal particles suspended. This speed can be determined by experiments and/or computational fluid dynamics (CFD) which can be costly. Previously developed empirical equations are often used in practice to determine the minimal agitational speed. One of the most commonly used equations is known as the Zwietering correlation [102]:

$$N_{js} = Z_c \nu^{0.1} d_p^{0.2} \left[\frac{g_c (\rho_c - \rho_{sol})}{\rho_{sol}} \right]^{0.15} X^{0.13} D_{im}^{-0.85} \quad (2.6)$$

where N_{js} denotes the minimum agitation rate required for particles of mass mean size d_p , Z_c is the Zwietering constant, unique to the geometric characteristics of the agitation system, which can be experimentally determined or found in literature and handbooks, ν is the kinematic viscosity of the solution, g_c is the gravitational acceleration constant (9.81 m/s^2), X is the weight percentage of solid to liquid content and D_{im} denotes the impeller diameter. An added complexity in crystallization is that agitation speed has a significant impact on crystal habits by affecting crystallization kinetics. While higher agitation speed improves mass transfer which improves local supersaturation, it can also induce particle breakage [103], attrition [104] and agglomeration [94] which is often undesirable. An optimal mixing scheme design relies on experiments, modeling and engineering experience.

Small bench scale MSMPR STCs range from 10s mL to 100s mL (an example of 500 mL STC is shown in Figure 2-21a) often equipped with ports for PAT tools [14], [17], [94], [105]–[108]. Pilot plant scale of a few liters (an example is shown in Figure 2-21b) to 15 liters in volume have also been demonstrated to successfully produce crystal products at the rate of several kilograms of API per day [109], [110]. Larger equipment is not necessarily required to meet

production demand at pharmaceutical scales and laboratory/development equipment is capable of matching batch scale production at equivalent or shorter time scale [27], [109] assuming that continuous crystallization can be sustainably operated for long periods of time, but it may be challenging. One of, if not the most challenging aspects of maintaining a sustainable continuous crystallization in an MSMPR, is slurry transfer.

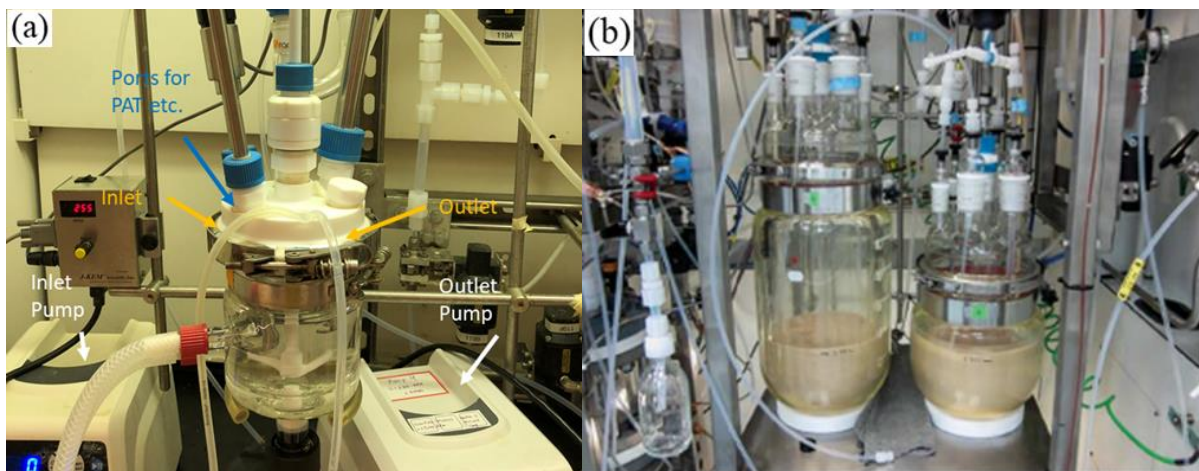


Figure 2-21 Equipment set-up of (a) a lab scale (500mL) stirred tank MSMPR [18] and (b) a kilo scale stirred tank MSMPR. Permission obtained from [110] Copyright © 2017, Copyright © 2017 The Authors, some rights reserved; exclusive licensee American Association for the Advancement of Science. No claim to original U.S. Government Works.

b. Slurry transfer

Continuous crystallization is a two-phase process where a mixture of solid and liquid must be transferred from one vessel to the next which presents a host of challenges. Slurry transfer failure, including inhomogeneous slurry removal and transfer tubing blockage, have been reported to be the top reason causing premature termination during continuous crystallization studies and summarized by Yang et al, a research group at the FDA, in a risk focused study [23] amongst other review literatures [27], [66], [98], [111], [112]. Representative or homogenous product removal refers to the practice where the product removed at the outlet has the same composition (and CSD) of the bulk slurry. Yang et al [23] pointed out that while it needs further discussion whether

representative product removal is strictly required, representative slurry removal is often preferred for a more stable steady-state continuous operation. To ensure representative slurry removal, not only a proper rotational speed needs to be determined for sufficient particle suspension, the location of the transfer line is also important. Three common slurry removal locations are demonstrated in Figure 2-22. Due to the nature of agitational mixing dynamics, particles tend to accumulate under the impeller, the inlet of the product removal line is recommended to be placed lower than the impeller if possible [23]. A drain may be used as the product removal outlet to further improve this issue.

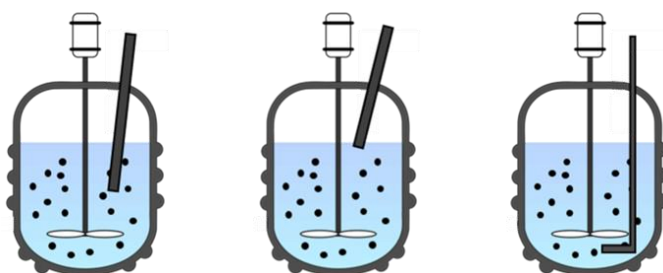


Figure 2-22 Animation illustration of MSMPR drawing schemes: skimming (left), submerged (middle), and metal pipe guided bottom drawing (right).

A bigger challenge is fouling and blockage of transfer lines (Figure 2-23 [23]). A wide removal tubing, which is often required to prevent blockage, coupled with slow removal rates, needed to maintain a certain residence time, poses a challenge to sustain turbulence in the transfer line [27], [73], [113]. Lack of turbulence may cause particles to settle and/or block the transfer line completely. Moreover, unconsumed supersaturation that is naturally present during MSMPR operation can cause further crystallization in the transfer line which worsens the particle settling issue and onsets encrustation on the tubing wall. This in turn can result in lowered yield, line blockage and in some cases process failure. Therefore, transfer lines should only be as long as needed without unnecessary kinks and pinches and slurry transfer should take place as quickly as

possible. Temperature control can also be implemented on the transfer line to prevent further crystallization [23].



Figure 2-23 A blocked slurry transfer line of a lab scale MSMPR. Permission obtained from [23] Copyright © 2017, ACS.

Pump driven slurry transfer is commonly used in conjunction with soft Teflon tubing to transfer slurries as shown in the MSMPR set-up in Figure 2-21a [16], [18], [78], [114]–[116]. Programmable peristaltic pumps also enable a simple yet effective slurry transfer scheme to prevent transfer line fouling: intermittent product removal. It has been reported that intermittent removal significantly improves transfer line fouling compared to continuous operation. During intermittent operation, the slurry transfer pump remains idle for some time followed by high flowrate removal of the accumulated volume. This accumulation is recommended to be less than 10% of the total volume in the vessel to avoid significant disturbances. It has been shown to produce similar products as true continuous operation both by experiments and by mathematical modeling [117].

c.State-of-control operation

State-of-control is a more accurate description of stable continuous crystallization operation where small deviations from steady state may occur but system dynamics and/or applied control strategies

can correct such a deviation without causing significant changes in product CQAs [10], [12], [100]. Such a dynamic or sometimes oscillatory state is considered a steady and stable operation of continuous crystallization and is more appropriately called a ‘state-of-control’ operation. During state-of-control operation, product quality attributes such as CSD, solution concentration, impurity level and polymorphic form remain constant or in an acceptable range. The final state-of-control product qualities are often governed by the operating conditions; For example, if the temperature of the MSMPR is low during a cooling continuous crystallization process aiming to improve yield, CSD is likely to be small because of excessive nucleation but is observed to improve if residence time increases [106], [118]. Incorporation of milling or ultrasound also affects state-of-control CSD by inducing particle breakage and/or accelerating nucleation. Yield is another important property to consider when designing a suitable state-of-control operation. It is often of economic interest to maximize yield. To achieve this, several studies have been carried out to investigate potential strategies to improve yield. Recycling being an obvious choice has been shown to significantly improve the overall yield in MSMPR operation. Alvarez et al. [119] showed that implementing a recycling stream increased the yield from 71% to 87% while decreasing purity by ~2% for the cooling crystallization of cyclosporine (Figure 2-24). Thus, recycling may be an unacceptable strategy for certain compounds. Lowering the MSMPR crystallizer temperature has also been shown to improve yield but it may result in smaller crystal size [65], [120], [121]. Inclusion of wet-mill (Figure 2-25) and sonication (Figure 2-26) can improve particle uniformity but it is a trade-off with crystal size [68], [122], [123]. Increasing residence time can improve yield without compromising CSD and often times improving state-of-control crystal size [14], [105], [124]. However, it will require lowering the flow rate thus decreasing throughput or implementing

more stages which increases cost. Depending on the kinetics, a combination of the aforementioned techniques can be applied to obtain an optimal state-of-control.

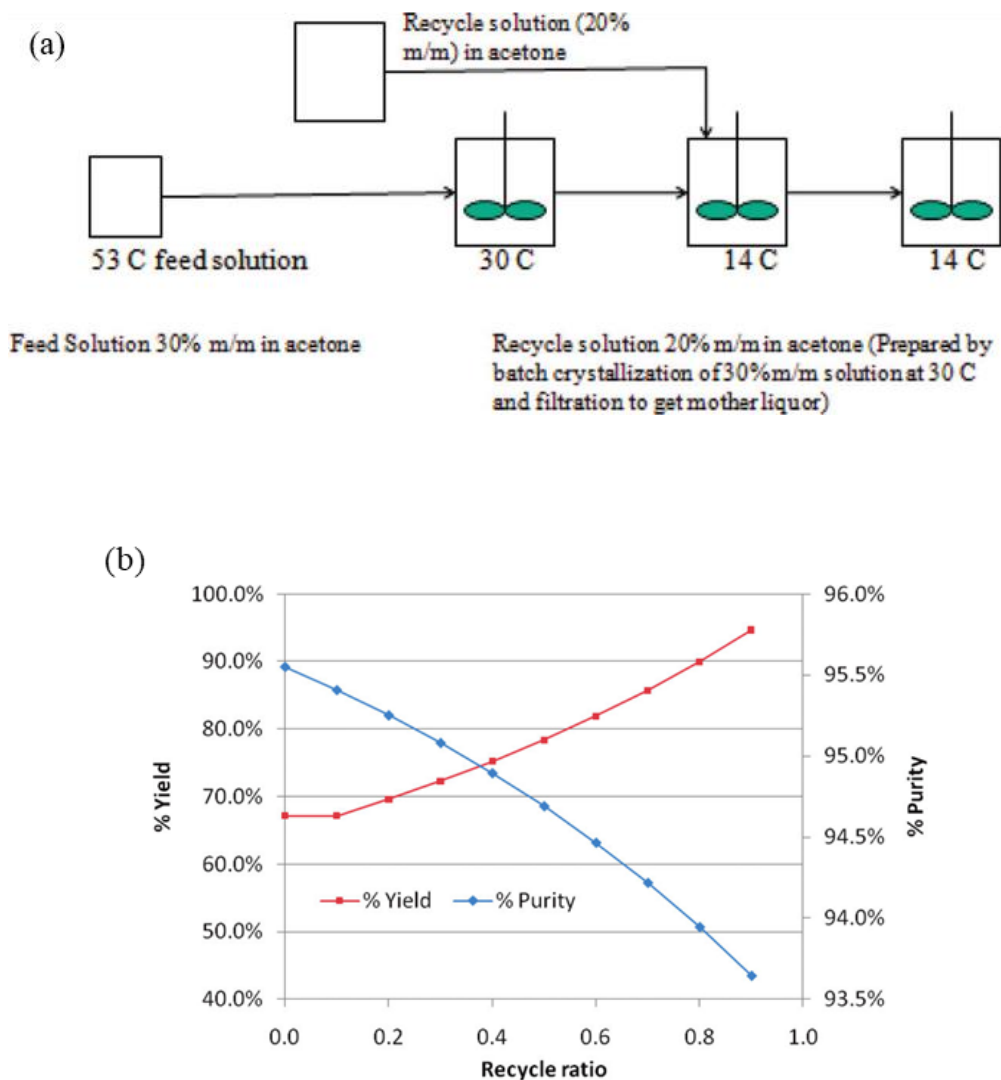


Figure 2-24 (a) Schematic of multistage MSMPR continuous crystallization of cyclosporin with recycle; (b) effect of recycle ratio on product purity and process yield. Permission obtained from [119] Copyright © 2011, American Chemical Society.

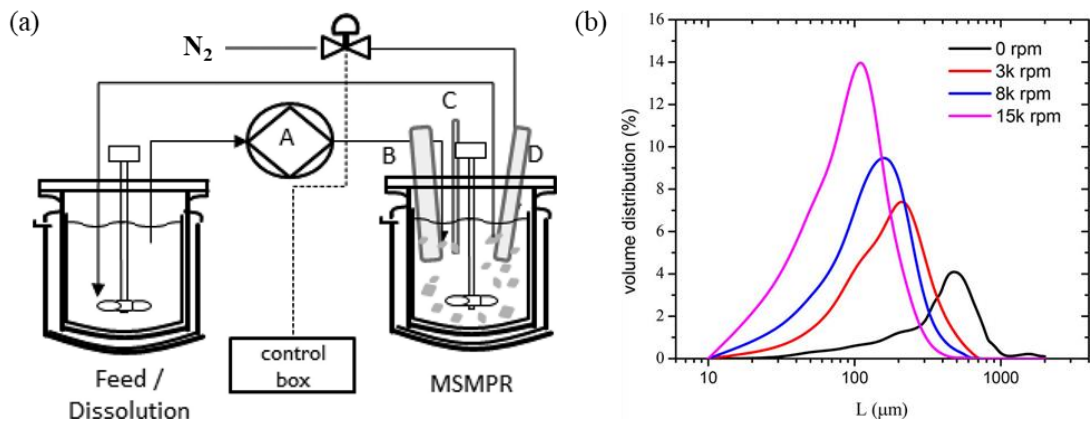


Figure 2-25 (a) Schematic of an in-situ wet mill in the MSMPR experimental set-up and (b) volume-based size distribution at different wet mill rpm. Permission obtained from [16] Copyright © 2017, American Chemical Society.

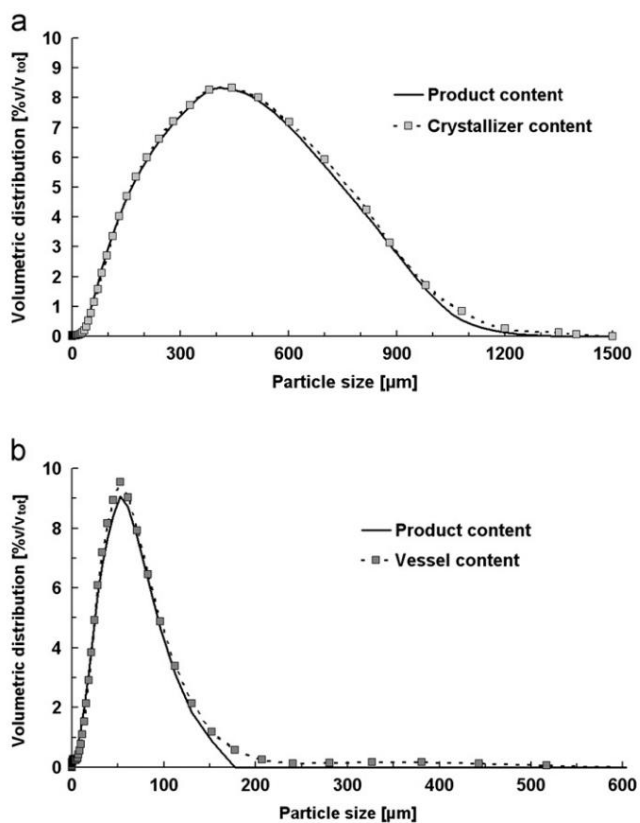


Figure 2-26 Volume-based size distribution of particles in crystallizer implemented with sonication and product vessel at (a) silent conditions and (b) 40% power amplitude sonication. Permission obtained from [123] Copyright © 2010 Elsevier Ltd.

Polymorph (and chirality) control is another important but perhaps more subtle advantage that comes with MSMPR operations. Unlike batch, one MSMPR state-of-control operation fixates on a single point in the phase diagram consistently producing the polymorphic form favored at that point. A batch operation curve may inevitably pass through regions in the phase diagram that favor an undesired polymorphic form. Thus, maintaining a specific state-of-control operation can achieve tight control of the polymorphic form. Lai et al. [125] demonstrated this aspect by manipulating the temperature and residence time of the MSMPR operation to selectively produce a β -form of L-glutamic acid which is relatively difficult to obtain with batch crystallization processes. Similarly, Steendam and Horst [126] established a single stage MSMPR continuous process to consistently produce chirally pure crystals by manipulating residence time, feed concentration and start-up strategy to tune for a desirable state-of-control operation.

As of now, MSMPR continuous crystallization of pharmaceuticals remains in research stage. Fouling and blockage is often vaguely reported or kept off records. In addition, the robustness and reproducibility of these studies are not tested rigorously. Therefore, the issue of fouling may take place more frequently and cause more serious consequences than what current literature suggests. Further study of the robustness of continuous crystallization in MSMPR mode is still needed to establish a systematic process development strategy to achieve a robust state-of-control operation.

2.4.2 Plug-flow crystallizers

Plug flow crystallizers (PFC) are tubular reactors in which the content flows at a near constant velocity. The obvious appeal of a PFC over an MSMPR vessel is that the axial mixing is minimal in the PFC producing a near uniform RTD compared to the broad RTD in an MSMPR crystallizer as illustrated by Figure 2-27. The spatial gradient (i.e. the length) of a PFC is equivalent to that of

batch time which would require several MSMPR crystallizers in series to achieve the same operating profile. However, in order to maintain turbulence in the PFC, a high flowrate is usually required resulting in short residence times or extended reactor length. While plug flow reactors have been successfully applied for single phase reaction processes, the added complexity of particle suspension poses a challenge for successful crystallization operations. It is difficult to produce high enough turbulence in PFCs to ensure homogenous mixing of the liquid phase and the solid phase. Therefore, a bench scale PFC is rarely demonstrated to be successful. However, there are a few nonconventional PFCs that incorporated unique designs such as static mixing, sonication, and micro channels to enhance mixing for successful continuous crystallization operations with short residence times [127]–[132]. Encrustation and fouling is another challenge in maintaining the state-of-control in the PFC (Figure 2-28). Cleaning procedures can also be very complex for long PFCs.

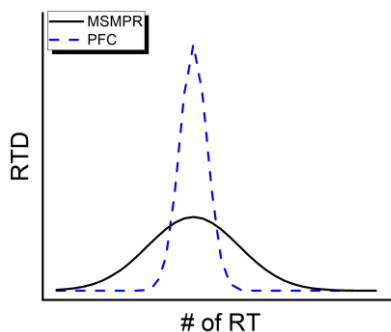


Figure 2-27 Typical RTD of MSMPR versus PFC.



Figure 2-28 Image of an encrusted tube section of a tubular PFC.

A particular near plug-flow oscillatory crystallizer has been gaining popularity in recent years for its ability to suspend particles at relative low net flow rates: an oscillatory flow baffled crystallizer (OFBC) also known as a continuous oscillatory baffled crystallizer (COBC) or simply oscillatory baffled crystallizer (OBC) [133]–[140]. It superimposes oscillatory motion onto the flow by a plunger in a baffled tubular reactor to aid particle suspension as shown in Figure 2-29. A combination of oscillatory motion and static baffles generates sufficient turbulence at laminar net flow conditions attaining far longer residence times (10 - 30 minutes) compared to static PFCs (up to a few minutes). Oscillatory mixing also brings additional advantages such as improved heat and mass transfer and low shear rate. Lawton et al. (2009) [133] was amongst the first to demonstrate successful continuous crystallization of an API in an OFBC (Figure 2-30). In the same study, a cost analysis was carried out which suggested a potential £300k saving annually compared to equivalent batch operations (Table 2-3) providing financial incentives of switching to continuous crystallization.

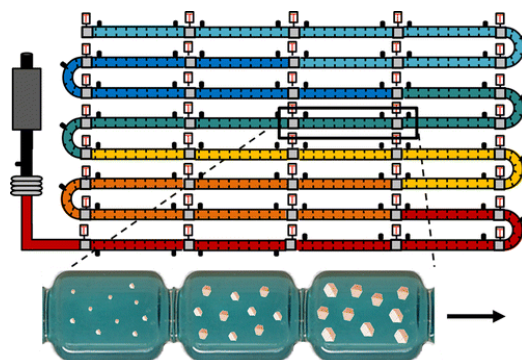


Figure 2-29 Schematic of the tubular OFBC and a zoomed-in view on a baffled tube segment. Permission obtained from [140] Copyright © 2015, American Chemical Society.



Figure 2-30 A custom built stainless steel OFBC unit. Permission obtained from [133] Copyright © 2009, American Chemical Society.

Table 2-3 Cost analysis of a continuous operation in an OFBC compared to a traditional batch isolation process. Permission obtained from [133] Copyright © 2009, American Chemical Society.

	Potential saving (£) from traditional batch
New build	20% lower
Operating costs	300k per annum
Crystal engineering without milling	50% lower +> 300K per annum

2.5 Population balance modeling

Mathematical modeling is a useful tool in process development of crystallization. A population balance model (PBM) is often used to describe crystallization as it tracks the population of particles of different sizes in suspension as well as concentration in solution. The basic concept of a population balance is to balance the number of particles generated/destroyed by nucleation, agglomeration and/or breakage as well as to track the flux of particles travelling between size bins by crystal growth. To describe this idea mathematically, let us introduce a (univariate) population distribution function $f(L,t)$ such that $f(L,t)dL$ describes the number of particles between size L to $L + dL$ per unit slurry volume at time t (Figure 2-31).

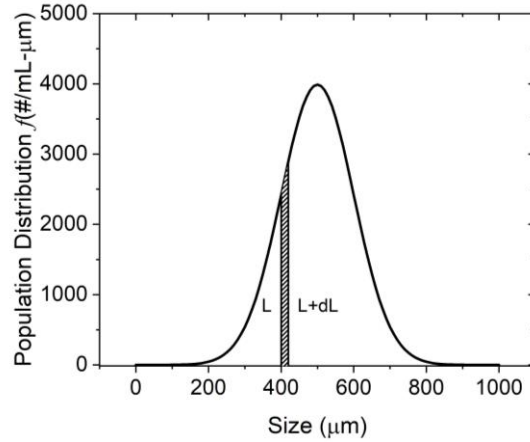


Figure 2-31 Population distribution function where shaded area represents the number of particles between size L and $L+dL$ in a unit slurry volume.

2.5.1 Batch

For a batch crystallization process, population balance is written as:

$$\frac{\partial f}{\partial t} + \frac{\partial(Gf)}{\partial L} = Q_{nuc} + Q_{agg} + Q_{break} \quad (2.7)$$

where Q denotes particle generation or disappearance mechanisms and *nuc*, *agg*, *break* subscripts stand for ‘nucleation’, ‘agglomeration’ and ‘breakage’ respectively [141]–[143]. If agglomeration and breakage are negligible, Eq(2.7) can be simplified as:

$$\frac{\partial f}{\partial t} + \frac{\partial(Gf)}{\partial L} = B\delta(L - L_0) \quad (2.8)$$

where $\delta(L - L_0)$ is the dirac delta function that engages nucleation only at nucleus size L_0 (usually taken to be very small or 0):

$$\int_{-\infty}^{\infty} \delta(L)dL = 1 \quad \text{if } L = L_0$$

$$\delta = 0 \quad \text{if } L \neq L_0 \quad (2.9)$$

To close the system of equations, a mass balance can be written to relate solid and liquid phase concentration:

$$\frac{dC}{dt} = -3k_v \rho_c \int_{L_0}^{\infty} GL^2 f dL \quad (2.10)$$

where C is the mass concentration of the solute in solution, k_v represents the shape factor (1 for cube, 0.5 for sphere, 10 for needle shape etc.), and ρ_c is the crystal density. An energy balance can also be written which is especially important for strongly exothermic or endothermic crystallization processes:

$$\frac{dT}{dt} = \frac{-hA(T - T_w)}{V \rho_{sol} C_p} - \frac{\Delta H_c 3k_v \rho_c}{\rho_{sol} C_p} \int_{L_0}^{\infty} GL^2 f dL \quad (2.11)$$

where h represents heat transfer coefficient, A is the heat exchanging area of the crystallizer, T_w is the temperature at the heat exchanging wall, V stands for the slurry volume, ρ_{sol} is the density of the solution, C_p denotes the specific heat of the solution, and ΔH_c represents heat of crystallization. Solving Eq(2.8) Eq(2.10) and Eq(2.11) together yields particle population distribution, solution concentration, and bulk temperature profile over time [141], [144]. Initial concentration (and temperature), and seed population (if seeded) must be obtained as the initial conditions to solve the system of equations.

2.5.2 MSMPR

In a single stage MSMPR, the population balance model can be written as

$$\frac{\partial(Vf)}{\partial t} + \frac{\partial(VGf)}{\partial L} = \dot{Q}_{in} f_{in} - \dot{Q}_{out} f + V(Q_{nuc} + Q_{agg} + Q_{break}) \quad (2.12)$$

where V is the slurry volume in the crystallizer, \dot{Q}_{in} and \dot{Q}_{out} represent the inlet and outlet volumetric flow rate, f_{in} is the population distribution of the seed carried into the system with feed (taken as zero if the system is not continuously seeded). If agglomeration and breakage are negligible, Eq(2.12) can be simplified as:

$$\frac{\partial(Vf)}{\partial t} + \frac{\partial(VGf)}{\partial L} = \dot{Q}_{in}f_{in} - \dot{Q}_{out}f + VB\delta(L-L_0) \quad (2.13)$$

A mass balance can also be written for a single stage MSMPR operation:

$$\frac{d(VC)}{dt} = \dot{Q}_{in}C_{in} - \dot{Q}_{out}C - 3Vk_v\rho_c \int_{L_0}^{\infty} GL^2 fdL \quad (2.14)$$

where C_{in} denotes the feed concentration. Initial conditions can be written based on the start-up method:

$$\begin{aligned} f(@t=0) &= \text{population of initial seed, if seeded} \\ f(@t=0) &= 0 \text{ for all } L, \text{ if unseeded} \\ C(@t=0) &= \text{initial concentration} \end{aligned} \quad (2.15)$$

This PBM makes two additional assumptions: (1) the crystallizer is well mixed: solid PSD and solution concentration is uniform spatially, and (2) product removal is representative: solid PSD and solution concentration in the removal line are the same as the bulk.

At steady state, the first term of Eq(2.13) and Eq(2.14) becomes zero and the solution gives steady state concentration and particle population. Therefore, the population balance of a constant volume single-stage MSMPR crystallization without continuous seeding at steady state becomes:

$$\frac{\partial(Gf)}{\partial L} + \frac{f}{\tau} - B\delta(L-L_0) = 0 \quad (2.16)$$

where τ is the residence time. Eq(2.16) is an ODE and can be solved to estimate size independent linear growth rate:

$$\begin{aligned} \frac{df}{dL} &= -\frac{f}{G\tau} \\ \text{B.C. } f_0 &= \frac{B}{G} = \text{population of nuclei} \end{aligned} \quad (2.17)$$

Solving the ODE analytically:

$$\ln(f) = -\frac{1}{G\tau}L + \ln(f_0) \quad (2.18)$$

Linear growth rate can be estimated by plotting logarithmic steady-state population f against size L as shown in Figure 2-32 [107].

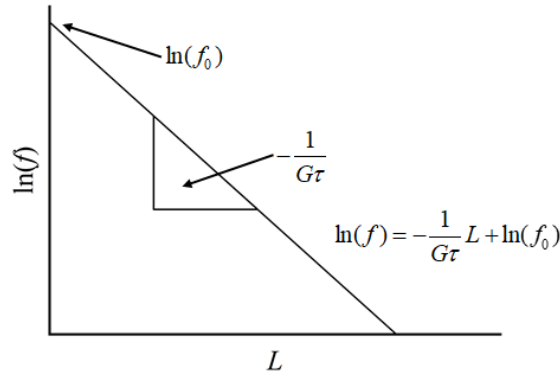


Figure 2-32 Semilogarithmic population density versus size plot to predict growth rate.

Similar system of equations can be written for multistage MSMPR operations. Consider the i th stage of a multistage MSMPR system, the inlet flow of the i th stage is equal to the outlet flow of the $i-1$ th stage:

$$\begin{aligned} \frac{\partial(V_i f_i)}{\partial t} + \frac{\partial(V_i G f_i)}{\partial L} &= \dot{Q}_{i-1} f_{i-1} - \dot{Q}_i f_i + V_i B \delta (L - L_0) \\ \frac{d(V_i C_i)}{dt} &= \dot{Q}_{i-1} C_{i-1} - \dot{Q}_i C_i - 3V_i k_v \rho_c \int_{L_0}^{\infty} GL^2 f_i dL \end{aligned} \quad (2.19)$$

Eq(2.19) can be solved for each stage with $i-1$ th stage being the feed for when $i = 1$. Initial conditions can be written similarly to Eq(2.15) based on the start-up procedure.

2.5.3 PFC

PBM can also be used to simulate continuous crystallization in the PFC with an added dependence along the length z of the crystallizer. f then becomes dependent on t , L and z (i.e. $f = f(t, L, z)$).

Assuming crystal nucleation and growth are the only two significant mechanisms, the population balance equation can be written as:

$$\frac{\partial(f)}{\partial t} + \frac{\partial(Gf)}{\partial L} + \frac{\partial(vf)}{\partial z} = B\delta(L - L_0) \quad (2.20)$$

where v is the velocity of the particles which equals to volume flow rate divided by cross sectional area. During steady-state, the PBM becomes:

$$\begin{aligned}\frac{\partial(Gf)}{\partial L} + \frac{\partial(vf)}{\partial z} &= B\delta(L - L_0) \\ \frac{\partial(vC)}{\partial z} &= -3k_v\rho_c \int_{L_0}^{\infty} GL^2 fdL\end{aligned}\tag{2.21}$$

from which the particle size distribution and concentration traveling through the length of the PFC can be solved.

2.5.4 Kinetic parameter estimation

To solve PBM, kinetic parameters listed in Eq(2.1), Eq(2.2) and Eq(2.3) must be known. In practice, they are often estimated from carefully designed experiments by minimizing the sum of square residuals of simulated concentration to experimental data with computer programs such as MATLAB's '*lsqnonlin*' and '*fmincon*'. This approach can be challenging because crystallization models are complex and may present many local solutions. More intelligent optimization frameworks have been developed to systematically improve parameter estimation algorithms from the basic least-square nonlinear optimization methodology [145], [146]. Summarizing these techniques, two general approaches are often taken: algorithmic improvement and physical insight incorporation. Algorithmic improvements include applying superior algorithms in attempt to find a global and unique solution to the least-square optimization problem. An example of this is applying genetic algorithm (GA) to find the best initial guesses by evolution. Uneducated initial guesses often result in local solutions especially when solving highly nonlinear systems like crystallization PBM. Other algorithm improvement techniques include model discrimination, estimability analysis, identifiability analysis and other mathematical means to improve parameter estimation meaningfulness and solution uniqueness. The other approach is to gain and apply physical understanding of the system. Performing representative design of experiments (DoE),

applying PAT guided experiments, sequential kinetic estimation [26], [29] are all examples of how to gain better understanding of the process. From these understandings, sensible constraints on crystallization rates and particle size can be imposed onto the optimization algorithm steering the system away from nonsensical solutions and limiting the search region significantly.

2.6 Integration of continuous crystallization and filtration

Operated as a slurry, crystallization is inseparable from its immediate unit operations such as filtration, drying and granulation. Integration of continuous crystallization with downstream operations is an important step towards end-to-end continuous manufacturing. However, there are many challenges associated with the integration of unit operations including slurry transfer, spatial constraints and scheduling. The immediate unit operation that follows crystallization is filtration. Filtration is a difficult unit operation to run continuously and most continuous crystallization–filtration studies apply an alternating semi-batch filtration system. Acevedo et al. [15] was amongst the first to demonstrate a commercially available continuous filtration carousel (CFC system from Alconbury Weston Ltd, AWL) which is shown in Figure 2-33. It consists of a wash solvent tank, a clean in place (CIP) solvent tank and a five-port filtration carousel. A Poremet metal mesh filter is installed at the bottom of the carousel covering port 1, 2, 3 and 4 while leaving port 5 uncovered. The CFC withdraws slurry from a hold-up tank and dispenses the slurry into port 1 via gravity, wash solvent and CIP solvent are dispensed into port 2 and 3. Port 4 inlet is blanked. Vacuum is applied under the filter mesh to remove filtrate/solvent and air-dry the filter cake residing in port 1-4. Then the carousel is rotated one index counter-clockwise i.e. port 1 becomes port 2 for wash, port 2 becomes port 3 for CIP etc. Port 5 is equipped with a piston at the top to push the filter cake into the collector vessel at the bottom. The coupling of an MSMPR crystallizer and a CFC was demonstrated in the study to obtain filtered paracetamol particles of an average moisture content

of 22%. A similar unit with the addition of drying abilities has also been developed by AWL and an initial study comparing to a batch bench-scale vacuum filtration unit has been carried out by Ottoboni et al. [147]. However, there is a lack of detailed study aimed to develop mechanistic understanding of operating parameters.

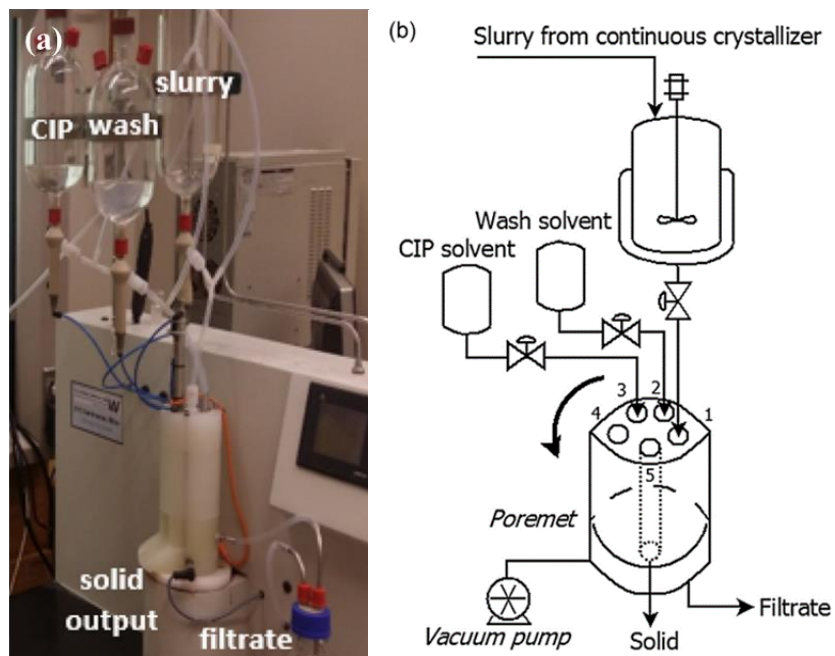


Figure 2-33 (a) A picture of CFC manufactured by AWL and (b) schematics of the CFC. Permission obtained from [15] Copyright © 2016 Elsevier B.V.



Figure 2-34 A continuous filtration drying unit developed by AWL. Permission obtained from [147] Copyright © 2019 American Pharmacists Association® Published by Elsevier Inc.

3. POPULATION BALANCE MODEL DEVELOPMENT, VERIFICATION AND VALIDATION OF CARBAMAZEPINE CRYSTALLIZATION IN A TRADITIONAL STIRRED TANK CRYSTALLIZER

3.1 Disclaimer

The results obtained to construct this chapter was obtained at DPQR/OPQ/CDER at the FDA Silver Spring campus (Maryland). The content in this chapter only reflects the views of the author and should not be construed represent the FDA's views or policies.

3.2 Introduction

Modern pharmaceutical development approaches emphasize product and process understanding. This understanding forms the foundation for quality-by-design (DbQ) methodology to identify the design space, the multidimensional combination of inputs and process parameters demonstrated to provide assurance of product quality [148]. Mathematical and knowledge-based modeling is a great tool to enhance the mechanistic understanding of different processes and potentially aid design space investigation. While process modeling has been adopted by other industries for decades, the adoption and implementation of process modeling in the pharmaceutical industry is in the early stages. Pharmaceutical processes are unique compared to other industries because it frequently requires solid and solid/liquid slurry handling at small throughputs with tight quality requirements. The use of modeling of such processes can be challenging. A typical example of such processes is crystallization.

To represent a crystallization process mathematically, the two main mechanisms, namely nucleation and growth, must be incorporated to quantify the changes in and between solid and solution states. Population balance modeling (PBM) does so by combining population balance

equation and mass balance equation to simulate both solid particle population and solution concentration. PBM can be developed by fitting simulated results such as solution concentration and solid PSD to experimental results to estimate kinetic parameters of predefined kinetic expressions [61], [62], [149]–[153]. Because of the pharmaceutical industry’s high requirement of product quality, it is crucial to identify model limitations and applicability based on the model risk. While many studies have been carried out to develop, optimize and control crystallization processes using PBM [67], [81], [91], [116], [125], [154], [155], there is a lack of studies in the current literature that discuss the applicability of the crystallization PBM in a systematic manner. In this work, a risk-based approach is taken to develop, verify and validate a PBM for the cooling crystallization of carbamazepine in ethanol, the kinetics of which, to the best of my knowledge, have yet to be studied in current literature.

As the industry move towards QbD, continuous processes have gained industry and regulatory attention for its steady-state, or more accurately state-of-control, operation and online monitoring capabilities [3], [10], [12], [14], [15], [18], [156]. PBM modeling is an especially useful tool for understanding continuous crystallization. In the current literature, continuous crystallization models are often developed by writing the PBM with added continuous terms while keeping the kinetic parameters the same as batch experiments [17], [156], [157], whereas in practice there might be deviations between continuous and batch kinetics depending on the operating conditions. An additional short discussion is carried out in this work on the applicability of the PBM developed with batch experiments on continuous processes for cooling crystallization of carbamazepine.

3.3 Material and Methods

3.3.1 Experimental material and crystallizer setup

Carbamazepine (CBZ, purity 99.8% form III, Ria International) and ethanol (anhydrous histological grade, Fisher Chemical) was chosen as the model system. CBZ has multiple well characterized polymorphic forms [158]–[160] amongst which, Form III, block-like shaped, is the most stable form at room temperature up to 78°C [161]. X-ray powder diffraction (XRD) and Raman (Kaiser Optical Systems, Inc.) as well as microscopic imaging confirmed all material and product of CBZ in this study were Form III. Experiments were performed in a 400mL jacketed glass vessel (EasyMax) featuring multiple ports capable of holding in-situ PAT tools. The temperature and stirring speed were controlled via an EasyMax 402 system (Mettler Toledo). The temperature was measured with a Pt100 resistant temperature detector. A Raman Rxn2 system from Kaiser Optical Systems, Inc. (785 nm, 150-3425 cm^{-1}) was used to measure solute concentration by applying a previously developed and validated calibration model [78]. A Focused Beam Reflectance Measurement (FBRM, Mettler Toledo G400) was used to monitor chord length distributions and particle counts. The volume-based PSD of the resulting CBZ crystals were characterized offline using laser diffraction (HELOS, Sympatec). CBZ Form III solubility in ethanol was measured in-house and fitted to a second order polynomial equation shown in Figure 3-1.

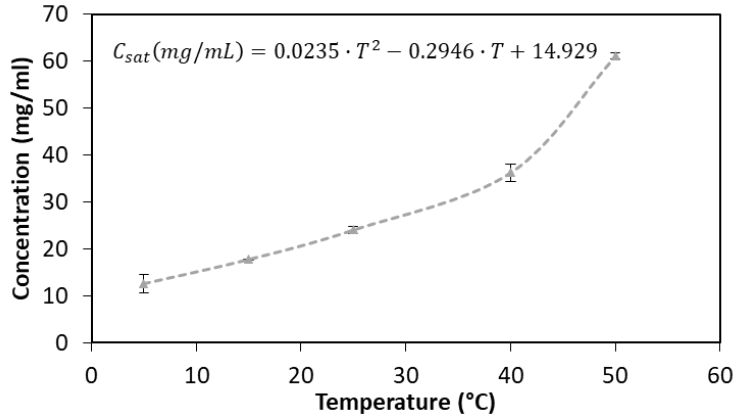


Figure 3-1 Solubility of Carbamazepine Form III in Ethanol and its fitted empirical equation determined in-house.

3.3.2 Kinetic expression

While the exact mechanisms are not understood, growth, nucleation and dissolution rates are generally formulated as supersaturation, temperature and size or magma density dependent semi-empirical expressions. They are not entirely empirical. Instead, they have some basis in crystallization theories and provide some mechanistic understanding of the process [28], [32], [33], [47]:

$$G = k_g (C - C_{sat})^g \text{Exp}\left(-\frac{E_g}{RT}\right) (1 + \alpha_g L)^{L_g} \quad (3.1)$$

$$B = k_s (C - C_{sat})^s \text{Exp}\left(-\frac{E_s}{RT}\right) M^{M_s} \quad (3.2)$$

$$D = k_d (C_{sat} - C)^d \text{Exp}\left(-\frac{E_d}{RT}\right) (1 + \alpha_d L)^{L_d} \quad (3.3)$$

where M (mg solid CBZ/mL EtOH) denotes solid concentration and k_g ($\mu\text{m} \cdot \text{min}^{-1} \cdot \text{mL}^g \cdot \text{mg}^{-g}$), g , α_g (μm^{-1}), L_g , E_g (J/mol), k_s ($\# \cdot \text{mL}^{-1} \cdot \text{min}^{-1} \cdot \text{mL}^{s+M_s} \cdot (\text{mg solution CBZ})^{-s} \cdot (\text{mg solid CBZ})^{-M_s}$), s , M_s , k_d ($\mu\text{m} \cdot \text{min}^{-1} \cdot \text{mL}^d \cdot \text{mg}^{-d}$), d , E_d (J/mol), α_d (μm^{-1}), L_d are kinetic parameters. These kinetic parameters are estimated by a least-square based optimization algorithm which tries to fit

concentration obtained described in section 2.5.4 and product volume-based PSD quantiles D10, D50 and D90 to experimental results. The PBM is solved numerically using a high-resolution finite volume (HRFV) method which is discussed in detail in the Appendix. Elimination of several kinetic parameters is possible which may improve or worsen the fitting of the model. The exercise of testing different formulations of the rate expressions is a form of ‘model discrimination’ practice [162], [163] which was carried out during the development of PBM in this study. Parameter estimation and confidence intervals (related to variable correlation) in each model discrimination exercise were performed with MATLAB function ‘*lsqnonlin*’ (trust-region-reflective algorithm) and ‘*paramci*’. The final selection of the rate expression formulation was based on the goodness of fit and the correlation between parameters.

3.3.3 Experimental methods for kinetic model development

Batch cooling crystallization of CBZ in ethanol were carried out to estimate the values of dissolution, growth and nucleation parameters. To simplify the estimation of parameters, experiments were designed in such a way that only one phenomenon occurs/dominates in each set of experiment [29], [164]. As a result, the correlation between kinetic parameters may be reduced or eliminated. For each phenomenon (growth, nucleation, and dissolution), 4 experiments were performed, all of which were carried out in the EasyMax system at 350 rpm and 350 mL batch volume. To study growth, cooling crystallization experiments were carried out at slow cooling rates and high seed loading to prevent nucleation. FBRM was utilized to monitor particle counts. Initial concentration (40 mg CBZ/mL EtOH), seeding temperature (35 °C), final temperature (20 °C) and seed loading (10 wt%) were unchanged among the set of four growth experiments. Seed size was varied between (1) 75-125 μm or (2) 125-212 μm and cooling rate (β) was varied between 0.05 °C/min or 0.1 °C/min. To conduct nucleation dominated experiments, faster cooling

rates were applied. Growth was minimal as confirmed by offline size measurement. Initial concentration (40 mg/mL), seeding temperature (35 °C), final temperature (15 °C) and seed size (125 – 212 μm) were fixed while seed loading was varied between 5 wt% or 10 wt% and cooling rate was varied between 0.5 °C/min or 0.35 °C/min. For dissolution, a set of four isothermal experiments were carried out at 15 °C, 20 °C, 25 °C and 35 °C. Sieved ‘seed’ crystals of size 75-125 μm were added into the pre-heated/cooled solvent at the beginning of the experiment at the amount corresponding to the solubility at that temperature. A summary of dissolution, growth and nucleation experiments is shown in Table 3-1.

Table 3-1 Experimental conditions of dissolution, growth and nucleation experiments.

Experiment	$C_{initial}$ (mg/mL)	$T_{initial}$ (°C)	T_{final} (°C)	β (°C/min)	Seed Loading	Seed Size (μm)
Growth1	40	35	20	0.05	1.6g (10%)	75-125
Growth2	40	35	20	0.05	1.6g (10%)	125-212
Growth3	40	35	20	0.1	1.6g (10%)	75-125
Growth4	40	35	20	0.1	1.6g (10%)	125-212
Nucleation1	40	35	10	0.35	0.8g (5%)	125-212
Nucleation2	40	35	10	0.35	1.6g (10%)	125-212
Nucleation3	40	35	10	0.5	0.8g (5%)	125-212
Nucleation4	40	35	10	0.5	1.6g (10%)	125-212
Dissolution1	0	15	15	0	6.4g	75-125
Dissolution2	0	20	20	0	7.6g	75-125
Dissolution3	0	25	25	0	9.2g	75-125
Dissolution4	0	35	35	0	14g	75-125

While nucleation may be suppressed by cooling slowly, growth of crystals in supersaturated solution is inevitable in supersaturated conditions, thus growth rate must also be considered during parameter estimation for the set of nucleation experiments. The strategy is to first obtain growth parameters and use them to aid the parameter estimation for nucleation. Then during nucleation parameter estimation, growth parameters were allowed to refit along with

nucleation parameters to nucleation experimental data because in retrospect, some nucleation could have taken place and gone undetected by the FBRM; growth kinetics obtained from growth experiments should still be close to their true values and thus can serve as an initial guess during the nucleation parameter estimation and its range was restricted to $\pm 20\%$ to minimize the search space during optimization. Dissolution phenomenon is completely isolated since the solution was not supersaturated at any point in dissolution experiments.

3.3.4 Model verification and validation

The PBM was developed to simulate carbamazepine crystallization. The context of use (COU) for the model is to enhance the mechanistic understanding of the batch and continuous crystallization of CBZ. The PBM is being used to support process development and can be classified as low impact. There are limitations and assumptions associated with any given computational model that must be understood to assess whether the model is fit for use. To assess the credibility of the developed PBM for the specific COU, a series model verification and validation (V&V) activities were conducted using a risk-based framework [165], the overview of which is illustrated in Figure 3-2. The rigor of each activity is dependent on the models COU and example levels (level a \rightarrow d with increasing credibility goal) of detailed V&V activities are given in the referenced guide published by American society of Mechanical Engineers (ASME) [165]. The verification and validation activities conducted as part of this study are summarized in Table 3-3; All model verification activities as well as governing equation model input uncertainty validation activities are evaluated with a hypothetical cooling batch experiment: seeded CBZ crystallization at 8% seed loading with 75-125 μm size operated at 0.4 $^{\circ}\text{C}/\text{min}$ cooling rate from 35 $^{\circ}\text{C}$ to 20 $^{\circ}\text{C}$. If the COU of the model changes, additional V&V activities may need to be performed to establish the credibility of the model for its expanded role.

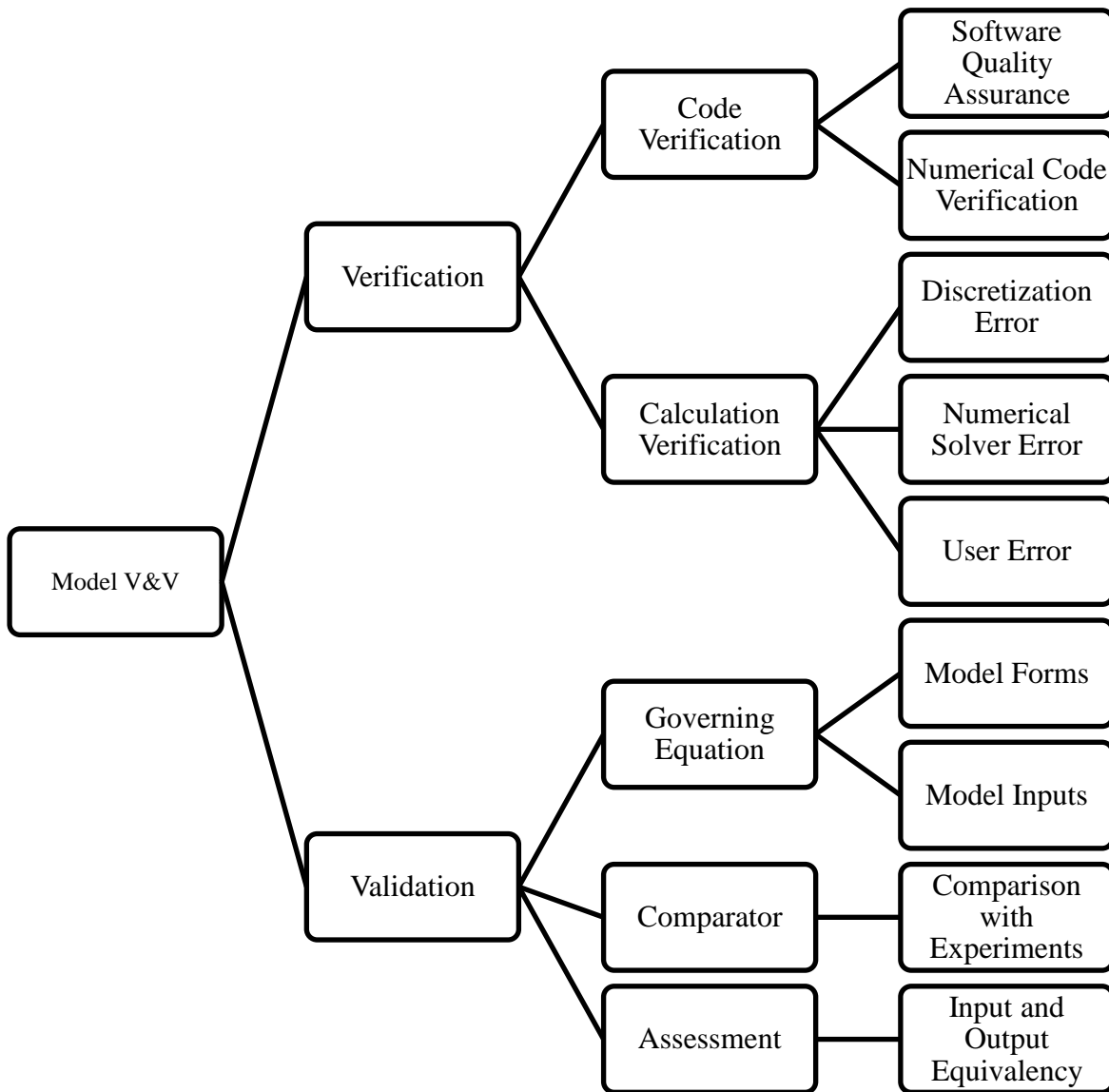


Figure 3-2 A short overview of risk-based model V&V activity structure according to AMSE V&V 40 standard [165].

Table 3-2 Detailed model verification and validation activities entailed in this study and rationale of the level of rigor selected for each activity according to ASME V&V40 [165].

Detailed Activity	ASME V&V 40 Example Activity Level and Rationale
Model verification → code verification	
Little to no SQA or NCV performed.	Low-level (a level) rigor is selected: MATLAB software is widely accepted as reliable and consistent. Thus, SQA was not carried out. The HRFV solution method of crystallization PBM has been shown in past literature to have second order accuracy. Discontinuities in input and solution are not expected.
Model verification → calculation verification	
<i>Discretization error:</i> size discretization of 50, 60, 70, 90, and 100 tested to observe convergence.	Mid-level (b level) rigor is practiced: discretization convergence analysis without error estimation. The coarsest discretization, at which further discretization does not increase accuracy, should be selected. Discretization in time is not examined because the ode solver determines the step size in time in each time step.
<i>Numerical solver error:</i> ‘ode45’ solver parameter settings changed around their default values as well as two other MATLAB ode solvers were tested.	High-level (c level) credibility is achieved by accessing the convergence of solution when the solver parameter settings were changed and when the solution method (solver choice) was changed for a crystallization experiment in silico.
<i>User error:</i> Verification of key inputs by author and colleague	Mid-to-high level (c level) rigor of exercise is carried out: key inputs are verified by the practitioner and an internal peer.
Model validation → computational model	
<i>Model form:</i> Model discrimination carried out to examine different kinetic expressions.	Mid-level (b level) exercise is carried out to observe the influence of key model form by comparing it to other possible forms.
<i>Model inputs:</i> Uncertainty and sensitivity analysis performed for key inputs (kinetic parameters).	Mid-level (b level) practice is performed to examine the model sensitivity to its inputs (kinetic parameters) and the uncertainties of the inputs which are calculated using MATLAB’s ‘paramci’.
Model validation → comparator	
Four additional batch crystallization experiments (Table 3-3) performed to compare with simulated concentration and product quantile results.	Mid-level (b-c level) of credibility is achieved by comparing experimental results to simulation results. The experimental conditions were different than those for model development but in the same range.

Table 3-2 continued

Model validation → assessment

Little to no input and output parameters equivalency activity performed. Low-level (a level) of rigor is practiced because the input and output parameters are straight forward. Concentration measurement was validated in previous work. PSD measurement was carried out in well-established equipment and procedure (however not yet experimentally validated).

Table 3-3 External batch validation experimental conditions.

Experiment	$C_{initial}$ (mg/mL)	$T_{initial}$ (°C)	T_{final} (°C)	β (°C/min)	Seed Loading	Seed Size (μm)
Val1	40	35	10	0.2	1.28 (8%)	125-212
Val2	40	35	10	0.4	0.96 (6%)	125-212
Val3	40	35	10	0.2	1.6 (10%)	125-212
Val4	40	35	10*	0.2*	1.6 (10%)	75-212

*In Val4, the crystallizer was first cooled from 35°C to 10°C at 0.2°C/min followed by a rapid heating step from 10°C to 45°C at 1°C/min.

3.3.5 Continuous crystallization

The verified and validated batch model was then used to simulate two continuous crystallization experiments, one in a single stage MSMPR system and the other in a two-stage MSMPR system. Both continuous crystallization experiments were cooling crystallization of CBZ where both feed and product removal were operated continuously with peristaltic pumps. The detailed experimental conditions are listed in Table 3-4. In the single stage experiment, 350mL of saturated solution was preloaded with 10% seed loading in the crystallizer at 20 °C as the start-up condition. The continuous operation started about 1 minute after the seed was loaded to achieve uniform suspension. The two-stage continuous experiments featured the same start up procedure in the first stage, but the second stage started empty. The slurry transfer between stage 1 and 2 started at the same time as the feed into stage 1 started while the product removal of stage 2 started after the volume of stage 2 reached 350mL. The level was maintained via a previously developed level control system [23]. In the two-stage continuous crystallization experiments, a disturbance of stepwise increase and decrease in temperature was applied in the second stage.

Table 3-4 Single stage and two-stage continuous crystallization experimental conditions.

Exp	C_{feed} (mg/mL)	seed loading	T (°C)	Volume (mL)	τ (min)
SingleStage	39	10%	20	350	20
TwoStage	40	10%	20*	350	40, 20 of each stage

*A stepwise up and then down disturbance in temperature was applied to the second stage.

3.4 Results and Discussion

3.4.1 Kinetic model discrimination and parameter estimation

Model discrimination can help identify a superior kinetic expression for parameter estimation. Growth kinetics was estimated using slow cooling experiments listed in Table 3-1 where nucleation was assumed to be absent. One example experimental profile (Growth1) is shown in Figure 3-3 where the particle count (red solid line) did not increase and square weighted mean chord length (SWMCL, green dashed line) increased indicating a likely growth dominated process. The following 5 growth models (GMs) were the main growth models tested in the following order with the previous fitted results serving as the initial guess for the following model:

$$GM1 = k_g (C - C_{sat}) \quad (3.4)$$

$$GM2 = k_g (C - C_{sat})^g \quad (3.5)$$

$$GM3 = k_g (C - C_{sat})^g \text{Exp}\left(-\frac{E_g}{RT}\right) \quad (3.6)$$

$$GM4 = k_g (C - C_{sat})^g \text{Exp}\left(-\frac{E_g}{RT}\right)(1 + \alpha_g L) \quad (3.7)$$

$$GM5 = k_g (C - C_{sat})^g \text{Exp}\left(-\frac{E_g}{RT}\right)(1 + \alpha_g L)^{L^g} \quad (3.8)$$

Each model was fitted using ‘*lsqnonlin*’ in MATLAB by minimizing the sum of square residuals of simulated concentration as well as final product quantiles to experimental data obtained in the growth experiments:

$$j = \sum_{i=1}^{100} (C_{\text{exp},i} - C_{\text{sim},i})^2 + w_D \cdot \sum_k^{10,50,90} (D_{\text{exp},k} - D_{\text{sim},k})^2 \quad (3.9)$$

where j denotes the objective function value, $C_{\text{exp},i}$, $C_{\text{sim},i}$ represents the experimental and simulated concentration at i th time step, respectively, w_D is some weight given to product quantile comparisons and $D_{\text{exp},k}$, $D_{\text{sim},k}$ represents the experimental and simulated product size at k th quantile where $k = 10, 50$ or 90 , respectively. If concentration data was not measured exactly at the i th time step, linear interpolation was applied. Higher weight was given to D50 than D10 or D90. In addition to the residual of the fit, the correlation matrix was also calculated based on the Jacobian to ensure little to no correlation was present amongst the parameters. If correlated parameters were present, for example if parameter g is highly correlated with k_g and E_g , a new ‘*lsqnonlin*’ optimization would be run with g fixed at either the previously fitted value or another value that makes physical sense based on past experience. For a highly nonlinear system like a crystallization PBM, it is extremely difficult to prove global optimality. However, efforts were put in during this study by perturbing and drastically changing the initial guesses while repeating ‘*lsqnonlin*’ optimizations for a more stable ‘optimal’ solution. The mean square error (MSE) of concentration and product quantiles are compared in Table 3-5: GM5 was chosen to be the best growth rate formulation because it fitted well to experimental data and no correlations between parameters were observed. GM5 considers the effect of supersaturation and temperature on first order size dependent growth rate. Simulated and experimental results of growth experiments are shown in Figure 3-4 and Table 3-6. The MSE of GM5 fitted concentration is 5.73 (mg/mL)^2 which corresponds to 8.0% relative error. The MSEs of D10, D50 and D90 are $5319 \text{ }\mu\text{m}^2$, $349.7 \text{ }\mu\text{m}^2$, and $3448 \text{ }\mu\text{m}^2$ which correspond to 71%, 11%, and 24% relative error respectively. D50 is much better represented by the model than D10 and D90 which is to be expected because D10 and D90 were given much less weight than D50 in the objective function. The errors associated with the

measurement of D10 and D90 are known to be much higher than D50 by laser diffraction type of PSD measurement such as HELOS.

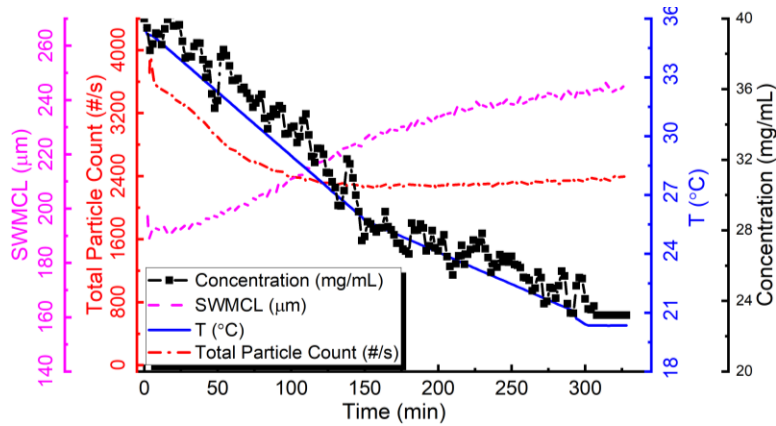
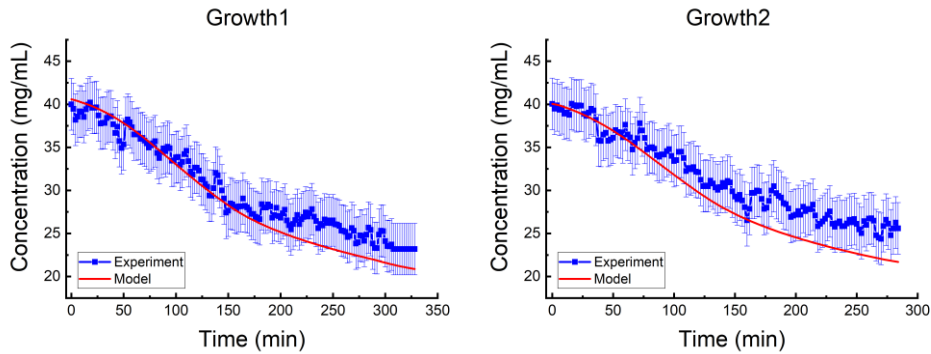


Figure 3-3 Operating profile of slow cooling growth experiment ‘Growth1’.

Table 3-5 Comparison of the mean square error (MSE) in concentration and PSD quantiles of five growth models.

	Conc MSE (mg^2/mL^2)	Quantile MSE (μm^2)
GM1	13.6	7246.1
GM2	5.32	7309.7
GM3	6.45	7291.7
GM4	8.44	3039.0
GM5	5.73	2363.2



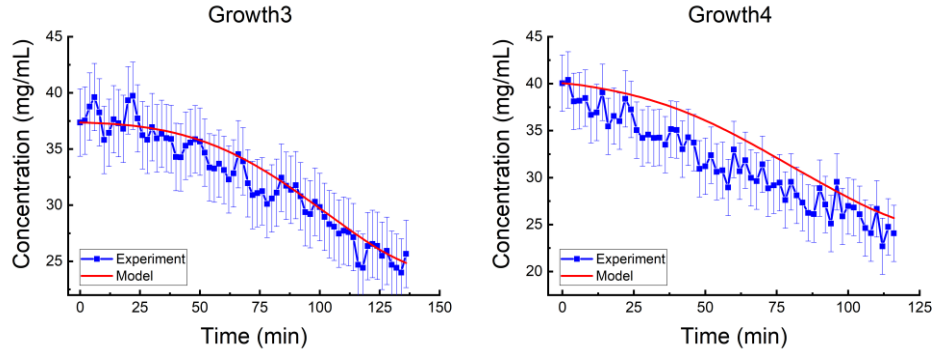


Figure 3-4 Fitted concentration result of GM5 compared to experimental concentration results of growth experiments 1-4.

Table 3-6 Simulated product PSD quantiles of GM5 compared to experimental results of growth experiments 1-4.

	D10 (μm)		D50 (μm)		D90 (μm)	
	Exp	Model	Exp	Model	Exp	Model
Growth1	75.52	25.84	132.5	119.0	183.3	232.9
Growth2	112.8	32.91	212.3	222.3	287.8	348.3
Growth3	89.87	69.52	144.2	121.3	197.5	225.9
Growth4	122.4	32.04	195.7	219.9	258.8	341.7

Secondary nucleation kinetics was estimated using fast cooling crystallization experiments described in Table 3-1. An example operating profile of exp ‘Nucleation4’ is plotted in Figure 3-5 where total particle count increased significantly indicating nucleation while SWMCL also increased suggesting that growth was also present. Therefore, both nucleation and growth must be considered. Growth kinetics had already been determined which can be used directly in secondary nucleation parameter estimation. However, it can improve the model without much burden on the optimizer to allow growth parameters to refit in a small range ($\pm 20\%$ of its originally fitted values) along with nucleation parameter estimation. While GM5 is fixed, nucleation kinetic expressions (BM) were varied for model discrimination:

$$\text{BM1} = k_s (C - C_{sat}) \quad (3.10)$$

$$\text{BM2} = k_s (C - C_{sat})^s \quad (3.11)$$

$$\text{BM3} = k_s (C - C_{sat})^s \text{Exp}\left(-\frac{E_s}{RT}\right) \quad (3.12)$$

$$\text{BM4} = k_s (C - C_{sat})^s \text{Exp}\left(-\frac{E_s}{RT}\right) M^{M_s} \quad (3.13)$$

$$\text{BM5} = k_s (C - C_{sat}) \text{Exp}\left(-\frac{E_s}{RT}\right) M^2 \quad (3.14)$$

BM1-3 formulations are also commonly used to describe primary nucleation while BM4-5 are exclusive secondary nucleation rate expressions where the solid effect is taken into consideration. BM5 is a variation of BM4 where s and M_s were fixed to be 1 and 2 respectively because the correlation matrix of BM4 fitted parameters showed high correlation between s , M_s , k_s and E_s . Different initial guesses were tested to obtain a more stable solution for each of the rate expression. In addition, different combinations of GM's and BM's were also tested but other GMs significantly underperformed compared to the combinations of GM5 with various BMs. The MSE of concentration and product size quantiles of GM5 combined with various BM's are shown in Table 3-7. BM5 outperformed other nucleation models with little to no correlations amongst the parameters. The comparison between simulated concentration based on GM5-BM5 and experimental results is shown in Figure 3-6 and the comparison of product size quantiles is shown in Table 3-8. The concentration MSE is 6.49 (mg/mL)^2 or relative error of 9.1%. The MSE of D10, D50 and D90 are $14589 \text{ }\mu\text{m}^2$, $171.8 \text{ }\mu\text{m}^2$, and $5793 \text{ }\mu\text{m}^2$ which corresponds to the relative errors of 85%, 4.1%, and 24% respectively. Similar to growth parameter estimation results, the errors of D10 and D90 are much larger than that of D50 because they were not given much weight in the objective function.

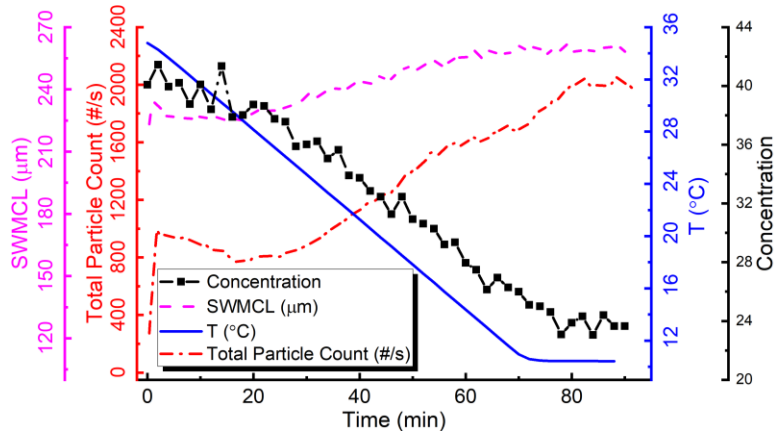
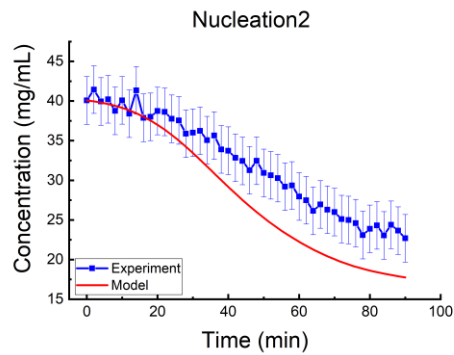
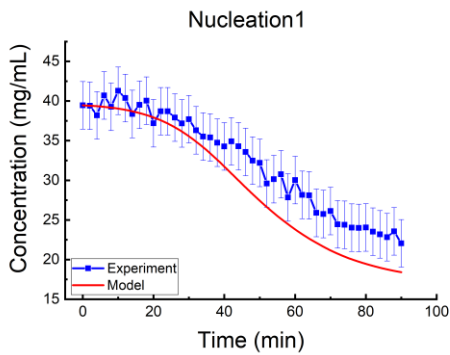


Figure 3-5 Operating profile of a fast cooling experiment ‘Nucleation4’.

Table 3-7 Comparison of the MSE in concentration and product PSD quantiles of the five nucleation models.

	Conc MSE (mg^2/mL^2)	Quantile MSE (μm^2)
BM1	53.7	51338
BM2	35.6	50382
BM3	8.44	6852.6
BM4	8.28	6854.4
BM5	6.49	6528.8



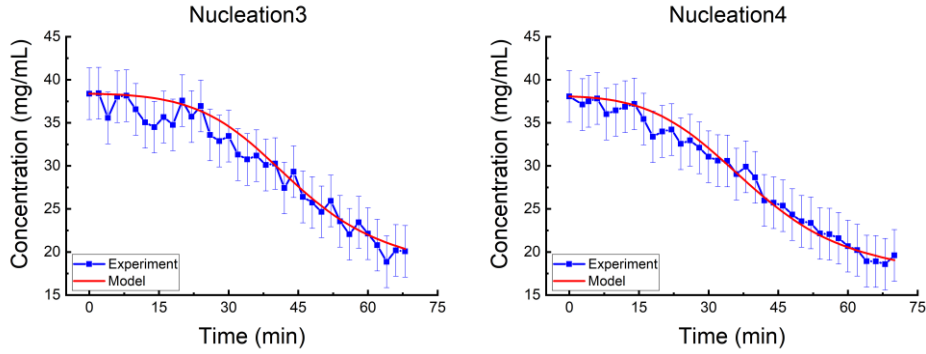


Figure 3-6 Fitted concentration results of GM5-BM5 compared to experimental concentration results of nucleation experiments 1-4.

Table 3-8 Simulated product PSD quantiles of BM5 compared to experimental results of nucleation experiments 1-4.

	D10 (μm)		D50 (μm)		D90 (μm)	
	Exp	Model	Exp	Model	Exp	Model
Nucleation1	129.8	22.19	229.9	228.1	301.4	400.1
Nucleation 2	141.2	17.42	227.5	214.2	291.1	347.7
Nucleation 3	143.2	25.81	236.8	236.0	301.4	394.8
Nucleation 4	153.2	20.25	241.6	219.1	306.2	344.9

Dissolution kinetics were estimated with concentration data of isothermal dissolution experiments listed in Table 3-1 along with a model discrimination exercise. The concentration, temperature and particle count profiles of the experiment ‘Dissolution1’ are plotted in Figure 3-7. The three dissolution kinetic models are as follows:

$$\text{DM1} = k_d (C_{sat} - C)^d \quad (3.15)$$

$$\text{DM2} = k_d (C_{sat} - C)^d \text{Exp}\left(-\frac{E_d}{RT}\right) \quad (3.16)$$

$$\text{DM3} = k_d (C_{sat} - C)^d \text{Exp}\left(-\frac{E_d}{RT}\right) (1 + \alpha_d L)^{L_d} \quad (3.17)$$

The three models fitted similarly as shown in Table 3-9 with DM1 slightly outperforming DM2 and DM3. Therefore, DM1, the simplest formulation of dissolution kinetics was selected. Fitted

concentration data of the four experiments are plotted in Figure 3-8. The concentration MSE of DM1 is 20.78 (mg/mL)^2 which corresponds to 10.6% relative error.

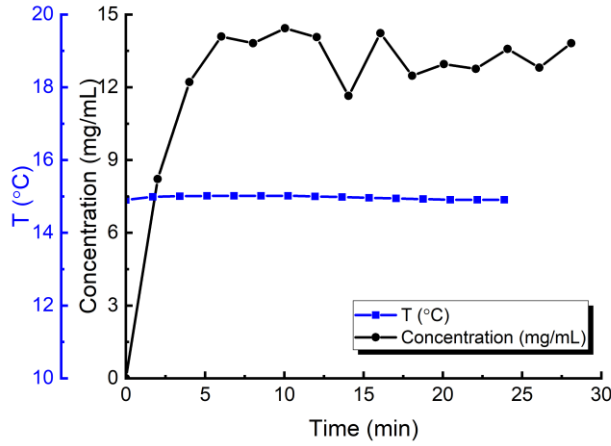
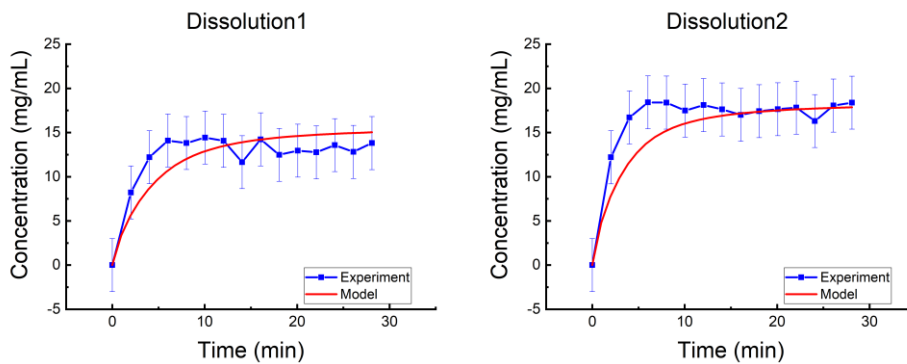


Figure 3-7 Operating profile of an isothermal dissolution experiment ‘Dissolution1’.

Table 3-9 Comparison of the MSE in concentration and product PSD quantiles of the three dissolution models.

Model	Conc MSE (mg^2/mL^2)
DM1	20.78
DM2	21.35
DM3	21.22



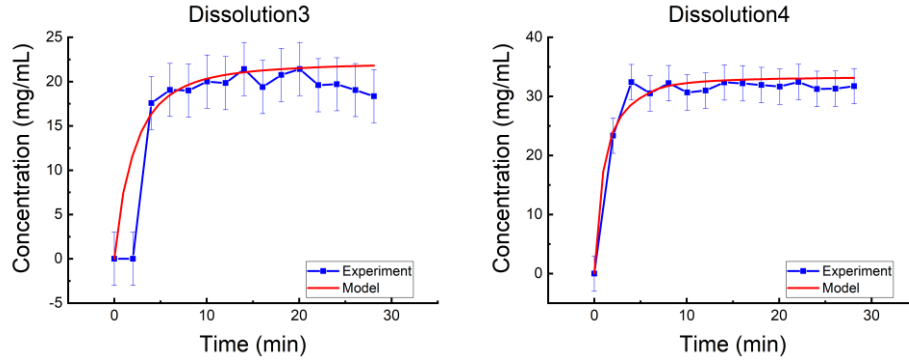


Figure 3-8 Fitted result of DM1 compared to experimental concentration data.

In summary, GM5, BM5 and DM1 were selected so that the PBM becomes Eq(3.18) when supersaturated and Eq(3.19) when undersaturated. Estimated kinetic parameter values and their 95% confidence interval (CI) are listed in Table 3-10. The confidence interval of each parameter is of a reasonable range as a result of correlation matrix examination during parameter estimation to eliminate correlated parameters eliminating extremely wide confidence intervals.

$$\left\{ \begin{array}{l} \frac{\partial f}{\partial t} + \frac{\partial(Gf)}{\partial L} = B\delta(L - L_0); \quad \frac{dC}{dt} = -3k_v\rho_c \int_{L_0}^{\infty} GL^2 fdL \\ \text{where } G = k_g (C - C_{sat})^g \text{Exp}\left(-\frac{E_g}{RT}\right)(1 + \alpha_g L)^{L_g} \\ \text{and } B = k_s (C - C_{sat}) \text{Exp}\left(-\frac{E_s}{RT}\right)M^2 \end{array} \right. \quad (3.18)$$

$$\left\{ \begin{array}{l} \frac{\partial f}{\partial t} + \frac{\partial(Df)}{\partial L} = 0; \quad \frac{dC}{dt} = -3k_v\rho_c \int_{L_0}^{\infty} DL^2 fdL \\ \text{where } D = k_s (C_{sat} - C)^d \text{Exp}\left(-\frac{E_d}{RT}\right) \end{array} \right. \quad (3.19)$$

Table 3-10 Estimated PBM kinetic parameter values and their 95% confidence interval.

Param.	Unit	Value	95%CI-	95%CI+
k_g	$[\mu\text{m}\cdot\text{min}^{-1}\cdot\text{mL}^g\cdot\text{mg}^{-g}]$	0.15695	0.15676	0.15713
g	[-]	2.17415	2.17372	2.17458
E_g	[kJ/mol]	10.3325	10.3305	10.3345

Param.	Unit	Value	95%CI-	95%CI+
α_g	$[\mu\text{m}^{-1}]$	0.01168	0.01153	0.01182
L_g	[-]	1.17650	1.17619	1.17681
k_s	$[\#\cdot\text{mL}^{-1}\cdot\text{min}^{-1}\cdot\text{mL}^{s+M_s}\cdot\Delta C^{-s}\cdot\text{M}^{-M_s}]$	1.0002×10^6	0.99997×10^6	1.0003×10^6
E_s	[kJ/mol]	26.572	26.566	26.578
k_a	$[\mu\text{m}\cdot\text{min}^{-1}\cdot\text{mL}^d\cdot\text{mg}^{-d}]$	-0.04414	-0.04414	-0.04414
d	[-]	1.79373	1.79373	1.79374

3.4.2 Model verification

Size discretization was studied to identify discretization errors as the first model verification activity. Size discretization examination is an important yet often neglected step during model development. The finer the grids, the more accurate the solution will be while finer discretization increases computational cost, in some cases so much so that the simulation time becomes unrealistic. Therefore, it is crucial to find a fine enough discretization such that increasing discretization no longer changes the solution significantly which is how the number of discretization was determined in this study: the same ‘in-silico’ experiment described in section 3.3.4 was simulated at 50 to 100 discretization with an increase of 10 between each simulation. Finer discretization was not considered because of the experimental limitation that the offline size measurement HELOS only gives 32 size discretization bins. Changes in simulated dynamic concentration and size quantiles solutions were quantified by the maximum relative difference at each time step:

$$C_{\text{RelDiff,max}} = \text{MAX}\left(\frac{|C_{p,i} - C_{st,i}|}{C_{st}}\right) \quad (3.20)$$

$$D10_{\text{RelDiff,max}} = \text{MAX}\left(\frac{|D10_{p,i} - D10_{st,i}|}{D10_{st}}\right) \quad (3.21)$$

$$D50_{RelDiff,max} = MAX\left(\frac{|D50_{p,i} - D50_{st,i}|}{D50_{st}}\right) \quad (3.22)$$

$$D90_{RelDiff,max} = MAX\left(\frac{|D90_{p,i} - D90_{st,i}|}{D90_{st}}\right) \quad (3.23)$$

where subscript ‘*RelDiff,max*’ denotes the maximum relative difference of all time steps and subscripts ‘*p,i*’ and ‘*st,i*’ represent the simulated data of perturbed settings (in this activity, 50, 60, 70, 90, 100 discretization bins) or standard/default settings (in this activity, 80 discretization bins) at *i*th time step respectively. The experimental relative errors of the D10, D60 and D90 measurements are conservatively taken to be 15%, 10%, and 15% respectively. The results are shown in Table 3-11 where simulated concentration, D10, D50 and D90 do not vary significantly compared to experimental errors at 80, 90 and 100 discretization however, coarser grids result in significant variations especially for D10. Therefore, discretization of 80 was the optimal choice because increasing discretization did not change the solution significantly anymore compared to experimental error.

Table 3-11 Maximum relative difference in dynamic concentration and PSD quantiles with various size discretization.

	# of Discre.	C_{RelDiff,max}	D10_{RelDiff,max}	D50_{RelDiff,max}	D90_{RelDiff,max}
Sim0	80	-	-	-	-
Sim1	100	0.62%	11.9%	2.37%	0.62%
Sim2	90	0.43%	6.31%	1.84%	0.38%
Sim3	70	1.04%	21.0%	5.47%	1.12%
Sim4	60	1.74%	34.3%	8.50%	1.91%
Sim5	50	1.73%	30.8%	6.50%	2.05%

To identify numerical solver errors, the ODE solver parameters were changed. The ODE parameter settings studied were relative tolerance (default value 1×10^{-5}), absolute tolerance (default value 1×10^{-6}), and maximum step size (default $0.1 \times |t_{final} - t_{initial}|$). Six simulation exercises were carried out with each parameter perturbed one at a time as shown in Table 3-12. The maximum relative differences of simulated concentration and size quantiles between perturbed simulations (Sim1-6) and the default simulation (Sim0) are extremely small. Therefore, the parameter settings presented negligible to no error to the numerical solution of the PBM.

Table 3-12 Maximum relative changes in concentration and size quantiles with varying ‘ode45’ parameter settings in MATLAB.

	ODE Parameter Setting			Maximum Relative Difference			
	TolRel	TolAbs	Max Step	C	D10	D50	D90
Sim0	1×10^{-5}	1×10^{-6}	1.5	-	-	-	-
Sim1	1×10^{-6}	1×10^{-6}	1.5	<< 0.01%	<< 0.01%	<< 0.01%	<< 0.01%
Sim2	1×10^{-4}	1×10^{-6}	1.5	<< 0.01%	<< 0.01%	<< 0.01%	<< 0.01%
Sim3	1×10^{-5}	1×10^{-7}	1.5	<< 0.01%	<< 0.01%	<< 0.01%	<< 0.01%
Sim4	1×10^{-5}	1×10^{-5}	1.5	<< 0.01%	<< 0.01%	<< 0.01%	<< 0.01%
Sim5	1×10^{-5}	1×10^{-6}	0.15	<< 0.01%	<< 0.01%	<< 0.01%	<< 0.01%
Sim6	1×10^{-5}	1×10^{-6}	15	<< 0.01%	<< 0.01%	<< 0.01%	<< 0.01%

Different choices of ODE solvers were also explored as a model verification activity. There are a number of ODE solvers specializing in solving different types of systems (stiff vs nonstiff) featuring different levels of accuracy and efficiency. ‘ode45’ specializes in solving nonstiff problems at medium accuracy and should be the first solver to try as recommended by MATLAB software. Two other solvers tested in this study are: ‘ode113’ and ‘ode15s’. ‘ode113’ specializes in solving nonstiff problems at low to high accuracy and ‘ode15s’ can solve stiff problems with low to medium accuracy. A detailed description of MATLAB ode solvers can be found in the work by Shampine & Reichelt (1997) [166] and a summarized guide to choose an ODE solver can be

found in MATLAB helpfiles. Settings of each ODE were kept as default values. The maximum relative difference of concentration and size quantiles are listed in Table 3-13. The differences in solutions caused by different ODE solver choices were very small. By studying the sensitivity of solution to ODE solver settings and choices of ODE solver, numerical solver errors were identified and confirmed to be minimal and negligible compared to experimental errors.

Table 3-13 Maximum relative changes in concentration and size quantiles with different ODE solvers in MATLAB.

	Solver	C_{RelDiff,max}	D10_{RelDiff,max}	D50_{RelDiff,max}	D90_{RelDiff,max}
Sim0	ode45	-	-	-	-
Sim1	ode15s	< 0.01%	1.21%	< 0.01%	0.02%
Sim2	ode113	0.01%	1.66%	0.01%	0.04%

3.4.3 Model validation

An uncertainty study of model output to kinetic parameter values was carried out as a part of governing equation validation. 100 sets of kinetic parameters were randomly selected in their 95% confidence interval space. This random sampling technique is commonly known as the Monte-Carlo method. The in-silico batch experiment described in section 3.3.4 was simulated for every sample set of kinetic parameters. The final concentration, and final product size quantiles were simulated. The mean, standard deviation and coefficient of variation (C.V., the ratio of standard deviation to mean) are shown in Table 3-14. The uncertainty in concentration and product size quantiles caused by uncertainties in estimated kinetic parameters is minimal and neglectable compared to experimental errors.

Table 3-14 The mean, standard deviation and coefficient of variation of the final concentration and PSD quantiles in the kinetic parameter sensitivity study.

C(mg/mL)	D10(μm)	D50(μm)	D90(μm)
-----------------	----------------	----------------	----------------

μ	28.09	18.81	117.9	221.4
σ	0.021	0.019	0.404	0.370
CV	0.07%	0.10%	0.34%	0.17%

The four validation experiments listed in Table 3-3 were carried out as model validation comparators. The comparison of predicted and experimental concentration is plotted in Figure 3-9 where simulated concentration followed the experimental trend with some underprediction. The MSE for concentration predictions in experiment 1-3 are 17.9 (mg/mL)², 8.34(mg/mL)², and 2.70 (mg/mL)² which correspond to 13.8%, 8.2%, and 2.70% relative errors. In validation experiment 4, simulated concentration followed the general decrease followed by increase trend but underpredicted towards the end of the cooling cycle and during dissolution. The MSE is 37.2 (mg/mL)² or 18.4% relative error. The lack of fit during dissolution may be caused by the design of dissolution parameter estimation experiments during which sieved seeds were used whereas in validation experiments, crystallization products were dissolved directly after crystallization. In addition, validation 4 dissolution was induced by a fast heating ramp while dissolution model development experiments were isothermal. The simulated PSD quantiles and the relative errors are listed in Table 3-15. D50 as the most heavily weighted parameter in the estimation objective function was well predicted in experiment 1 and 2 where the error is less than 15% but significantly overpredicted in experiment 3. This is likely due to the seed size being unseen by the model during development. Nucleation kinetics are highly sensitive to seeding conditions and consequently, it is commonly observed that the kinetic parameters would change drastically for different seeding strategies which in turn causes size prediction to underperform using the same kinetics for different seeding strategies [28], [32], [33], [87], [167], [168]. Nucleation kinetics are generally expected to be difficult to estimate because of its stochastic nature but they significantly influence product PSD. In addition, there are a few sources of errors associated with offline PSD measurements that may

contribute to the discrepancy between model prediction and validation experiments including inevitable inconsistency of sampling, handling, filtration and drying procedures, as well as instrument error. Volume based laser diffraction PSD measurement techniques has been criticized for its lack of accuracy [169]–[173]. Perhaps less obviously, there are also numerical errors when converting volume-based PSD to number-based population distribution (and back) when solving the PBM. Therefore, it is reasonable to conclude that the model is validated only for experiments that use 125-212 μm seeds at low to medium risk. Application of the model to predict product size that do not apply the same seeding strategies as training experiments requires further investigation.

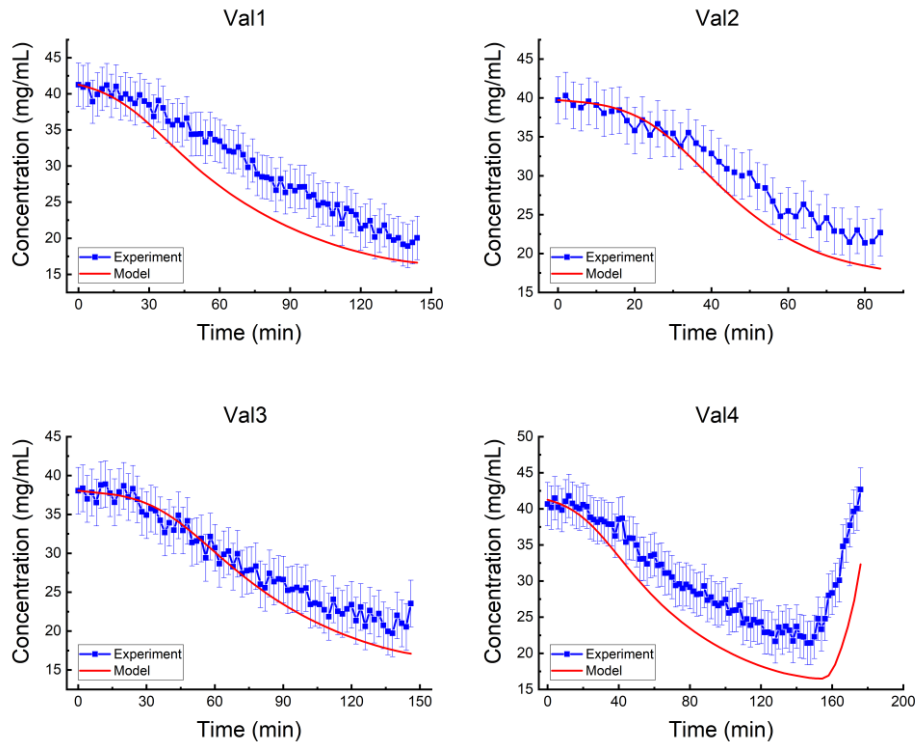


Figure 3-9 Comparison of experimental and simulated dynamic concentration of batch validation experiments.

Table 3-15 Simulated product PSD quantiles compared to validation experimental results.

D10(μm)			D50(μm)			D90(μm)		
Exp	Model	Rel Err	Exp	Model	Rel Err	Exp	Model	Rel Err

Val1	80.07	14.86	81.44%	284.3	248.2	12.70%	373.9	405.1	8.34%
Val2	124.5	21.58	82.67%	254.6	224.9	11.67%	341.0	384.1	12.64%
Val3	95.34	15.69	83.54%	159.4	203.9	27.92%	227.2	339.7	49.52%

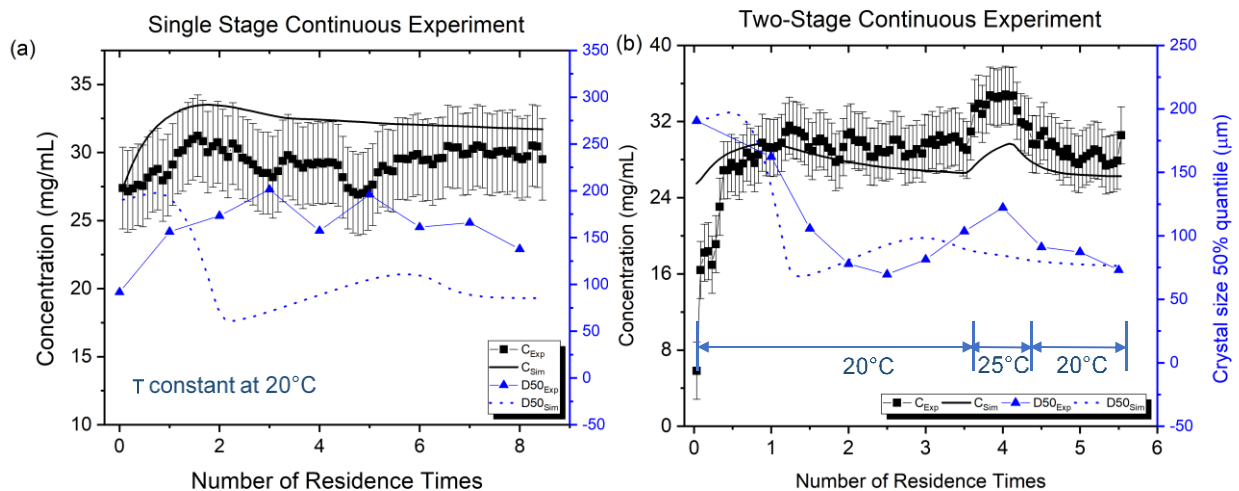
3.4.4 Discussion of model on continuous crystallization

In continuous crystallization, if the crystallizer dimension, hydrodynamics and solid concentration are similar to that of batch operations, the batch-validated model may transfer to continuous crystallization. To test this, two continuous experiments were carried out in a single stage and two-stage MSMPR system as shown in Table 3-4. The two continuous experiments dynamic concentration and D50 results were compared to simulated values using batch kinetics in Figure 3-10. In the single stage experiment shown in Figure 3-10a, the model slightly overpredicted concentration while underpredicted particle size (D50). The MSEs of concentration and D50 were 9.44 (mg/mL)^2 and $5875 \text{ }\mu\text{m}^2$ or mean relative errors of 9.94% and 39.2%. Growth rates were likely underpredicted by the model, which is to be expected because during parameter estimation, slow cooling batch experiments were carried out where supersaturation level was low (less than 7 mg/mL of absolute supersaturation) while in the single stage continuous experiment, supersaturation level was higher (~11 mg/mL). In the two-stage experiment on the other hand, both the concentration and particle D50 of the second stage were better predicted (Figure 3-10b) than the single stage experiment: the MSEs are 7.73 (mg/mL)^2 and $461.8 \text{ }\mu\text{m}^2$ or relative errors of 7.80% and 18.0% respectively. The supersaturation in the second stage (~9mg/mL) was lower compared to the single stage experiment as the first stage had consumed some supersaturation and the second stage supersaturation was closer to those of batch experiments. The concentration and

particle size in the first stage were not monitored during experiments because they are essentially repetitive information as the single stage experiment.

Figure 3-10 Comparison of experimental and simulated dynamic concentration, and D50 of (a) Single Stage and (b) Two-stage continuous crystallization experiments.

The number of particles in the crystallizer is another crucial process parameter to monitor. FBRM can be used for qualitative particle count analysis in experiments. It is important to note that FBRM measurement is not a quantitative indication of the actual number of particles in the crystallizer, nor is it a reliable indicator when comparing across different experiments to infer, for example, which experiments contained more particles. Depending on the equipment setup, the FBRM may give different readings of identical slurries if the FBRM has been moved. However, the trend of FBRM count measurement within one experiment gives important information about the changes in particle count over time. The FBRM measurement trend was compared to simulated particle counts which were obtained by calculating the zeroth moment (μ_0) of the population distribution f in Figure 3-11a&b.



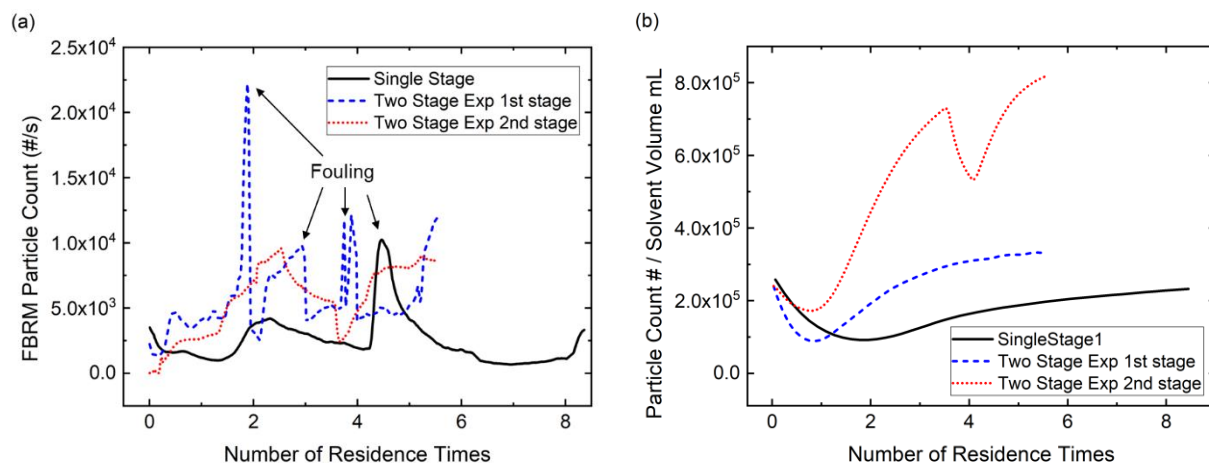


Figure 3-11 (a) FBRM total particle count measurement and (b) simulated particle count of the continuous experiments.

In the single stage experiment, the simulated μ_0 followed a similar trend as the FBRM measurement (black solid line) if the FBRM fouling events around 4.5 residence times are ignored: FBRM showed a decrease between 1-2 residence times as correctly predicted by the model indicating a washout event followed by an increase as a result of nucleation. This further reinforces the conclusion that the deviation of the model prediction of D50 to experimental results was likely due to the underprediction of growth kinetics instead of nucleation. In the two-stage experiment, the FBRM measurement in the first stage (blue dashed line) showed a slight decrease at around one residence time where the model also showed a decrease; However, it is inconclusive whether or not it is due to a washout as the model indicates or pure noise followed by fouling. FBRM measurement in the second stage (red dotted line) did not show a decrease where model predicted the first washout event because of the low slurry volume in the second stage during the first residence time. The model correctly predicted the particle count increase and decrease following the temperature step-up and down around 4 residence times shown by FBRM measurements.

Overall the model suggested similar events as experimental results of the two continuous operations tested.

However, the same level of performance as the two experiments discussed above was not observed for some of the other continuous experiments conducted (not specifically for this study) where the conditions were vastly different from the batch experiment. Because crystallization processes operate entirely in thermodynamically metastable conditions, the kinetics are heavily influenced by slurry conditions especially by supersaturation and seeding strategies. Different mechanisms of nucleation and growth (and potentially agglomeration, breakage etc) are present at different supersaturation levels and solid conditions [28], [32], [33], [47]. It is very difficult to capture the different mechanisms with a single empirical/semi-empirical model. The misrepresentation of crystallization kinetics leads to the misprediction the solution and solid concentration which subsequently further steer crystallization kinetics away from their true values. Therefore, it is important to carefully design parameter estimation experiments to match the solution supersaturation and solid properties to the intended processes design space. In addition, it is also important to ensure sufficient particle suspension and efficient slurry transfer as they are assumed by the model. Particle settling, inhomogeneous slurry removal and/or transfer line blockage may cause particle accumulation and system deviation from steady state operation as often observed in poorly designed stirred tank MSMPRs [18], [32], [96]. Sufficient mixing is also important to lessen or eliminate local supersaturation which may cause spontaneous primary nucleation despite of existing crystal particles in the slurry [32], [33], [174]–[176]. As primary nucleation is not well understood and extremely stochastic, this phenomenon usually cannot be accurately captured by simple kinetic models.

3.5 Conclusion

A PBM was developed for the cooling crystallization of CBZ. Growth, nucleation and dissolution kinetics were estimated sequentially with specially designed growth, nucleation and dissolution dominated experiments respectively. Model discrimination was carried out during parameter estimation to test for different formulations of the kinetic expressions. The final PBM fitted concentration within or close to the experimental concentration error range as well as product D50 while D10 and D90 were not well fitted due to their low weight in the objective function. To address the gap in the current literature of discussing the applicability of PBMs, verification and validation activities were carried out following the guideline of ASME V&V40 reaching the credibility goal of low risk applications (process understanding). Model verification activities included quantifying the errors associated with size discretization, solver parameter settings and solver choice which were verified to be negligible. For model validation, the governing equation was first validated by an uncertainty study that indicates negligible sensitivity of the system to the uncertainties in kinetic parameters. The validation comparators were examined by comparing the model performance to four additional validation experiments that featured ‘unseen’ seeding strategies and cooling rates. The concentration followed the experimental trend, but the product size quantiles were only validated for seed size 125-212 μm . Therefore, the model was not validated for particle size prediction applications where seeding strategies differ from training experiments. A final discussion was given on the ‘transferability’ of batch crystallization kinetics to continuous operations. For the system in this study, the kinetics were transferable in continuous operations under similar solution and solid conditions as batch training experiments. The model was observed to deviate severely from experimental results in continuous experiments that operated at vastly different supersaturations and solid concentrations from batch training experiments. Crystallization systems may exhibit different nucleation and growth mechanisms at

the microscopic scale under different supersaturations and solid concentrations which explains why a PBM developed with batch experiments would not be able to describe continuous operations of largely different conditions.

4. SYSTEMATIC PROCESS DEVELOPMENT OF CONTINUOUS CRYSTALLIZATION IN AN INNOVATIVE OSCILLATORY BAFFLE REACTOR: RESIDENCE TIME DISTRIBUTION STUDY

4.1 Introduction

There are limitations associated with impeller-induced mixing in a traditional STC such as poor local mixing and high shear. Another system that has been gaining interests in the crystallization community for its near plug flow residence time distribution (RTD) profile is the tubular oscillatory flow baffled crystallizer (OFBC) consisting of several baffled tube segments and an oscillating plunger. However, the OFBC often requires high oscillatory velocities to keep particles suspended leading to more widely spread RTD. To address the gap between the inherent poor mixing dynamics of a continuous STC and the complex design challenges of an OFBC, a dynamic baffle crystallizer, also known as an oscillatory baffle reactor (OBR) is systematically studied as a rising candidate for continuous crystallizer. An OBR is a jacketed crystallizer with baffles attached to an oscillating shaft to provide mixing. To operate continuously, it is designed to operate as an MSMR with an input and an output line similar to those commonly found on an STC.

Oscillatory mixing, provided by dynamic baffles, has been shown to improve heat and mass transfer while imposing less shear [177]–[182], promising for crystallization processes. The unique oscillatory fluid dynamics can be characterized by a number of dimensionless numbers [183]–[185], including oscillatory Reynolds number (Re_o) describing mixing intensity and Strouhal number (St) reflecting eddy propagation, as follows

$$Re_o = \frac{2\pi\omega x_o \rho D}{\mu} \quad (4.1)$$

$$St = \frac{D}{4\pi x_o} \quad (4.2)$$

where ω is the frequency of oscillations, x_o is the center to peak oscillation amplitude, D is the inner diameter of the tube, ρ is the fluid density and μ is the fluid viscosity. In comparison, impeller-induced mixing can be quantified by the impeller Reynolds number (Re_{im}) described by Eq(4.3).

$$Re_{im} = \frac{N \rho D_{im}^2}{\mu} \quad (4.3)$$

where N denotes agitation rate and D_{im} represents impeller diameter. Many studies have been carried out to demonstrate the improvement of heat and mass transfer in a batch oscillatory system compared to a traditional stirred tank [134], [136], [140], [180], [182], [186]–[190]. However, to the best of our knowledge, there is a lack of comparative study between continuous operations of an STC and a DBC. In this study, we aim to address this gap by studying RTD and continuous crystallization performance in a DBC versus an STC.

4.2 Experimental Methods and Material

4.2.1 Oscillatory baffled reactor and stirred tank crystallizer setup

The dynamic baffle crystallizer used in this study is the ‘Oscillatory Baffled Reactor’ (OBR) manufactured by Alconbury Weston Ltd. The OBR is an evaluation product featuring oscillating baffles in a jacketed glass vessel of an elongated geometry, shown in the schematic in Figure 4-1a. The vessel is made of Borosilicate glass and is jacketed for temperature control by a Huber Ministat125. The inner diameter of the glass vessel is 40 mm and the jacketed portion is 246 mm long. It can hold 300 mL content. There are four ‘donut’ shaped baffles with a hole in the middle (20 mm diameter) and an O-ring at the outer rim making the effective diameter of the baffles 40 mm, leaving no gap between the baffles and the wall. The baffles are equally spaced at 60mm apart, 1.5 times the tubing diameter which is an optimized design studied in past literature [177],

[191], [192]. A motor is used to oscillate the baffle shaft that can be operated at the frequency of 0.1 – 3 Hz in 0.1 Hz increments and the amplitude of 1 – 40 mm in 0.1 mm increments. However, the feasible operating range does not range from 0.1 Hz - 1 mm to 3 Hz - 40 mm. Instead, a simple set of experiments was conducted to obtain the range of operation that sustains extended periods of operation without motor failure or extremely violent mixing. This range is plotted in Figure 4-1d where the shaded region denotes the feasible operating space. Weaker oscillations are also achievable. The vessel also features four ports of various sizes to install PAT tools such as infrared (IR) spectrometer, focused beam reflectance measurement (FBRM) and thermostats, all of which were utilized in this study as shown in Figure 4-2. There are three openings at the top that can serve as inlets, outlets and/or addition ports and there is a drain at the bottom of the system that can be utilized as an inlet or outlet. Thus, the OBR design provides three different ways to configure the inlet and the outlet: feed at the top remove from the bottom, remove from the top feed at the bottom, and both inlet and outlets at the top. These options will be further discussed in Section 4.3.1.

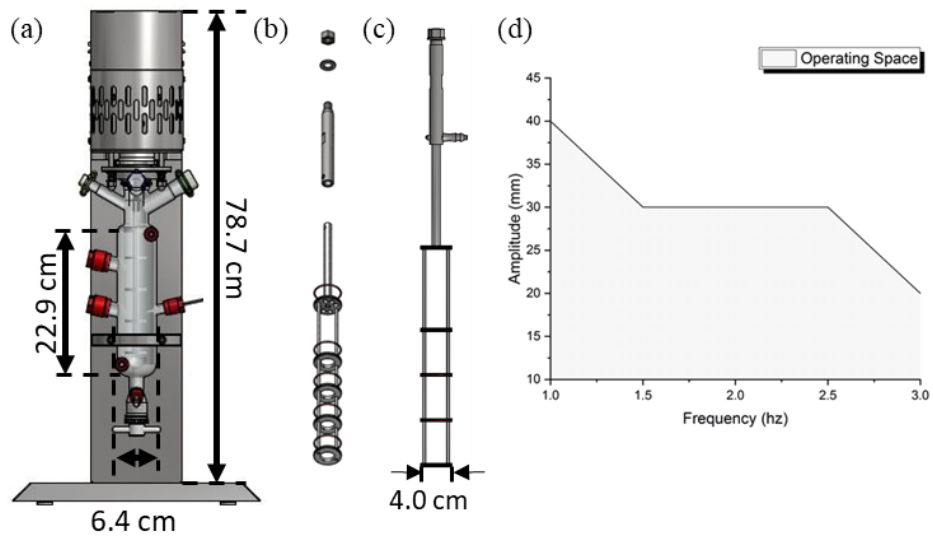


Figure 4-1 (a) Overall schematic of the OBR, (b) an exploded-view drawing of the baffle shaft, (c) sideview drawing of the baffle shaft, and (d) operating space of the OBR.

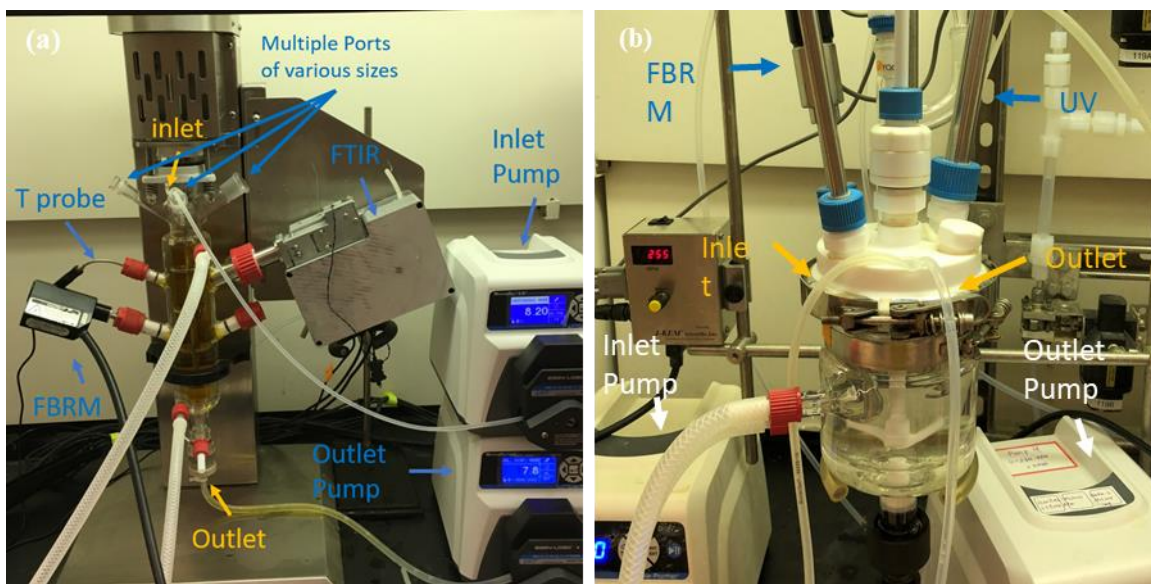


Figure 4-2 The continuous operational setup of (a) the OBR and (b) the STC.

The STC featured in this study consists of a 500 mL round-bottom jacketed glass vessel and a three-blade retreat curve impeller, illustrated in Figure 4-2b. The inner diameter of the round-bottom vessel is 100 mm and the jacketed height is approximately 180 mm. There are several ports at the top at which ultraviolet-visible spectrometer (UV), FBRM, and thermostat were inserted and secured for process monitoring. In addition, the ports also serve as inlets and outlets for continuous operation, as configured in this study, making a simple stirred tank type MSMPR.

4.2.2 Liquid and solid residence time distribution measurement

The first objective is to study the RTDs of the liquid phase content without solid present. It was achieved by quantifying the dilution process of a washout experiment. A washout experiment introduces a ‘reverse step change’ where concentrated feed, consisting of paracetamol (PCM, Alfa Aesar) in ethanol (EtOH, 200 proof, Decon Labs) at 0.1 g PCM/g EtOH, was replaced with pure solvent until all solute was removed from the reactor. Concentration was utilized to calculate the characteristics of the RTDs, which was recorded with in-situ Fourier transform infrared (FTIR)

spectrometer in the OBR every 18 seconds and UV in the STC every 15 seconds during washout experiments. To be consistent with later solid RTD and crystallization studies, the continuous operations in the two reactors feature a true continuous inlet and an intermittent product removal outlet. The feed was introduced continuously by a peristaltic pump (Cole-Parmer) at the flowrate determined according to the theoretical mean residence time (τ) and products were removed at the outlet also with a peristaltic pump every 2 minutes at 300 mL/min to remove the content accumulated during the 2 minutes in a few seconds. The level in the reactors was 240 mL in the OBR and 360 mL in the STC initially and after each removal. The temperature was maintained at 20 °C.

RTDs of solid particles suspended in solution were studied with pulse experiments described in Kacker et al. [139]: initially the reactors were filled to their respective operating level (240 mL in the OBR, 360 mL in the STC) with saturated PCM water solution at 20 °C. Prior to the injection of the pulse, the same saturated solution was run through the vessel continuously for about 15 minutes for baseline. At time zero, without changing the carrier solution, a small amount of solid PCM particle suspension tracer was injected quickly to the system with a syringe, serving as a pulse signal. Particle concentration was monitored in the form of particle count measurement by FBRM (Metler Toledo G400 unit in the STC and Lasentec S400 in the OBR) every 10 seconds until the solution in the crystallizer appeared clear. The saturated PCM water solution was prepared several hours prior to the experiment by adding PCM to water in slight excess. The solution was then stirred for at least 2 hours to ensure saturation before filtering. The tracer was prepared by adding 6.7 g of PCM to 10 mL of the saturated solution then stirred for at least 30 minutes. The long mixing time during the preparation of the solution and the tracer allows the mixtures to fully equilibrate to prevent dissolution and crystallization from taking place in the crystallizer as RTD

describes the digestion of signals solely by flow, not by phenomena of reactive natures such as dissolution or crystallization. As mentioned in Section 4.2.2, the operation also features a continuous inlet with an intermittent product removal every 2 minutes. Intermittent product removal is often employed for MSMPR systems to avoid outlet blockage.

In order to study the effects of the three main operating parameters of the OBR: baffle oscillating frequency (ω), baffle oscillating amplitude (x_0) and theoretical mean residence time (τ), on the liquid and solid residence time characteristics a three-level full factorial design was carried out for liquid and solid RTDs as shown in Table 4-1. Dimensionless numbers Re_o and St were also calculated and shown. Three-level factorial design provides insight into the curvature (i.e. secondary effect) of the model while producing easy-to-interpret visual plots of the results. The trade-off is the large number of experiments, which was acceptable in this study. The DOE range is a small subset chosen to avoid faint oscillations that will likely cause particle sedimentation and violent oscillations that can cause air bubble entrainment. In addition, the 'Exp#' is the randomized order to carry out the experiments. The experiments were not repeated. Initial repeatability study was carried out for 3-5 experiments which yielded repeatable results. The repeatability of the rest of the experiments was assumed to be acceptable. Analysis of Variance (ANOVA) was utilized to determine the significance of a factor or interaction of factors in addition to graphic interpretation of the results. ANOVA is a commonly used statistical technique with some assumptions: (1) observations are independent; (2) errors are normally distributed; and (3) variance is constant, all of which were verified and satisfied in this study, throughout all experiments.

Table 4-1 Three-level-three-factor full factorial design of experiment for RTD studies.

Exp#	ω (Hz)	x_0 (mm)	τ (min)	PD _L (W/m ³)	PD _S (W/m ³)	Re _{oL}	Re _{oS}	St
Exp1	2.0	15	30	221.5	264.5	5756	7511	0.2122
Exp2	2.5	10	45	128.2	153.1	4797	6259	0.3183
Exp3	1.5	10	30	27.7	33.1	2878	3756	0.3183
Exp4	1.5	15	45	93.5	111.6	4317	5633	0.2122
Exp5	2.0	10	30	65.6	78.4	3838	5007	0.3183
Exp6	2.0	20	15	525.1	627	7675	10015	0.1592
Exp7	1.5	15	15	93.5	111.6	4317	5633	0.2122
Exp8	2.5	20	45	1025.6	1224.6	9594	12519	0.1592
Exp9	2.0	10	45	65.6	78.4	3838	5007	0.3183
Exp10	1.5	20	45	221.5	264.5	5756	7511	0.1592
Exp11	1.5	15	30	93.5	111.6	4317	5633	0.2122
Exp12	2.0	10	15	65.6	78.4	3838	5007	0.3183
Exp13	1.5	20	15	221.5	264.5	5756	7511	0.1592
Exp14	1.5	10	45	27.7	33.1	2878	3756	0.3183
Exp15	2.5	15	45	432.7	516.6	7196	9389	0.2122
Exp16	2.0	15	45	221.5	264.5	5756	7511	0.2122
Exp17	2.0	20	30	525.1	627	7675	10015	0.1592
Exp18	1.5	10	15	27.7	33.1	2878	3756	0.3183
Exp19	1.5	20	30	221.5	264.5	5756	7511	0.1592
Exp20	2.5	15	15	432.7	516.6	7196	9389	0.2122
Exp21	2.5	10	15	128.2	153.1	4797	6259	0.3183
Exp22	2.5	15	30	432.7	516.6	7196	9389	0.2122
Exp23	2.0	20	45	525.1	627	7675	10015	0.1592
Exp24	2.5	10	30	128.2	153.1	4797	6259	0.3183
Exp25	2.5	20	30	1025.6	1224.6	9594	12519	0.1592
Exp26	2.5	20	15	1025.6	1224.6	9594	12519	0.1592
Exp27	2.0	15	15	221.5	264.5	5756	7511	0.2122

Another objective of RTD studies is to compare OBR with STC performance at equivalent conditions, i.e. yielding the same power density (PD). PD in an oscillatory system is estimated as follows:

$$PD = \frac{2\rho N_b}{3\pi c_D^2} \frac{1-\alpha^2}{\alpha^2} x_0^3 (2\pi\omega)^3 \quad (4.4)$$

where N_b denotes the number of baffles per length, c_D is the orifice discharge coefficient, which was taken to be 0.7, and α is the ratio of the area of the orifice to the total baffle area [193]. PD in an impeller driven system was estimated by the power number:

$$PD = \frac{P_0 \rho N^3 D_{im}^5}{V} \quad (4.5)$$

where P_0 is the power number, which was taken to be 1.27 for the type of impeller in our STC set up, N is the rotational speed, and V denotes the volume [194]. A set of liquid and solid RTD studies were carried out in the STC using the same methods. To limit the number of experiments required, τ was fixed at 30 min and agitation rates were chosen to correspond to the 7 achievable PDs in the OBR experiments, as listed in Table 4-2. The impeller Reynolds number is calculated for liquid and solid studies with Eq(4.3) and the order of experiments was also randomized.

Table 4-2 Experimental conditions of comparative liquid and solid RTD studies in the STC.

Exp#	N (rpm)	PD_L (W/m³)	PD_S (W/m³)	Re_{im,L}	Re_{im,S}	Equivalent Oscillation
STC1	351	221.4	264.4	11526	14570	1.5 Hz – 20 mm
STC2	439	433.2	517.2	14416	18222	2.5 Hz – 15 mm
STC3	263	93.1	111.2	8637	10917	1.5 Hz – 15 mm
STC4	176	27.9	33.3	5780	7306	1.5 Hz – 10 mm
STC5	234	65.6	78.3	7684	9713	2.0 Hz – 10 mm
STC6	293	128.8	153.8	9622	12162	2.5 Hz – 10 mm
STC7	468	524.8	626.7	15368	19426	2.0 Hz – 20 mm

4.2.3 Absorbance spectrometry

In the OBR, solution concentration was monitored by an in-situ FTIR spectrometer manufactured by Keit Spectrometers featuring a patented design based on the Sagnac interferometer to combat the interference of oscillations and vibrations to the spectrometer signal. To calibrate the FTIR, two sets of calibration experiments were performed: one set with low concentrations (<0.1 g/g) to

calibrate for liquid RTD experiments and another set at higher concentrations for continuous crystallization experiments. An example IR spectrum of PCM in EtOH obtained by the Keit FTIR is shown in Figure 4-3a where reference spectra were taken with pure EtOH. The peak at ~ 1250 cm^{-1} was identified as the only principle peak, possibly attributed to a $\nu\text{C-C}$ and $\delta\text{Ph-H}$ mode [195] in this concentration range. The calibration plot and equation are shown in Figure 4-3b. In the second set of calibration experiments followed the rapid calibration technique discussed in section 2.2: an excess amount of PCM was suspended in EtOH at ~ 15 $^{\circ}\text{C}$ and an FBRM was used to monitor particle counts. Then the solution was heated step-wise from 15 to 45 $^{\circ}\text{C}$ in increments of 5 $^{\circ}\text{C}$ with a 30 min hold at each step to allow for complete dissolution where the concentration was assumed to be the solubility concentration at the corresponding temperature obtained from literature [196]. The dynamic temperature and particle count profiles are shown in Figure 4-4a. As shown by the FBRM data, after 350 min where all solids dissolved, the concentration remained constant while temperature continued to increase, but the IR measurement stayed unvaried. Thus, temperature was eliminated from the calibration model and a linear model with the expression shown in Eq(4.6) was adopted where 15 significant peaks were identified by the ‘*stepwise fit*’ function in MATLAB.

$$C = a_1 Abs_1 + a_2 Abs_2 + \dots + a_i Abs_i + b \quad (4.6)$$

where C denotes concentration, a_i denotes fitted coefficients, Abs_i is the absorbance at a certain wavenumber and b is the fitted intercept, which was approximately zero as expected. An R^2 of 0.994 was obtained.

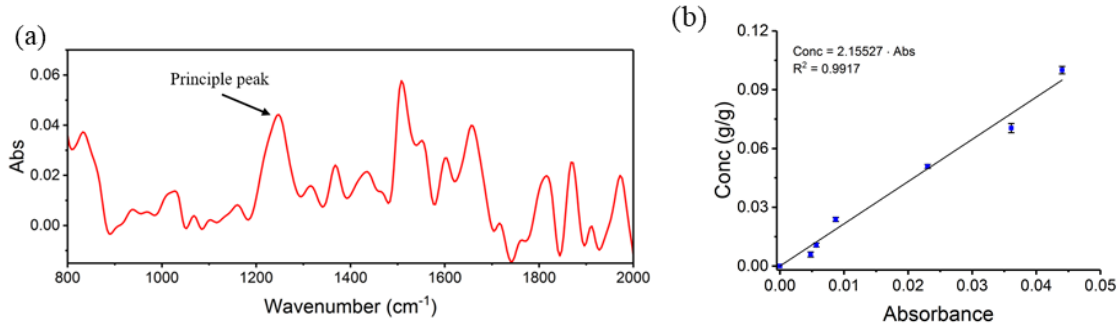


Figure 4-3 (a) Sample IR spectrum of 0.1 g/g PCM solution measured by the FTIR and (b) calibration model of PCM EtOH solution of concentrations lower than 0.1 g/g.

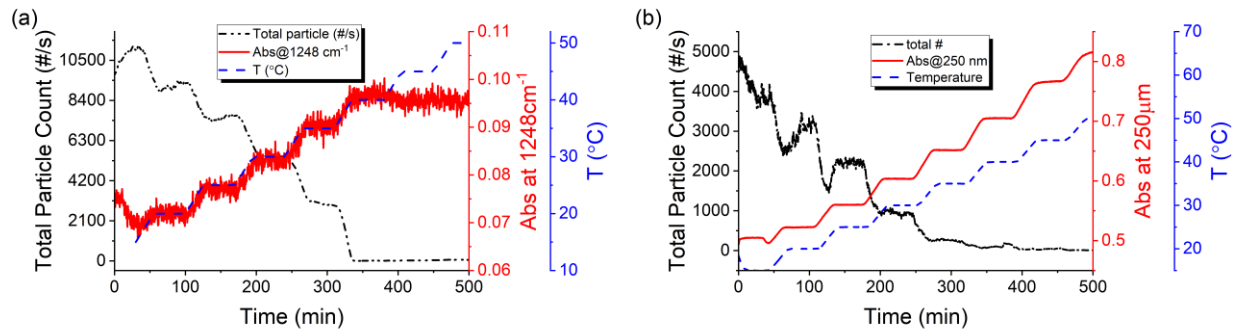


Figure 4-4 Operating profile of rapid calibration of (a) the FTIR in the OBR and (b) the UV in the STC.

In the STC, an in-situ UV was used to monitor concentration. As shown in Figure 4-4b, a similar rapid calibration of PCM in EtOH was carried out. First derivative of the UV spectrum was taken by the software during measurement. A single principle peak was identified at 250 nm, the maximum peak position of PCM UV spectrum. In contrast to the IR, temperature is included in the calibration model for UV absorbance is sensitive to temperature change:

$$C = a_1 Abs_1 + a_2 Abs_2 + \dots + a_i Abs_i + b \quad (4.7)$$

where T denotes temperature. The R^2 value of the model was 0.998. A lower concentration calibration was not performed. Eq(4.7) can be reduced to Eq(4.8) at constant temperature with pure EtOH at the same temperature taken to be the reference. While the value of a may take

different values in a lower concentration range, liquid RTD characteristic calculations do not call for a precise calibration model as long as:

$$C = a \cdot Abs \quad (4.8)$$

4.2.4 Analysis of liquid and solid residence time distributions

Residence time distribution can be represented either by the residence time distribution function (E-curve) or by the cumulative residence time distribution function (F-curve). The E-curve and F-curve contain the same information of the RTD and are interchangeable by:

$$E(t) = \frac{dF(t)}{dt} \quad (4.9)$$

To quantitatively characterize the RTDs, the mean of the RTD can be calculated to describe the average time that a particle spends in the vessel. Another important characteristic of an RTD is the variance (σ^2), or the ‘spread’ of the RTD [197]. The smaller the variance, the narrower/more uniform the RTD profile, the more consistent the end-product is likely to be.

For washout liquid RTD experiments, the F-curve can be easily calculated:

$$F(t) = 1 - W(t) = 1 - \frac{C(t)}{C_0} \quad (4.10)$$

where $W(t)$ is the washout function, $C(t)$ denotes the concentration measured by IR or UV at time t and C_0 is the initial concentration before the reverse step change. As demonstrated in Section 4.2.3, a linear model of a single absorbance with zero intercept was obtained for both UV and IR in this concentration range. Therefore, F-curve is simply calculated using the absorbance at the appropriate wavelength/wavenumber directly:

$$F(t) = 1 - W(t) = 1 - \frac{Abs(t)}{Abs_0} \quad (4.11)$$

The mean residence time \bar{t} corresponds to the first moment of the RTD:

$$\bar{t} = \int_0^{\infty} W(t) dt \quad (4.12)$$

To scale across experiments with different theoretical mean residence time, dimensionless experimental mean residence time or t_m is calculated as:

$$t_m = \frac{\bar{t}}{\tau} = \frac{\int_0^{\infty} W(t) dt}{\tau} \quad (4.13)$$

In a true continuous process, regardless of idealness, t_m should be equal to one. When $t_m > 1$, it indicates potential stagnant areas or ‘dead zones’. When $t_m < 1$, it suggests possible bypassing issues. Variance can be obtained by the second moment. Similarly, the variance is scaled by \bar{t}^2 :

$$\sigma^2 = \frac{2 \int_0^{\infty} t \cdot W(t) dt}{\bar{t}^2} - 1 \quad (4.14)$$

Variance describes the spread of the RTD. An ideal CSTR will have yield σ^2 of 1 and ideal plug flow produces completely uniform RTD, i.e. 0 variance.

Meanwhile solid RTDs are studied using pulse experiments and thus it is more accurate to obtain the mean and the variance directly from the E-curve [139]:

$$E(t) = \frac{X(t)}{\int_0^{\infty} X(t) dt} \quad (4.15)$$

where $X(t)$ is the FBRM particle count measurement at time t . Thus, the dimensionless experimental mean residence time t_m and dimensionless variance σ^2 can be obtained by Eq(4.16) and Eq(4.17)

$$t_m = \frac{\bar{t}}{\tau} = \frac{\int_0^{\infty} t \cdot E(t) dt}{\tau} \quad (4.16)$$

$$\sigma^2 = \frac{\int_0^{\infty} (t - \bar{t})^2 \cdot E(t) dt}{\bar{t}^2} \quad (4.17)$$

4.2.5 Continuous crystallization

Two sets of crystallization experiments were carried out; within each set, there was one experiment in the OBR and one experiment in the STC at similar power densities as shown in Table 4-3. The mean residence time was chosen to be 45 minutes for all four experiments. For each experiment, cooling crystallization of PCM from EtOH was carried out continuously. The feed tank consisted of a 0.3 g/g PCM solution ($T_{\text{sat}} \approx 45 \text{ }^\circ\text{C}$) maintained at $\sim 60 \text{ }^\circ\text{C}$ to avoid crystallization in the feed tank. The initial batch was filled with 0.18 g/g PCM solution ($T_{\text{sat}} = 20 \text{ }^\circ\text{C}$) at $20 \text{ }^\circ\text{C}$ and remained at $20 \text{ }^\circ\text{C}$ for the whole duration of the experiment. Before the start of continuous operation at time zero, PATs were turned on for a period of time to establish a ‘baseline’ of the initial batch. After time zero, feed was continuously charged to the crystallizer and product was removed intermittently every 2 min until ~ 2 residence times after steady state had been established, maintaining the volume to be 300 mL in the OBR/ 360 mL in the STC after each product removal. Solution concentration was monitored by IR in the OBR or UV in the STC with the appropriate calibration models while particle counts and the square weighted mean chord length (SWMCL) were tracked by FBRM. In addition, samples were drawn from the reactor at the end of every residence time, then filtered and dried for offline analysis including particle size distribution (PSD) and microscopy with Malvern Morphologi G3. Morphologi analyzes number-based PSD, which can be converted to volume weighted circle equivalent (CE) PSD as well as statistical information such as mean particle size (μ) and standard deviation (σ). Coefficient of variance (CV), defined as the ratio of μ over σ , was used to compare the uniformity of different PSDs.

Table 4-3 Experimental conditions of continuous crystallization studies in the OBR and the STC.

Exp #	Crystallizer	PD (W/m ³)	ω (Hz)	x_0 (mm)	τ (min)
			Agitation (rpm)		
Exp1	OBR	128.2	2.5	10	45
Exp2	ST	128.8		293	45
Exp3	OBR	432.7	2.5	15	45
Exp4	ST	433.2		439	45

4.3 Results and Discussion

4.3.1 Configurations of the OBR

The OBR offers three possible configurations of inlet and outlet positions when operating continuously: inlet at the bottom and outlet at the top (Configuration 1), inlet at the top and outlet at the bottom (Configuration 2), and both inlet and outlet at the top (Configuration 3) as shown in Figure 4-5. Each configuration can be a logical choice for continuous operation: Configuration 1 (Figure 4-5 left) offers an easy but precise way to control the level in the reactor by fixing the outlet tubing at a certain level with an ‘overdraw’ setting at the outlet pump; Configuration 2 (Figure 4-5 middle) utilizes gravity to aid product removal at the outlet. It also provides the opportunity to use a PID controlled valve instead of a removal pump for gentler handling of crystal products; Configuration 3 (Figure 4-5 right) closely resembles the STC configuration. Moreover, in some dynamic baffle vessels, a bottom outlet is not available for continuous operation thus leaving configuration 3 as the only way of operating in certain situations. The OBR set-up in this study allows all three configurations. Liquid RTD studies and solid RTD studies were conducted to examine all three configurations. Experiments were carried out at the same operating conditions where the baffles oscillate at the frequency of 2 Hz and amplitude of 15 mm and the theoretical mean residence time was set to be 30 min with three different configurations.

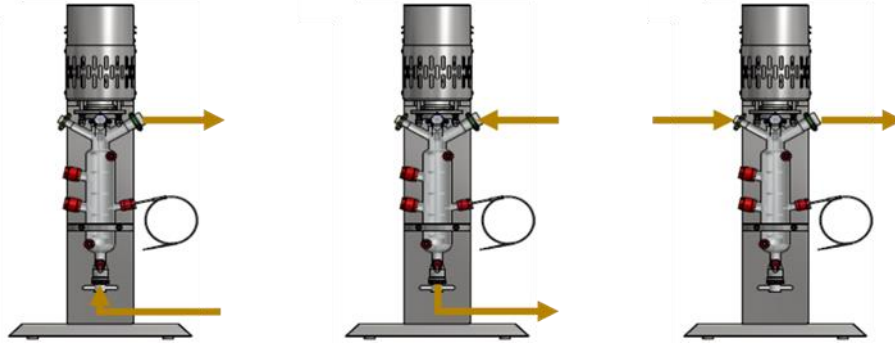


Figure 4-5 Three possible OBR configurations: inlet at the bottom, outlet at the top (left); outlet at the bottom, inlet at the top (middle); inlet and outlet both at the top (right).

The F-curves vs residence times Θ of the three configurations are shown in Figure 4-6a. Liquid RTDs in Configurations 2 and 3 were very similar to each other while Configuration 1 yielded a slightly steeper F-curve. While it can be anti-intuitive, the steepness of cumulative distributions is not a clear representation of the ‘spread’ or the variance of a distribution, as the steepness is affected by both the mean and the variance. Therefore, the calculation results of t_m and σ^2 are also listed in Table 4-4 which shows that Configurations 2 and 3 yielded very similar t_m and σ^2 while config. 1 produced small t_m and larger σ^2 which is less desirable. But overall, the three configurations performed similarly. Pulse experiments were also carried out in these three configurations to study solid RTDs. E-curves (Figure 4-6b) were constructed based on FBRM particle count. From visual inspection, Configurations 1, 2 and 3 are not exceedingly different except for around $\Theta = 2$ where FBRM might have fouled and defouled in Configuration 3. In addition, it is also desirable to have particles of different sizes to have similar RTDs. This aspect was investigated utilizing the chord length distribution measured by the FBRM. While chord length is not an accurate representation of true particle size, it may be acceptable to investigate the general differences in RTDs of particles of different chord lengths to infer the trend in RTDs of particles of different sizes. For each configuration, all particles were categorized into ‘small’ (10

$\mu\text{m} - 100 \mu\text{m}$) or ‘large’ ($100 \mu\text{m} - 1000 \mu\text{m}$); fines smaller than $10 \mu\text{m}$ were neglected. The E-curves are plotted in Figure 4-7 and the mean and variance values are listed in Table 4-5. Configurations 2 and 3 produced very similar RTDs between small and large particles in contrast to Configuration 1, which produced significantly different RTDs. Configuration 2 was slightly more consistent than Configuration 3.

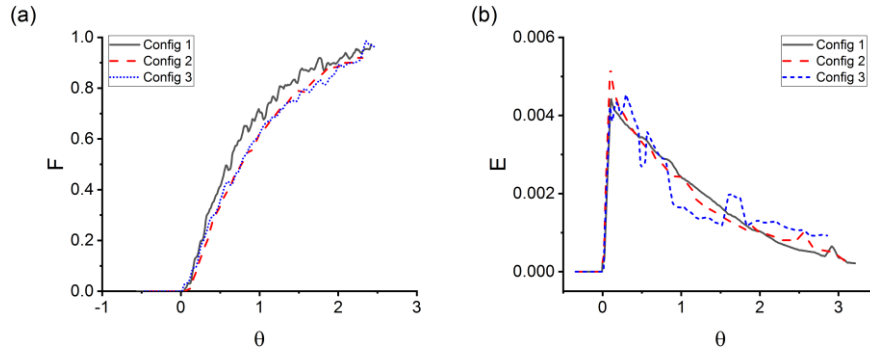


Figure 4-6 (a) F-curves of liquid RTD and (b) E-curves of solid RTD in Configuration 1,2 and 3.

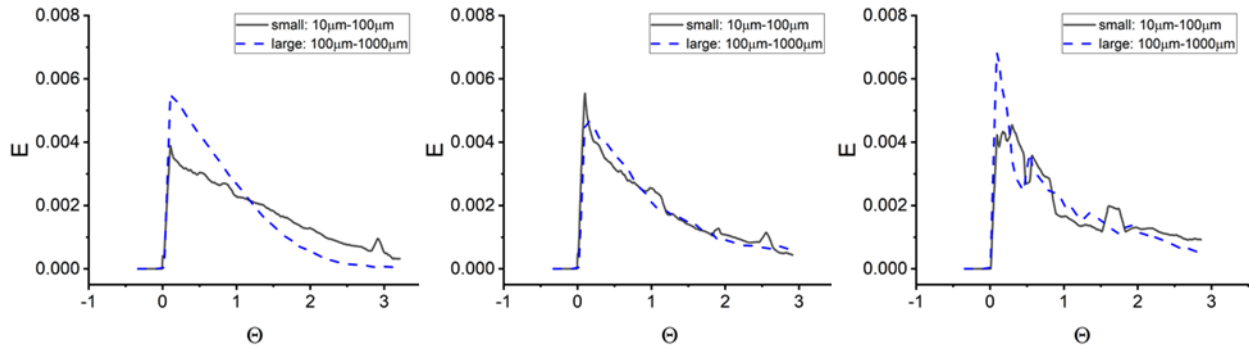


Figure 4-7 RTD function of small and large particles in Configuration 1 (left), Configuration 2 (middle), and Configuration 3(right).

Table 4-4 Dimensionless mean residence time t_m and variance σ^2 of liquid RTD in Configurations 1, 2, 3.

	Configuration1	Configuration2	Configuration 3
LRTD t_m	0.803	0.938	0.937
LRTD σ^2	0.658	0.522	0.59

Table 4-5 t_m and σ^2 of solid RTDs of small and large particles as well as total particle count in Configurations 1, 2, 3.

	Configuration1	Configuration2	Configuration3
SRTD $t_{m,total}$	1.017	1.008	1.036
SRTD $t_{m,10-100\mu m}$	1.138	1.005	1.065
SRTD $t_{m,100-1000\mu m}$	0.781	1.015	0.955
SRTD σ^2_{total}	0.542	0.592	0.573
SRTD $\sigma^2_{10-100\mu m}$	0.493	0.584	0.556
SRTD $\sigma^2_{100-1000\mu m}$	0.534	0.610	0.620

Taking both liquid and solid RTDs into consideration, Configuration 1 produced less desirable liquid RTD because of its small t_m (< 80 %) and its large variance. Configuration 1 also produced less consistent solid RTDs between small and large particles. Therefore, it was concluded that Configuration 1 (feeding from the bottom, removing from the top) is not a desirable method of continuous operation. This could be caused by the inlet pump being burdened by the task of charging at a small flowrate while counteracting the gravity of the full volume in the vessel. Configuration 2 and 3 on the other hand, produced similar liquid and solid RTDs with Configuration 2, with Configuration 3, being slightly better. Therefore, Configuration 2 was selected to be the optimal configuration and all following RTD and crystallization experiments were carried out in Configuration 2.

4.3.2 Liquid residence time distribution

Selective E-curves of the liquid RTD experiments, converted from F-curves, are plotted in Figure 4-8 over dimensionless time θ scaled by theoretical mean residence time, i.e. $\theta = t/\tau$. The values of t_m and σ^2 , as listed in Table 4-6 and Table 4-7, were calculated based on the F-curves using Eq(4.13) and Eq(4.14).

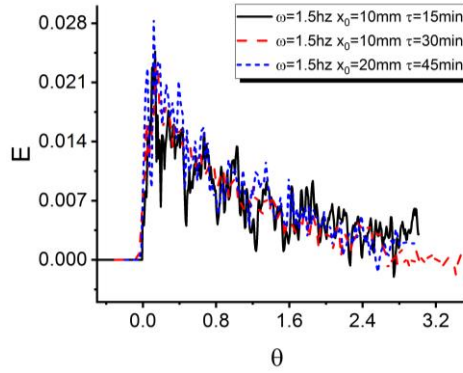


Figure 4-8 Converted liquid RTD E-curves under various conditions in the OBR.

Table 4-6 Dimensionless mean residence time (t_m) results of liquid RTD experiments.

ω (Hz)	τ (min)								
	15			30			45		
	x_0 (mm)								
	10	15	20	10	15	20	10	15	20
1.5	1.351	1.033	1.228	0.893	1.189	0.55	0.829	1.005	0.949
2	1.227	1.179	1.353	0.978	0.938	0.779	0.924	0.728	0.94
2.5	1.085	1.197	1.014	1.045	0.971	0.689	0.916	1.004	0.626

Table 4-7 Dimensionless variance (σ^2) results of washout experiments.

ω (Hz)	τ (min)								
	15			30			45		
	x_0 (mm)								
	10	15	20	10	15	20	10	15	20
1.5	1.349	0.815	0.936	0.65	0.574	0.606	0.765	0.726	0.63
2	1.27	0.703	1.444	0.701	0.522	0.761	0.713	0.669	0.709
2.5	0.845	0.725	0.825	0.76	0.854	0.729	0.527	0.806	1.027

The mean residence time appeared to be consistently larger when $\tau = 15$ min, with 4 out of 9 experiments larger than 1.2, suggesting a ‘dead zone’ issue while being generally smaller for $\tau = 30$ min and 45 min. Five out of the 18 experiments of $\tau = 30$ min and 45 min yielded t_m less than 0.8 suggesting that under certain conditions, the vessel exhibits bypassing issues, which should be avoided for future operations. Similarly, variances of $\tau = 15$ min were generally larger than those of $\tau = 30$ min and 45 min. Figure 4-9 plots the mean and variance over Re_o : t_m and σ^2 did not vary

significantly across Re_O , instead they varied across different τ values. ANOVA was carried out to study the statistical effect of ω , x_0 , τ , their secondary effect (ω^2 , x_0^2 , τ^2) and the two-way interactions of them ($\omega \times x_0$, $\omega \times \tau$, and $x_0 \times \tau$) on t_m and σ^2 responses. The same conclusion was reached by ANOVA, that only changes in τ had a significant impact on liquid RTD. Furthermore, t_m and σ^2 did not vary greatly among the $\tau = 30$ min and $\tau = 45$ min experiments. Thus, when designing future liquid reaction processes, if τ is determined to be relatively large, moderate changes in oscillation or flowrate will not affect RTD significantly. It should be emphasized here that even though often assumed so, experimental mean residence time may not be identical to volume divided by flowrate and should be measured when encountering a new reactor vessel.

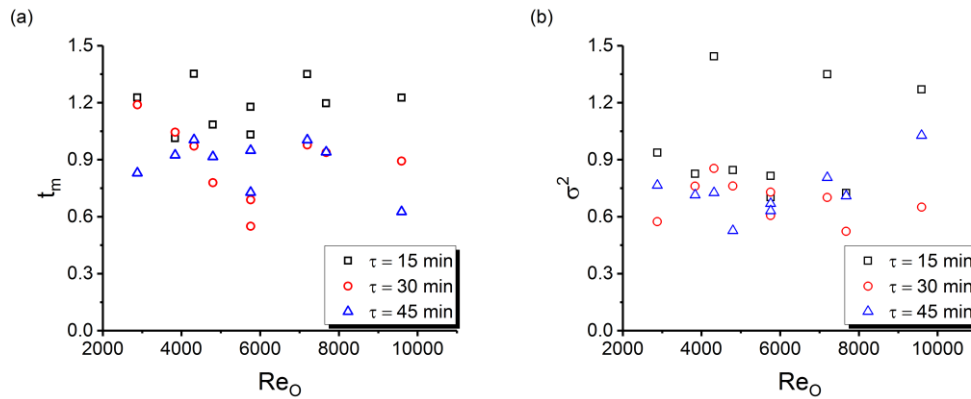


Figure 4-9 Plot of (a) t_m and (b) σ^2 of liquid RTDs against oscillatory Reynolds number Re_O .

To compare with the STC, F-curves were obtained and t_m and σ^2 were calculated (Figure 4-10) for the STC experiments. Figure 4-10a shows that t_m varied in a much larger range with varying power densities in the STC than the OBR. More importantly, the OBR yielded smaller variances in almost all the experiments as demonstrated in Figure 4-10b. As a result, the OBR may indeed be preferred compared to traditional stirred tanks under the conditions investigated here. For very small and very large agitation rates in the STC, mean residence times were not well

behaved and should be avoided when designing a continuous process in the STC as there may be bypassing or dead zone issues.

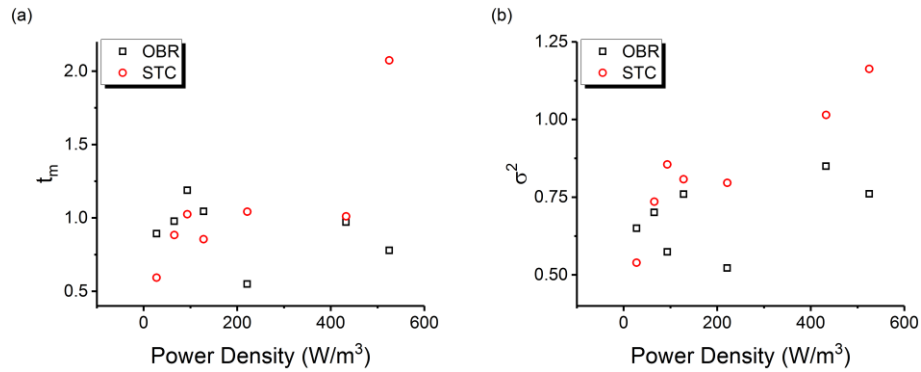


Figure 4-10 (a) Comparison of liquid RTD t_m in the OBR and in the STC; (b) comparison of liquid RTD σ^2 in the OBR and in the STC.

4.3.3 Solid residence time distribution

Selective E-curves of solid RTDs are plotted against θ in Figure 4-11. The values of t_m and σ^2 were calculated for each experiment based on the E-curve and are listed in Table 4-8 and Table 4-9. The parameter t_m appeared to be more sensitive to oscillation changes than changes in τ . Meanwhile, σ^2 stayed relatively unvaried throughout all 27 experiments. In Figure 4-12, the same result can be observed where t_m generally increased with respect to Re_o while σ^2 remained constant. At extremely weak oscillations (small Re_o), solid particles were not well suspended and thus ‘fell’ through the vessel causing a bypass directly to the outlet leading to small t_m values. At very intense oscillation conditions, the particles were possibly trapped, leading to prolonged mean residence times. Therefore, these extreme conditions should be avoided. In addition, ANOVA was carried out to confirm this observation statistically and indeed ω , x_0 as well as their nested effect were significant on t_m responses, while no factors or interactions of any factors had significant impact on σ^2 . Therefore, only the oscillation intensity affected the solid particle RTD but in a consistent way without causing much change in the uniformity of the RTD. It was also observed that τ was

less influential on RTDs in a solid-liquid process than in a liquid only process within the investigated range. The variance was also generally smaller of the solid particle RTDs than liquid RTDs promoting the potential usage of the OBR as a continuous crystallization system.

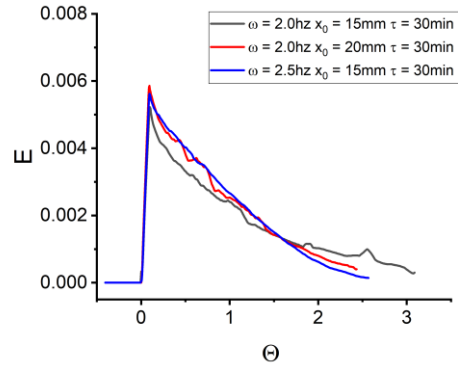


Figure 4-11 Measured solid RTD E-curves of various conditions in the OBR.

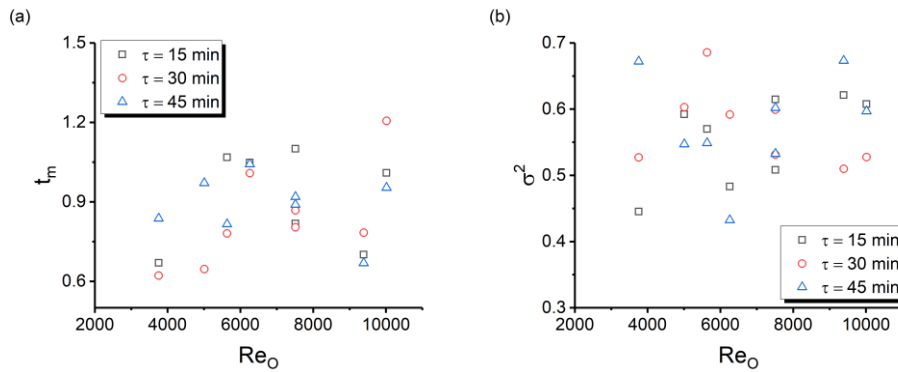


Figure 4-12 Plot of solid RTD (a) t_m and (b) σ^2 over Re_o .

Table 4-8 t_m results of pulse experiments.

ω (Hz)	τ (min)								
	15			30			45		
	x_0 (mm)								
	10	15	20	10	15	20	10	15	20
1.5	0.669	1.068	0.818	0.781	0.646	0.622	0.837	0.816	0.889
2	1.321	1.1	1.009	0.923	1.008	0.804	0.971	0.919	0.953
2.5	1.048	0.7	1.639	0.868	0.783	1.206	1.042	0.669	1.341

Table 4-9 σ^2 results of pulse experiments.

ω (Hz)	τ (min)								
	15			30			45		
	x_0 (mm)								
	10	15	20	10	15	20	10	15	20
1.5	0.615	0.57	0.592	0.686	0.603	0.527	0.672	0.549	0.602
2	0.571	0.607	0.483	0.495	0.592	0.531	0.547	0.533	0.597
2.5	0.621	0.445	0.508	0.599	0.51	0.527	0.432	0.673	0.463

Similarly, E-curves were constructed for the solid RTD experiments in the STC and σ^2 and t_m were calculated and plotted in Figure 4-13 against power density. Stirred tank experiments yielded small t_m for many experiments indicating an underlying bypassing issue during which particle settling was observed. More importantly, it is observed that the variance in the OBR was consistently smaller than the STC throughout all experiments as shown in Figure 4-13b. It suggests that the uniformity of solid RTD was significantly improved by oscillatory mixing which is especially beneficial for crystallization.

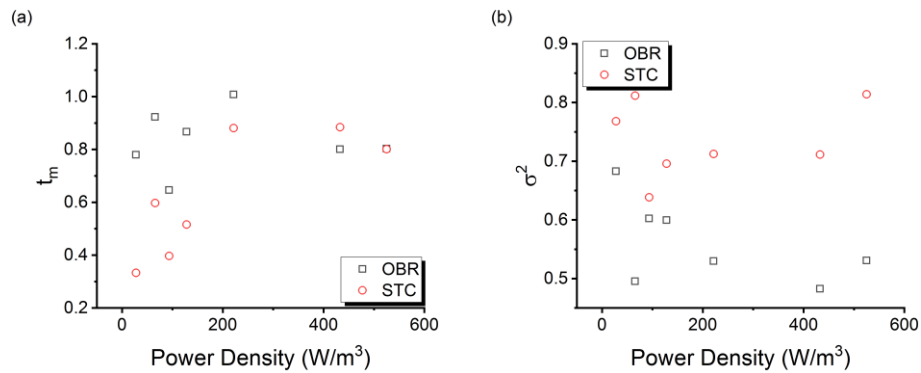


Figure 4-13 (a) Comparison of solid RTD t_m in the OBR and in the STC; (b) comparison of solid RTD σ^2 in the OBR and in the STC.

4.3.4 Continuous crystallization

Two sets of crystallization experiments were carried out in the STC and in the OBR under different mixing conditions as listed in Table 4-3 and their solid RTD E-curves are plotted in Figure 4-14;

The first set was chosen based on the solid RTD results of $\tau = 45$ min in the OBR. As shown in Figure 4-15, 2.5 Hz - 10 mm was chosen as an optimized condition because it yielded solid particle RTD with the lowest variance and mean residence time close to 1. Thus, the corresponding condition in the STC was back-calculated to be 293 rpm based on power density which yielded small t_m and slightly less uniformity. The second set was chosen for a higher agitation rate, 439 rpm, in the STC to avoid particle settling. The equivalent oscillation rate was 2.5 Hz – 15 mm in the OBR. Both experiments in this set have similar t_m with the uniformity improved in the OBR as discussed in Section 4.3.3.

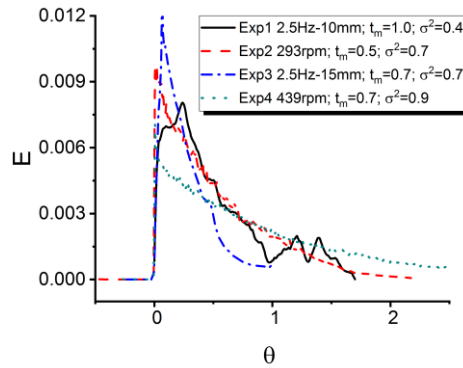


Figure 4-14 Solid RTD E-curves of the four continuous crystallization experiment conditions.

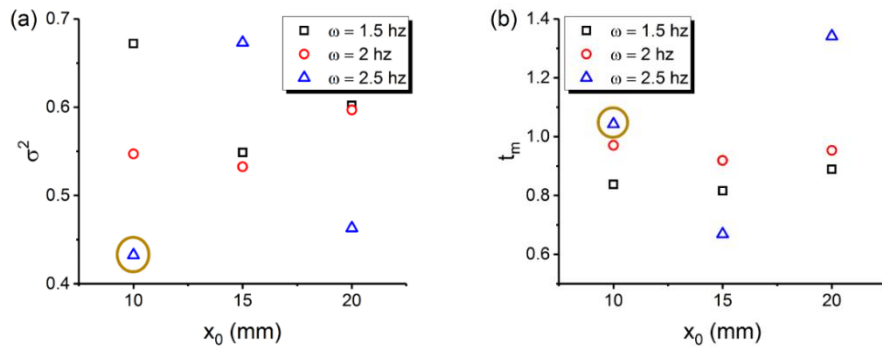


Figure 4-15 (a) σ^2 results and (b) t_m results of solid RTD studies in the OBR at $\tau = 45$ min. The circle represents the optimal operating conditions chosen (2.5 Hz frequency of oscillations and 10 mm amplitude).

Particle count, SWMCL, and concentration were monitored and plotted in Figure 4-16. The overall trends in all four operating profiles were similar: concentration increased as continuous operation began until nucleation took place where concentration decreased rapidly as particle count increased sharply; eventually steady-state should be reached. Across both sets of experiments, faster nucleation was observed in the OBR, occurring at around 1 residence time, while in the stirred tank, nucleation took place at approximately 2 residence times, which can be explained by the enhanced mixing in the OBR. Nucleation being a highly stochastic process, stronger, more thorough mixing mechanism can increase the chances of molecules coming together to form critical clusters, which can increase nucleation rate or decrease induction time [198].

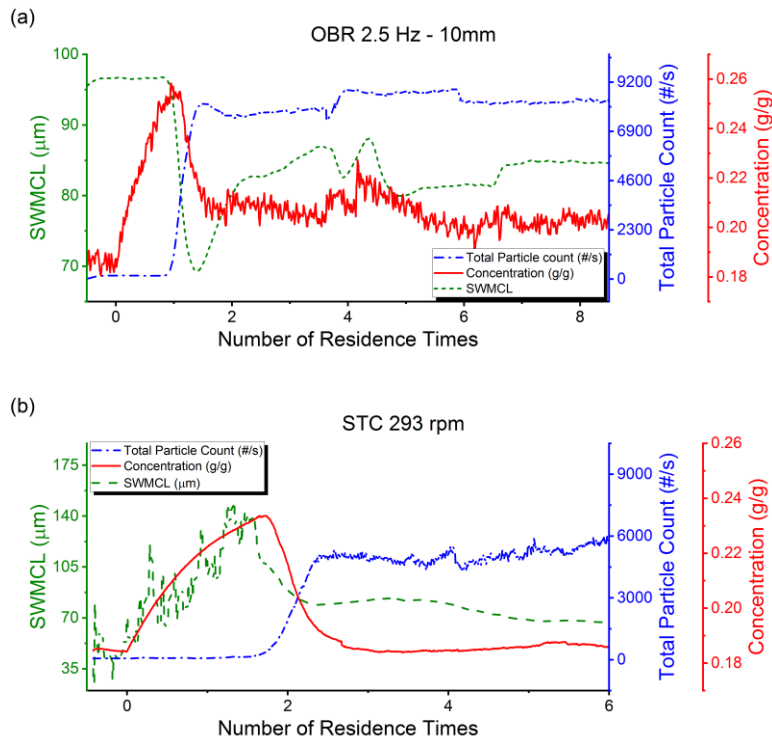
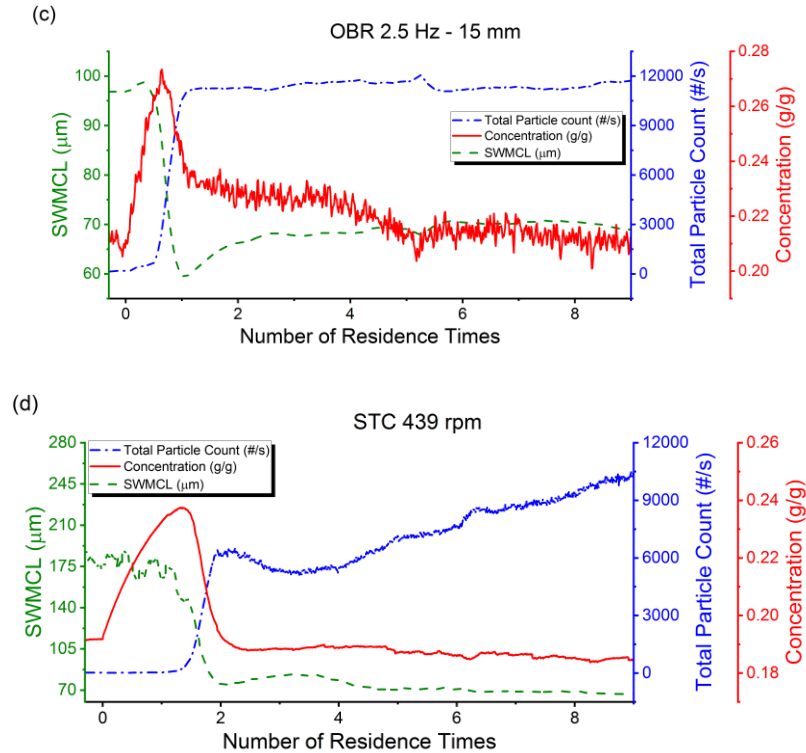


Figure 4-16 Total particle count, concentration and square weighted mean chord length (SWMCL) profiles over time of continuous experiments: (a) Exp1 OBR 2.5 Hz – 10 mm (b) Exp2 STC 293rpm (c) Exp3 OBR 2.5 Hz – 15 mm and (d) Exp4 STC 439rpm.

Figure 4-16 Continued.



After initial nucleation, crystals continued to nucleate and grow dynamically until steady state was reached indicated by stable particle count, SWMCL and concentration. During this time, slurry samples were taken at each residence time for offline PSD analysis (Figure 4-17 & Table 4-10) and microscopy (Figure 4-18). In the OBR, steady state was reached at 5-6 residence times in both experiments (Figure 4-16a,b) where FBRM measurement, UV measurement and offline PSD measurements became steady. The particle size distribution measured offline remained relatively unvaried across all residence times in each OBR experiment, which is also consistent with the microscopic images. However, the experiments in the STC were not as ‘uneventful’. In Exp2, the system seemingly reached steady state around 4-5 residence times as FBRM and UV data stabilized but the offline PSD measurement showed large variations between 5-6 residence times, which indicates that true steady state was perhaps not achieved (Figure 4-16c). Furthermore, particle sedimentation was observed after 6 residence times by visual inspection. The same

observation was made during a repeat experiment at this agitation speed in the STC. Eq(4.18), known as the Zwietering correlation, describes the empirical equation to calculate the minimum agitation rate required to suspend particle of a certain size in solid-liquid systems [102]

$$N_{js} = S \nu^{0.1} d_p^{0.2} \left[\frac{g_c (\rho_s - \rho_l)}{\rho_l} \right]^{0.15} X^{0.13} D_{im}^{-0.85} \quad (4.18)$$

where N_{js} denotes the minimum agitation rate required, S is the Zwietering constant, unique to the geometric characteristics of the agitation system, which is taken to be 4.5 according to literature [199], ν is the kinematic viscosity of the solution, d_p represents the mass mean particle size of interest, g_c is the gravitational acceleration constant (9.81 m/s), ρ_l and ρ_s are the densities of liquid solution and solid particles respectively, and X is the weight percentage of solid to liquid content. The Zwietering correlation has been commonly applied by chemical engineers for the last few decades to quickly determine a minimum required agitation speed for a slurry system. According to calculations based on the Zwietering correlation described in Eq(4.18), the agitation rate of 293 rpm was insufficient to suspend particles 360 μm or larger. On the contrary, in the OBR, particle sedimentation was not observed, which can be explained by the smaller crystal size and the enhanced oscillatory mixing. While, to the best of our knowledge, there is no such comprehensive correlation developed for oscillatory mixing, previous study has been conducted to demonstrate the ability to suspend solid particles at relatively low oscillation intensities [71].

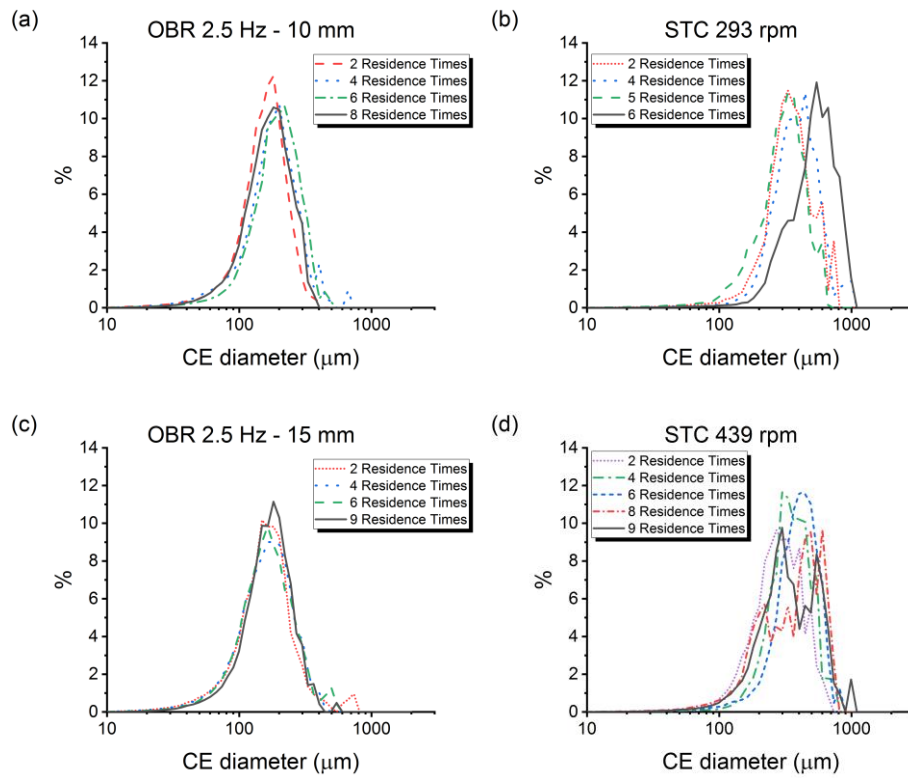


Figure 4-17 Volume weighted particle size distribution (PSD) of samples taken at various residence times of continuous experiments; (a) – (d): Exp1 - Exp4.

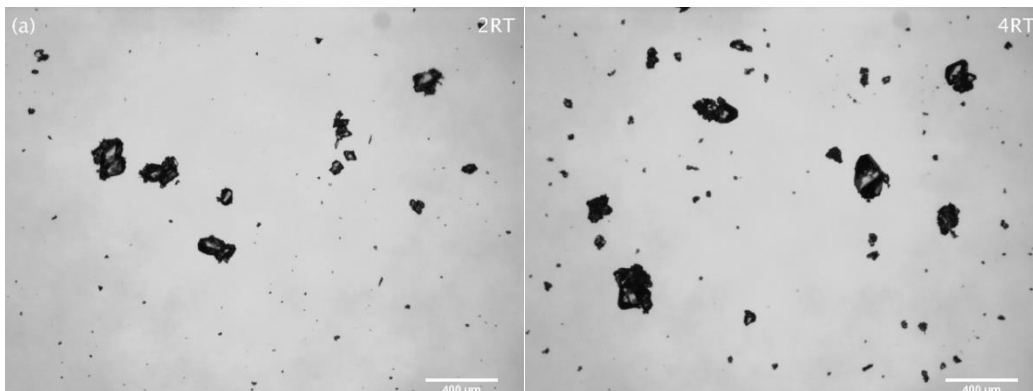


Figure 4-18 Microscopic images of samples taken at various residence times of continuous experiments; (a) – (d): Exp1 - Exp4.

Figure 4-18 Continued.

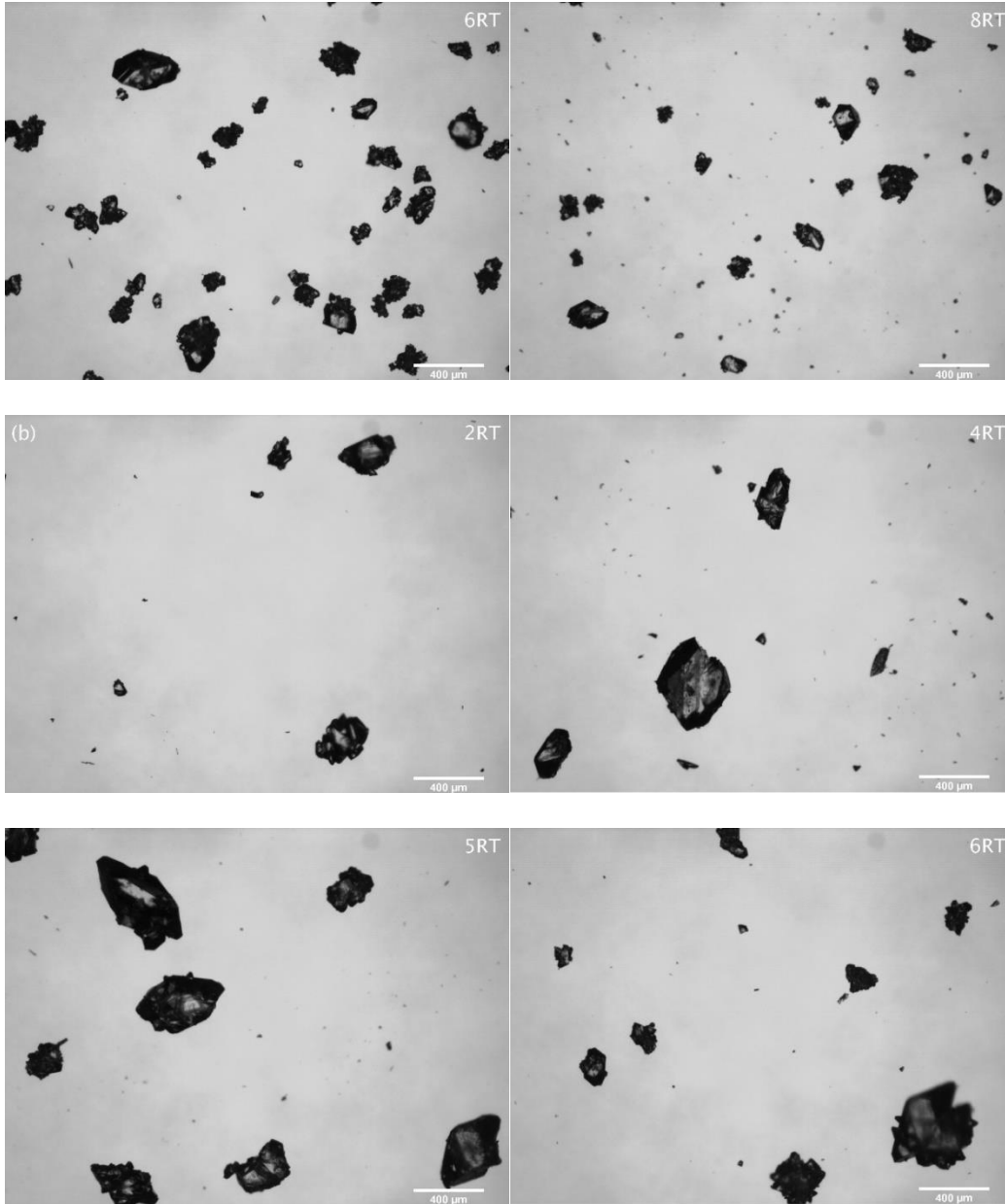


Figure 4-18 Continued.

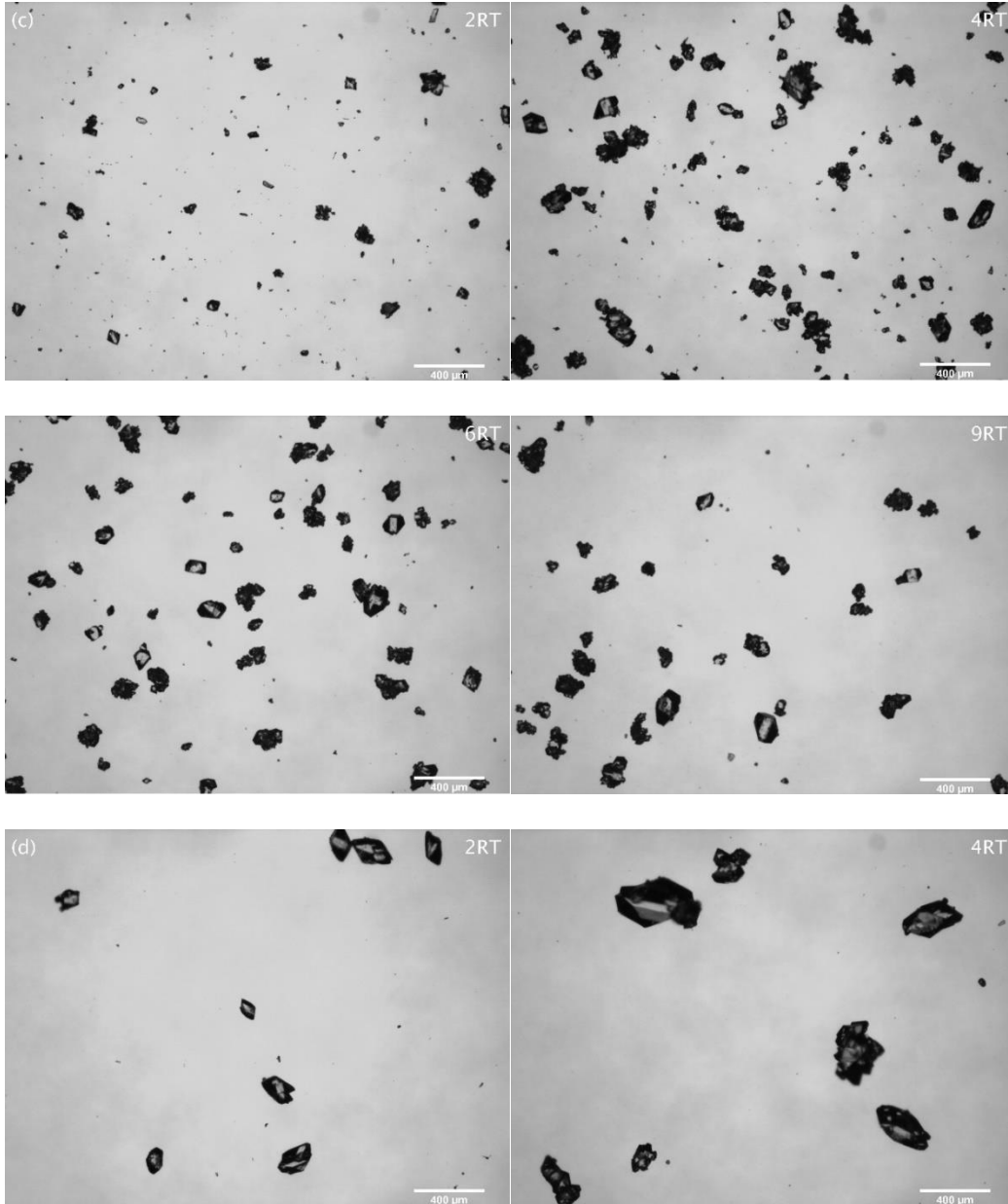


Figure 4-18 Continued.

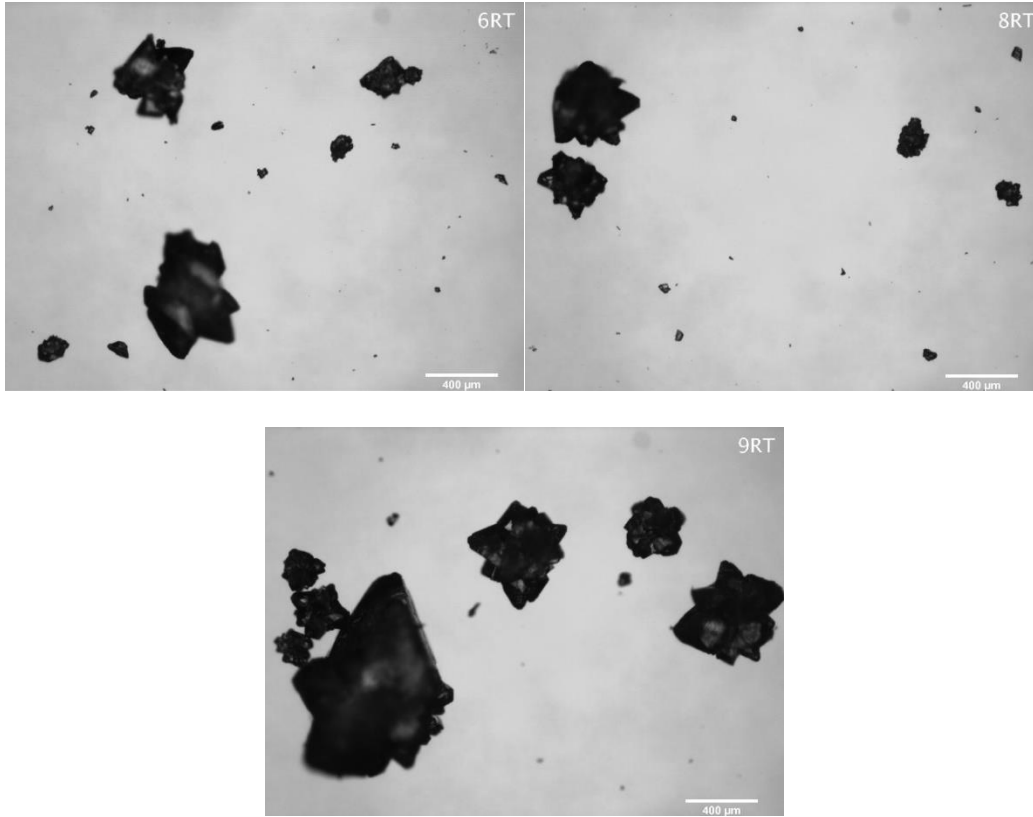


Table 4-10. The mean and the C.V. of the PSD at various residence times of continuous experiments Exp1-4.

		2RT	4RT	5RT	6RT	8RT	9RT
Exp1	μ	155.2	184.3	-	193.3	166.9	-
	C.V.	0.365	0.484	-	0.384	0.37	-
Exp2	μ	347.8	388.6	453.9	301.4	-	-
	C.V.	0.387	0.398	0.361	0.38	-	-
Exp3	μ	168.5	163.3	-	169.3	-	168.6
	C.V.	0.594	0.438	-	0.49	-	0.408
Exp4	μ	285.7	347.6	-	385.3	364.3	357.8
	C.V.	0.41	0.35	-	0.339	0.458	0.484

In Exp4 where agitation rate was increased to 439 rpm, sedimentation was not observed; however, the particle count continued to increase even at 9 residence times (Figure 4-16d). Taking a closer look at 6-9 residence times as shown in Figure 4-19: as particle count increased, the

SWMCL decreased, which indicates that breakage likely took place. The high shear rate exerted by the agitator possibly induced crystal breakage in the STC. The offline measurement also supports this assumption, where the PSD at 6, 8 and 9 residence times (Figure 4-17d and Table 4-10) yielded smaller average size. The PSD was also increasingly more spread out at 8 and 9 residence times, where it even exhibited bimodality, possibly due to breakage as well as agglomeration of small broken crystals, which can be observed in the microscopic images (Figure 4-18d). Breakage and agglomeration can also cause classified withdraw, also known as non-representative withdraw, which can further intensify size bimodality of the product. At the same power density, such breakage phenomenon was not observed in the OBR, which supports the claim that oscillatory mixing generally exerts less shear, possibly leading to less breakage [192], [200]. In addition, comparing Exp1 and Exp3, the uniformity of the final product PSD was slightly enhanced in Exp1 since an optimized condition was selected based on solid RTD results. Therefore, the experimental design of solid RTD studies demonstrated in this study can aid the selection of an optimized condition when designing a continuous crystallization process.

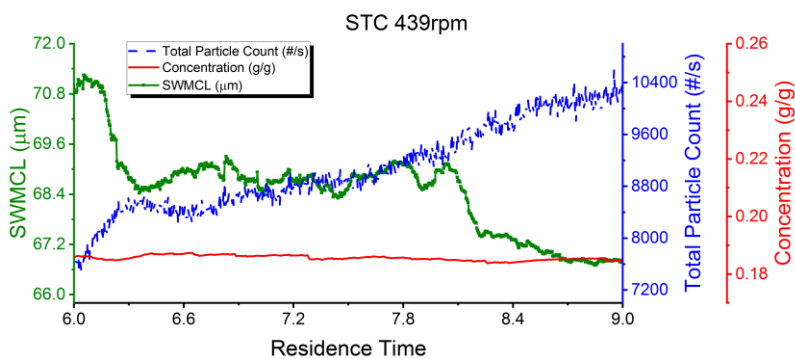


Figure 4-19 Close-up process profile of Exp4 at 6-9 residence times.

PSDs of the samples taken at the final residence times in all four experiments were compared in Figure 4-20. The final products of Exp1 and Exp3 are of comparable uniformity as

Exp2 in the STC before particle sedimentation occurred. Exp4, during which breakage likely took place, produced products of less uniform sizes. Therefore, the OBR shows potential as a promising candidate for continuous crystallization as it produced more consistent results without undesirable events such as particle settling, crystal breakage and heavy agglomeration. The improvement in RTD uniformity in the OBR is reflected in the improved CSD results in the experimental conditions studied. But the exact effect of improved RTD on the final product may also be dependent on the model compound and operating conditions which is an interest of future studies. Furthermore, many techniques can be applied to optimize the continuous crystallization process such as seeding and multistage operation which are worthy of further investigations.

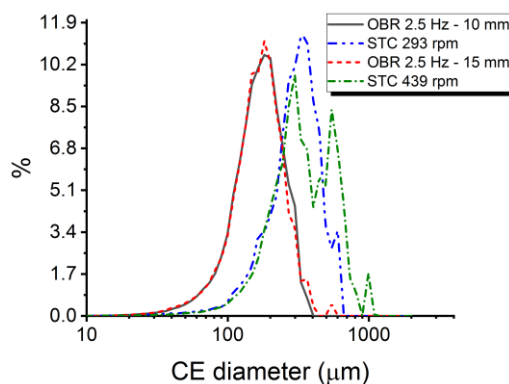


Figure 4-20 The PSD of samples taken at the last residence times in all 4 continuous experiments.

4.4 Conclusions

The gap between a well-studied stirred tank MSMR and the newly developed oscillatory flow baffled crystallizer is addressed by studying a dynamic baffle crystallizer, also known as the oscillatory baffle reactor, operated continuously as an MSMR. The results of liquid and solid RTD studies in the OBR have been discussed: according to ANOVA, theoretical mean residence time was the only significant factor affecting liquid RTD characteristics, while oscillating intensity affects the solid RTD by affecting the mean but not the variance. In comparison to the stirred tank

crystallizer, the RTDs, both liquid and solid, were more uniform in the OBR, which indicates the potential advantage of oscillatory mixing over traditional agitation in continuous processes. An initial crystallization study was carried out to compare the performances between the OBR and the STC on the continuous cooling crystallization of PCM. Nucleation occurred sooner in the OBR experiments. However, it was inconclusive whether steady state was established sooner or later in the OBR than in the STC. Even though the product was generally smaller in the OBR, the size distribution of the crystal product uniformity was comparable. More importantly, continuous crystallization in the OBR was stable and reliable while in the STC, undesirable events, such as particle sedimentation and crystal breakage, took place causing early termination and/or failure to establish steady state.

Our study showed that as an MSMR vessel, the OBR shows great potential in comparison to a traditional STC. Such potential calls for further studies of continuous crystallization design and control in the OBR as a continuous crystallization platform in conjunction with existing STC and OFBC.

5. SYSTEMATIC PROCESS DEVELOPMENT OF CONTINUOUS CRYSTALLIZATION IN AN INNOVATIVE OSCILLATORY BAFFLE REACTOR: MODEL AND EXPERIMENT GUIDED START-UP OPTIMIZATION

5.1 Introduction

Start-up of continuous MSMPR operation is an important aspect of achieving a desirable state-of-control operation. Improper start-up procedures could lead to fouling [123], prolonged dynamics [17] and even polymorph impurities [125], [201]. The start-up process should be optimized to minimize product loss and operational issue and, in the meantime, shortening the time to reach the state-of-control. Two general startup procedures have been seen in literature: immediate continuous operation or batch crystallization as start-up. Both has been ‘praised’ for different systems or different optimization objectives. Continuous MSMPR operation can start with a clear solution or a slurry. It is however not advisable to start the MSMPR crystallizer dry as it may result in excessive nucleation and fouling. If a clear solution is used during start-up, primary nucleation will take place and the primary particles can serve as seed. A slurry can also be used as start-up which serves as a seed bed. A batch crystallization can be performed first to create the crystalline slurry for start-up [65], [67], but an improper batch design can lead to significant fouling and blockage [123]. It is important to note that residence time must be long enough for both start-up choices to avoid excessive particle washout to prevent periodic primary nucleation resulting in large number of fines unless seed is carried in continuously with feed. Most studies in the current literature are simulation based STC MSMPR optimization studies where kinetic parameter errors are not quantified. As demonstrated in the last chapter, the mixing dynamics in the OBR is different from a STC. It may have a significant impact on crystallization kinetics which in turn may change process dynamics during continuous operation. In this study, the goal is to study the effects of

different start-up strategies of cooling crystallization of PCM by the means of modeling and experiments.

5.2 Material and Methods

5.2.1 Kinetic parameter estimation

Batch cooling crystallizations of paracetamol (PCM, Alfa Aesar, 98.0% purity) in ethanol (EtOH, 200 proof, Decon Labs) were carried out in the OBR to estimate the values of growth and nucleation parameters. Four experiments were performed, all of which were carried out in the OBR described in section 4.2.1. In-situ UV was used to measure concentration and FBRM was utilized to monitor particle counts. Initial concentration (240 mg PCM/mL EtOH), seeding temperature (43 °C), final temperature (15 °C) and oscillation intensity (2.5 Hz-10 mm) were unchanged among four experiments. Seed size was varied between (1) 75-180 μm or (2) 60-120 μm, seed loading was varied between 3wt% to 10wt% and cooling rate (β) was varied between 0.05 to 0.3 °C/min. Seed was sieved using Advantech L3P sonic sifter using sieve size 75μm and 180μm or 60μm and 120μm. End products were collected, filtered and dried for laser-diffraction based PSD analysis (Malvern Mastersizer300, Aero S) to obtain their 10%, 50% and 90% size quantiles (D10, D50, D90 respectively). Table 5-1 summarizes the experimental conditions discussed above.

Table 5-1 Experimental conditions of batch crystallization experiments in the OBR.

Exp#	$C_{initial}$ (mg/mL)	$T_{initial}$ (°C)	T_{final} (°C)	β (°C/min)	Seed Loading	Seed Size (μm)
Exp1	240	43	15	0.1	5.0g (10%)	75-180
Exp2	240	43	15	0.05	5.0g (10%)	60-120
Exp3	240	43	15	0.3	1.7g (3%)	75-180
Exp4	240	43	15	0.2	2.5g (5%)	75-180

The PBM described by Eq(2.8) and (2.10) was used to simulate PCM crystallization in the OBR. Semi-empirical kinetic expressions were used to describe secondary nucleation and growth:

$$\begin{aligned} B &= k_s (C - C_{sat})^s \text{Exp}\left(-\frac{E_s}{RT}\right) M^{M_s} \\ G &= k_g (C - C_{sat})^g \text{Exp}\left(-\frac{E_g}{RT}\right) \end{aligned} \quad (5.1)$$

where concentration has the unit of mg PCM/mL EtOH, k_g ($\mu\text{m}\cdot\text{min}^{-1}\cdot\text{mL}^g\cdot\text{mg}^{-g}$), g , E_g (kJ/mol), k_s ($\#\cdot\text{min}^{-1}\cdot\text{mL}^{s+M_s-1}\cdot(\text{mg solution CBZ})^{-s}\cdot(\text{mg solid CBZ})^{-M_s}$), s , and M_s are kinetic parameters. These kinetic parameters are estimated by a least-square optimization algorithm which attempts to fit the PBM simulated concentration to experimental concentration. Instead of attempting to assign a weight to PSD quantiles in the objective function, product quantiles were taken into consideration as constraints to force the model to produce reasonably sized products which narrows the search range of the algorithm. The optimization problem can be described as follows:

$$\min_{k_g, g, E_g, k_s, s, E_s, M_s} \sum_i (C_{sim,i} - C_{exp,i})^2 \quad (5.2)$$

such that

$$\begin{aligned} \left| \frac{D50_{end,sim} - D50_{end,exp}}{D50_{end,exp}} \right| &< 15\% \\ \left| \frac{D90_{end,sim} - D90_{end,exp}}{D90_{end,exp}} \right| &< 20\% \end{aligned} \quad (5.3)$$

Laser-diffraction PSD measurement is more accurate in D50 and D90 measurement than D10 which is emitted in the constraints. The relative errors of D50 and D90 was bounded to 15% and 20% respectively. MATLAB function 'fmincon' (sequential quadratic programming algorithm) was used and repeated with 100 sets of randomly generated initial guesses. The confidence interval was calculated based on the gradient matrix.

5.2.2 Start-up optimization

Five continuous experiments were carried out to examine the effect of different start-up strategies on the process dynamics and steady-state product. The continuous operating conditions were identical amongst all five experiments where 240 mg/mL PCM EtOH solution was fed into the OBR continuously at 5.44 mL/min and slurry was removed intermittently from the bottom outlet of the OBR every 2 minutes using a peristaltic pump (Cole-Parmer). The volume in the OBR was maintained around 245 mL after each removal yielding a residence time of 45 minutes. Samples were taken at the end of each residence time for PSD analysis. The temperature of the crystallizer was maintained at 20°C.

Each experiment employs a different start-up strategy which is summarized in Table 5-2. Start-up1 employed linear cooling seeded batch experiment identical to Exp3 described in Table 5-1 except for 2 grams of seed was added instead of 1.7; start-up2 featured a cooling profile optimized using the kinetics obtained in this study to maximize yield and steady-state product PSD uniformity. The optimization problem is described as follows

$$\min_{t_B, \mathbf{T}_b, m_s} \text{span} - \text{yield} \quad (5.4)$$

such that

$$\begin{aligned} 15 &\leq \mathbf{T}_b \leq 43 \\ \mathbf{T}_b(\text{end}) &= 20 \\ t_B &< 240 \\ 3\% &< m_s < 10\% \end{aligned} \quad (5.5)$$

where t_B is the batch start-up duration (min) which was limited to less than 4 hours, \mathbf{T}_b denotes the batch cooling profile which was discretized from 0 to t_B and m_s represents seed loading in wt% which was constrained within 3%-10%. The batch temperature profile was limited between 15°C to 43°C and the final temperature of the batch crystallization must be 20°C. Start-up3-5 feature

direct continuous operation at the constant temperature of 20°C where the reactor was initially filled with saturated solution (139 mg/mL). Start-up3 was identical to the experiment described in section 4.2.5 where clear solution was used. Start-up4 utilized pre-sieved seeds of size 75-180 μm which was also used in kinetic parameter estimation batch experiments. Start-up5 used the steady-state product of start-up2 experiment. In Start-up4 and Start-up5 2 grams of solids were added to the initial saturated slurry.

Table 5-2 Start-up procedures of continuous crystallization experiments in the OBR

Exp#	Mode	Seed	C₀ (mg/mL)	T₀ (°C)	Cooling
Start-up1	Batch	75-180μm	240	43	Linear
Start-up2	Batch	75-180μm	240	43	Optimized
Start-up3	Continuous	No	139	20	-
Start-up4	Continuous	75-180μm	139	20	-
Start-up5	Continuous	Steady-state product	139	20	-

5.3 Results and Discussion

5.3.1 Kinetic parameter estimation

A PBM was obtained for the cooling crystallization of PCM in EtOH by fitting simulated concentration to experimental results using the experiments described in Table 5-1. Only growth and secondary nucleation were considered; The estimated growth and nucleation kinetic parameter values and their 95% confidence interval is shown in the Table 5-3. The simulated concentration profile is shown in Figure 5-1. The model predicted concentration better in slow cooling experiments. The mean square error of concentration prediction is 187.1 mg²/mL² corresponding to the mean relative error is 6.67%. D50 and D90 of the products were slightly underpredicted while D10 was overpredicted. The MSE for D10, D50 and D90 were 442.7, 154.6, 1827.4 μm² corresponding to the mean relative error were 58.7%, 9.44% and 16.1% respectively. The large

error of D10 prediction was to be expected because a constraint was not put on D10 due to its large measurement error.

Table 5-3 Estimated secondary nucleation and growth kinetic parameter values and 95% their confidence interval.

Param.	Unit	Value	95%CI-	95%CI+
k_g	$[\mu\text{m}\cdot\text{min}^{-1}\cdot\text{mL}^g\cdot\text{mg}^{-g}]$	0.22984	0.22983	0.22984
g	[-]	1.61234	1.61234	1.61235
E_g	[kJ/mol]	0.1049	0.10489	0.1049
k_s	$[\#\cdot\text{mL}^{s+M_s-1}\cdot\text{min}^{-1}\cdot\text{mg}_{\text{sol}}^{-s}\cdot\text{mg}_{\text{crys}}^{-M_s}]$	55019.9	55018.5	55019.9
s	[-]	1.89644	1.89636	1.89644
E_s	[kJ/mol]	23.0179	23.0179	23.0179
M_s	[-]	1.95543	1.95502	1.95543

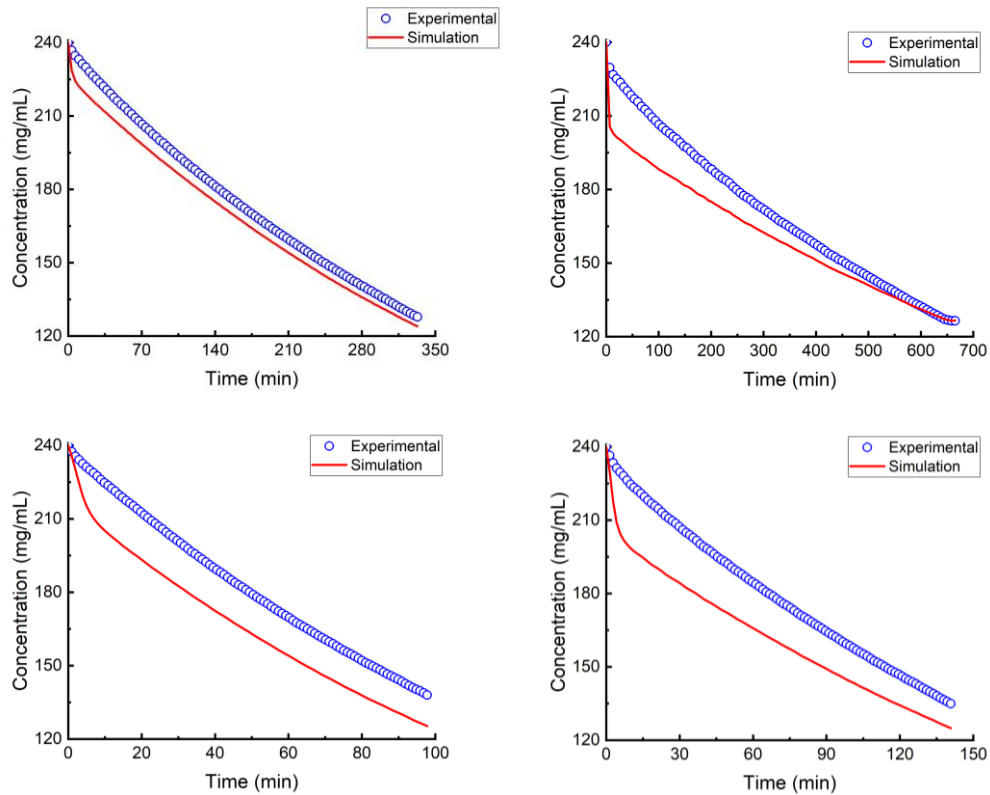


Figure 5-1 Simulated and experimental concentration profile of Exp1 (top left), Exp2 (top right), Exp3 (bottom left), and Exp4 (bottom right).

Table 5-4 Comparison of simulated and experimental batch product size quantiles

	D10(μm)		D50(μm)		D90(μm)	
	Exp	Model	Exp	Model	Exp	Model
Exp1	30.30	48.23	115.3	100.1	242.4	191.4
Exp2	36.52	50.14	104.8	104.0	224.4	174.3
Exp3	36.20	63.14	117.4	103.7	207.5	202.8
Exp4	36.21	59.36	115.6	101.7	247.6	200.9

PCM growth kinetics in EtOH have also been studied in STCs by Worlitschek and Mazzotti (2004) [196] and Mitchell et al. (2011) [153], [202] the results of which are converted into the units used in this study and shown in Table 5-4. A comparison of growth rates simulated at various supersaturation and temperature is shown in Figure 5-2 which suggests fast growth in the OBR possibly due to the gentler mixing dynamics. However, the PBM obtained in this model has not been verified and validated based on its risks. Further studies are required to make a confident conclusion.

Table 5-5 Growth kinetic parameters comparison to literature values.

	OBR	Worlitschek and Mazzotti	Mitchell et al.
k_g	0.2298	69.42	453.375
g	1.612	1.9	1.602
E_g	0.1049	41.6	40.56

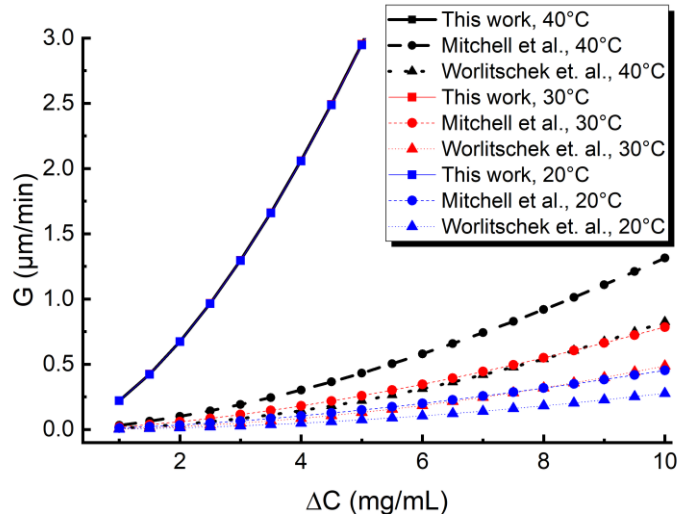


Figure 5-2 A comparison of growth rates of various absolute supersaturation and temperatures obtained in this work and from literature.

5.3.2 Model guided batch start-up optimization

The PBM model obtained was used to optimize a batch crystallization as the start-up procedure for start-up experiment 2. The duration of the batch start-up procedure was allowed to vary to obtain an optimized solution. The optimized operating temperature and the simulated concentration, particle count (0^{th} moment, noted as μ_0) and D50 are plotted in Figure 5-3. ‘Negative’ residence times indicate the batch start-up procedure which was optimized to be approximately 227 minutes while the seed loading was optimized to be approximately 5% (2 grams of seed) which is the same as the batch procedure in start-up experiment 1. At time zero, continuous feed was initiated by the model and the removal was assumed to be constant which has been shown mathematically equivalent to intermittent removal [117]. According to the simulation, particle count persisted to decrease while D50 increased steeply suggesting severe particle washout. The nucleation rate was likely underpredicted for continuous operation considering that the kinetic parameters were obtained with batch experiments. However, the optimized batch cooling profile has potential to produce uniform steady-state product because the particles at the end of the batch

procedure are large and uniform in size. The optimized batch cooling profile features fast cooling followed by slow cooling followed by a small heating cycle and eventually slow cooling to 20°C promoting growth and fines dissolution. Therefore, even though the model may not have made reliable prediction of continuous operation, it is worthwhile to compare with a fast cooling batch start-up procedure noted as start-up4 in Table 5-2.

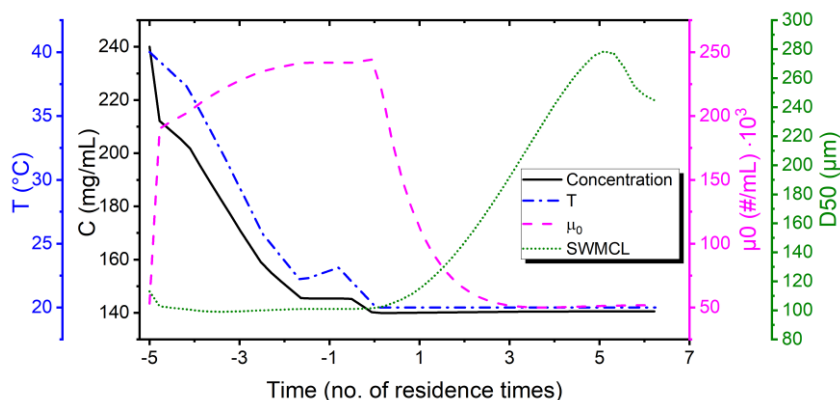


Figure 5-3 Simulated Start-up5 concentration, particle count (μ_0), and D50 profile applying the optimized start-up batch cooling procedure.

5.3.3 Experimental start-up strategy comparisons

Carrying out a batch crystallization first can be a plausible start-up strategy because many techniques can be applied to manipulate the end batch product which serves as seed during continuous operation. It can be especially beneficial if the model compound is not readily available in the desired crystalline form. Two batch start-up strategies were tested in this study: a fast-linear cooling experiment and an optimized experiment using the temperature profile described in section 5.3.2. The temperature, concentration, total particle count and SWMCL are shown in Figure 5-4. ‘Negative’ residence times represents the batch start-up procedure. During fast cooling start-up, the particle count quickly increased but a steady count was not reached before the start of continuous operation at ‘time zero’. A slight particle washout is observed at the beginning of the

continuous operation where total particle count decreased followed by a slow increase. Meanwhile SWMCL slightly increased followed by a sharp decrease and eventually oscillated to stability. The same dynamics can be clearly observed in the optimized batch start-up procedure. A zoom into residence time 0-2 is shown in Figure 5-5 during which particle washout took place immediately after the initiation of continuous operation resulting in particle count decrease. This is likely caused by the high solid concentration of crystals at the end of the batch procedure. High particle loading can result in growth promotion and nucleation suppression which also explains the SWMCL increase. As particle was being carried out of the vessel, nucleation was no longer suppressed thus the particle count increased accompanied by the sharp SWMCL decrease. As continuous operation carries on, nucleation and growth dynamic eventually stabilized around 3 residence times in experiment 1 and approximately 4 residence times in the second experiment. Both maintained very similar steady-state concentration. The steady-state products medium size and span were similar as shown in Table 5-6: Start-up1 yielded D50 of 110 μm and span of 1.72 while Start-up2 produced steady state product of 115 μm and 1.64 span as summarized in Table 5-6. As the objective function aimed to maximize yield and minimize span, indeed the span was slightly improved than fast linear cooling batch start-up procedure at a hefty price of 135 minutes longer in batch duration.

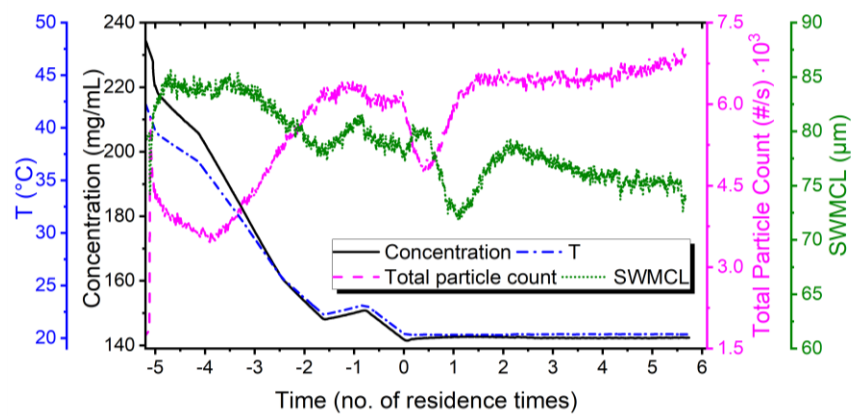
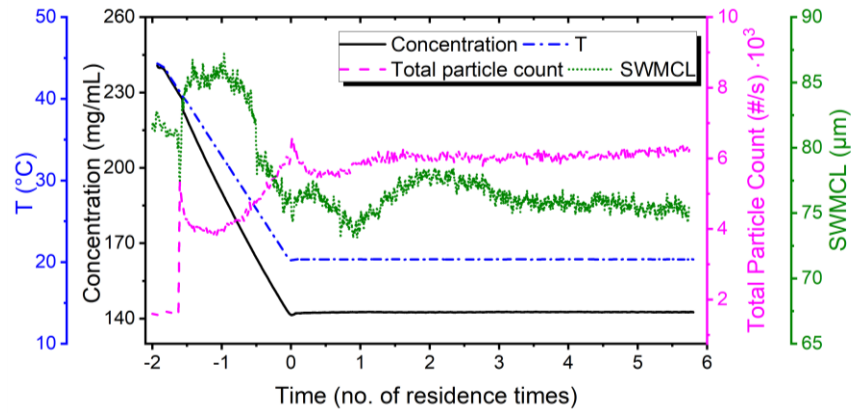


Figure 5-4 Concentration, temperature, total particle count and SWMCL profile overtime of Start-up1 (top) and Start-up2(bottom).

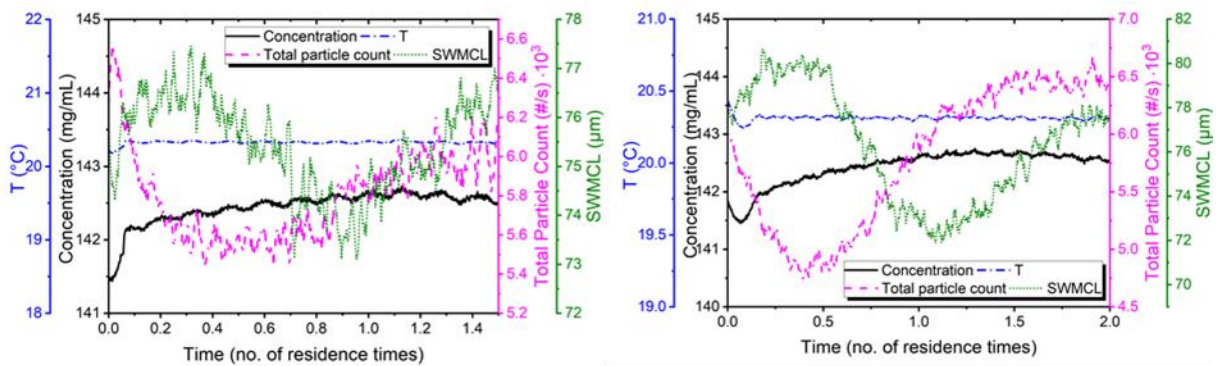


Figure 5-5 Zoom in operating profile of 0-2 residence times of Start-up1 (left) and Start-up2(right).

Direct continuous operation start-up strategies are also a popular choice. Three different strategies were tested in this study featuring the initial vessel filled with clear saturated solution,

sieved raw material suspension in saturated solution and previous continuous crystallization product (Start-up2) suspension in saturated solution listed in Table 5-2 as Start-up3, 4 and 5 respectively. The temperature, concentration, total particle count and SWMCL are shown in Figure 5-6. An FTIR was used to measure the concentration in Start-up3 and 4 and an in-situ UV was used in Start-up5. No feed or slurry removal was performed during ‘negative’ residence times. Start-up3 was unseeded, thus as continuous operation began, particle count remained at zero while concentration increases until primary nucleation was triggered. Concentration and FBRM measurement eventually reached stability around 4 residence times. Start-up4 started with sieved seeds suspended in saturated solution. The suspension was given time stabilize before continuous operation during which Ostwald ripening or agglomeration possibly took place indicated by the particle count decrease. A slight washout can be observed at the beginning of continuous operation as supersaturation was just starting to build up. Significant nucleation was triggered at 0.5 residence times which was slightly earlier than Start-up3. The initial solution in Start-up3 was slightly supersaturated which triggered nucleation earlier in time but at larger supersaturation than Start-up4 or 5. Primary nucleation requires a larger activation energy barrier. The washout was the least significant in Start-up5 likely due to that the steady-state product balanced nucleation and washout to establish an operating state similar to that of steady state operation. Start-up5 drove the system quickly to steady-state in about 3 residence times displaying a smooth operating profile without intense process dynamics.

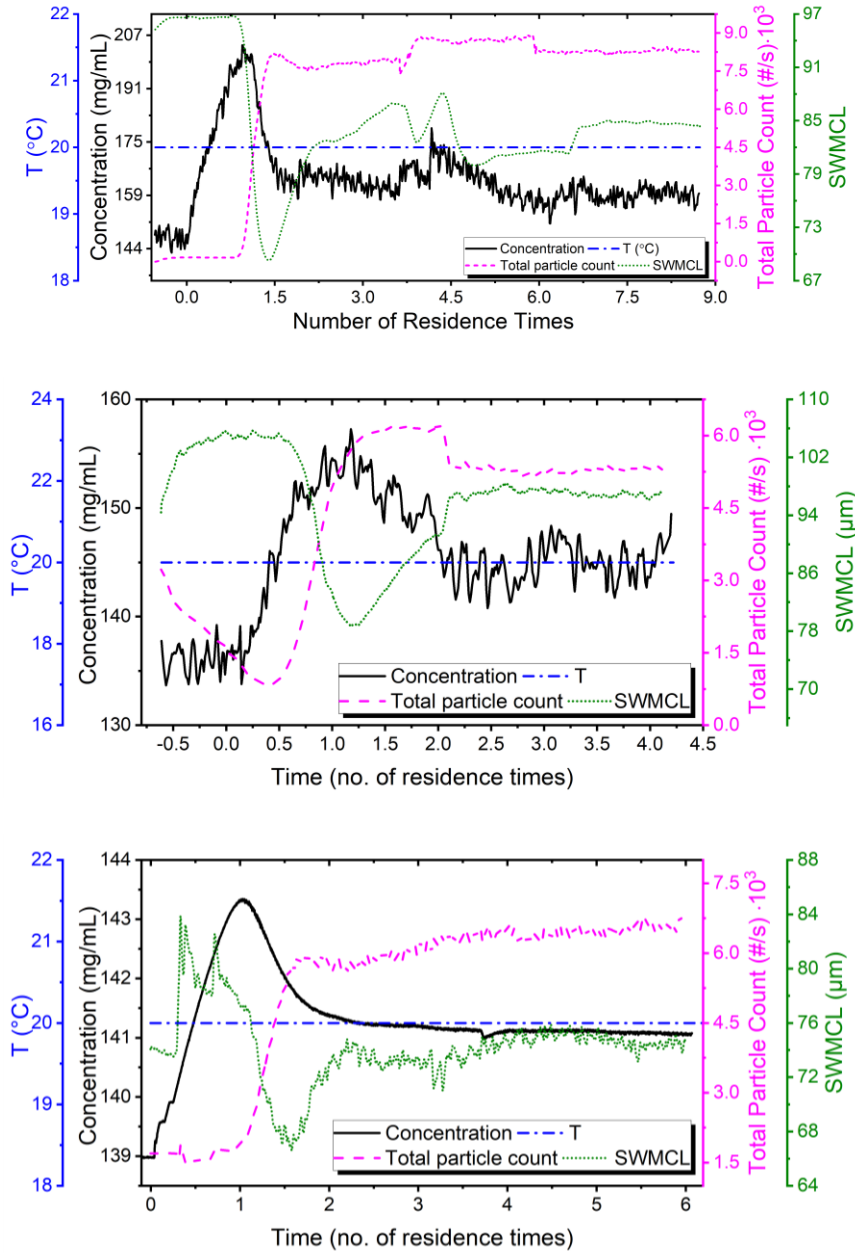


Figure 5-6 Concentration, temperature, total particle count and SWMCL profile overtime of Start-up3 (top), Start-up4 (middle) and Start-up5 (bottom).

The steady state product of Start-up4 and 5 were similar in medium size which were 111 µm and 117 µm as well as span which were 1.73 and 1.69 respectively. Both improved in uniformity compared to the unseeded start-up strategy in Start-up3 which produced steady state product of 115 µm D50 and 1.85 span. The detailed size quantiles and span are summarized in

Table 5-6. Primary nucleation resulted in larger number of fines and is generally undesirable. However, if premade seeds are not available, it is still a reasonable strategy which produced slightly less uniform products.

Table 5-6 Medium size (D50) and span of samples taken at various residence times (RT) of start-up experiments 1-5.

		1RT	2RT	3RT	4RT	5RT	6RT	7RT
Start-up1	<i>D50</i>	117	105	110	110	110	110	-
	<i>Span</i>	1.72	1.81	1.71	1.71	1.71	1.72	-
Start-up2	<i>D50</i>	126	100	105	117	105	115	-
	<i>Span</i>	1.55	1.97	1.71	1.69	1.76	1.64	-
Start-up3	<i>D50</i>	-	81.5	-	-	102	-	115
	<i>Span</i>	-	1.94	-	-	2.09	-	1.85
Start-up4	<i>D50</i>	-	-	-	-	110.6	-	-
	<i>Span</i>	-	-	-	-	1.73	-	-
Start-up5	<i>D50</i>	-	125	122	105	116	117	-
	<i>Span</i>	-	1.53	1.65	1.73	1.71	1.69	-

Taking all five start-up strategies into consideration, it took approximately similar amount of time to reach steady-state despite gentle or severe particle washout and produced products of similar size and uniformity. While continuous crystallization processes may generally present different steady states with different start-up procedures due to potential multiplicity, the particular system studied in this study did not exhibit such behavior. This is likely because the time scale of PCM nucleation and growth is much shorter than the residence time which also prevented periodic particle washout and nucleation.

Looking closely at steady state yield and product size uniformity, Start-up 2 which featured a computationally optimized batch cooling profile produced the highest yield and lowest span which was the optimization objective, but not by a significant amount at the price of a long batch duration which may be undesirable. On the other hand, Start-up5 featuring direct continuous operation with Start-up2 steady state product as seed produced products of the second lowest span

with the gentlest washout event. A smooth operating profile can be desirable to prevent sedimentation, pump failure and excessive fines. It can also be a preferred procedure for control strategy implementation or digitalization.

5.4 Conclusion

Start-up strategies were investigated in this study for the continuous cooling crystallization of PCM in the OBR. Five different strategies were explored: two featured batch start-up procedures including one batch optimized using kinetic parameters obtained with batch experiments carried out in the OBR; and the other three featured direct continuous operation. Batch start-up procedures caused washout at the beginning of continuous operation due to the suppressing effect of heavy solid concentration has on secondary nucleation. Overall, the optimized start-up strategy indeed resulted in highest yield and most uniform PSD but not significantly at the price of significantly longer start-up duration. Direct continuous operation featuring steady state products of a prior continuous experiment yielded the smoothest operating profile producing products of similar uniformity. It may be the most desirable for control framework implementation.

6. DEVELOPMENT OF CONTINUOUS FILTRATION IN A NOVEL CONTINUOUS FILTRATION CAROUSEL INTEGRATED WITH CONTINUOUS CRYSTALLIZATION

6.1 Introduction

Filtration has long been developed through practical and empirical knowledge instead of mechanistic understanding because of the complex nature of filter cake formation.[203], [204] Bench-scale vacuum filtration setups are often used during development to gain some empirical understanding of the slurry which may be unrepresentative of large scale behaviors. At manufacturing scale, filtration usually takes place in batch equipment of large and complicated geometry introducing greater uncertainties because of the complex interaction between the slurry feed and the complicated moving parts. Filtration performance is often characterized by the product moisture content which assesses the liquid removal during filtration. As the inseparable counterpart to crystallization, it is also important to assess the impact on particle properties such as product particle size distribution (PSD), particle morphology and polymorphism if applicable. Washing of the filter cake is a common practice to strip impurities, redissolve undesirable fine particles and to prevent filter media fouling [147], [205]–[207]. Continuous filtration is a relatively new area of study in the pharmaceutical industry and only a small number of publications on this topic have been found. Yazdanpanah et al. (2016) studied a novel falling film continuous crystallization technique that combines crystallization and removal of solvent in one step that separates crystals from their mother liquor to form a solid film. The crystalline film was then subsequently redissolved for purification purposes and the film could not be continuously collected as isolated solid products. Gursch et al. (2015 [208] & 2016 [209]) studied a small-scale cross flow membrane filtration device that utilized a high rpm rotor to drive filtration. The authors found a

material-specific linear relationship between the feed and permeate rate. However, the high shear of the motor may be unsuitable for brittle particles. The filtered filter cake layer also requires manual removal after concluding the operation.

To address this gap of the integration of continuous crystallization and filtration, a novel prototype continuous filtration carousel (CFC) is studied in conjunction with the OBR to develop a true continuous API separation step where supersaturated solution is crystallized and subsequently filtered to obtain the API in solid form continuously. The CFC consists of a small slurry drawing cell and a rotating multi-port filtering body to transfer and filter slurries continuously under vacuum. The unique vacuum facilitated slurry draw scheme, similar to that of a pressure-swing MSMPR transfer zone[116], is especially beneficial for direct coupling with crystallization to prevent transfer line fouling. It is also equipped with automated washing and cleaning-in-place (CIP) capabilities to prevent process shutdown due to filter fouling. This is an update to a previous version of the CFC that utilizes gravity for slurry transfer which requires an elevated hold-up tank. Our colleagues carried out a proof-of-concept study to demonstrate the feasibility of coupling the CFC (previous version) with continuous crystallization. Successful operation of integrated continuous crystallization and filtration of PCM and benzoic acid was demonstrated [15].

In this updated study, it is aimed to investigate CFC operating parameters and their effects on filter cake qualities via stand-alone filtration studies. PCM and benzoic acid are also used as model systems to investigate CFC performance on compounds of vastly different shape, size and crystallization procedures. Furthermore, direct coupling of CFC and the continuous crystallization without a hold-up tank are demonstrated using the optimal process parameters obtained during filtration experiments.

As the pharmaceutical manufacturing sector starts to adopt the quality-by-design approach, risk management becomes the ‘centerpiece’ when developing and evaluating a new or updated process[3], [148]. It can be of great values to consider potential risks of a novel technology even at its early development stage. Here a short discussion is carried out on the risk considerations of continuous filtration operations in hopes to encourage its application in the pharmaceutical industry to advance the transformation from traditional batch to end-to-end continuous manufacturing of oral solid dosage form drugs.

6.2 Experimental Methods and Material

6.2.1 Materials

Two model compounds were selected to study the integration of continuous crystallization and continuous filtration. Paracetamol (PCM, Alfa Aesar, 98.0% purity) in ethanol (EtOH, 200 proof, Decon Labs) is the first model system selected for its filterability: PCM crystals are of prism-like cubic shape which is less likely to cause fouling and EtOH is volatile and easy to dry. To challenge the CFC, benzoic acid (BA, Fisher Scientific Education, 99% purity), EtOH and water mixture was selected as the second model system: BA crystals are of plate-like, elongated shapes which are much more difficult to filter and the addition of water as antisolvent poses an extra challenge for drying.

6.2.2 System setup

The continuous filtration carousel (CFC, Figure 6-1) is a prototype product designed and manufactured by Alconbury Weston Ltd (AWL). The main filter body as illustrated in Figure 6-1Figure 2-33b consists of 5 ports with ports 1-4 covered by a Poremet metal filter at the bottom. During automated operation, the CFC utilizes vacuum to transfer slurry into the charge cell which is located higher than the filter carousel as well as the upstream vessel. A check valve is placed

between the inlet tubing and the charge cell which opens for a set time (noted in this study as ‘charge time’) allowing a certain amount of slurry to be drawn. Once it closes, the slurry drawn up the inlet tubing falls back into the upstream vessel while slurry already drawn into the charge cell remains in the charge cell. The pinch valve is subsequently opened allowing slurry in the charge cell to fall into port 1. In the meantime, wash solvent is dispensed into port 2 for a set time determined by the user (noted in this study as ‘wash time’). Wash time determines the amount of wash solvent dispensed into the carousel. Port 3 is blanked at the inlet during normal operation but is connected to the cleaning solvent tank and is utilized for CIP procedure when the filter mesh is fouled which can be detected by the pressure sensor installed at the filter mesh. During automated CIP, slurry is no longer drawn into the system, but the same filtration time is performed until all 4 ports are emptied followed by high flowrate washing of the filter body with CIP solvent while the filter rotates clockwise continuously for four revolutions. Port 4 is blanked off completely but allows extra time for drying. Vacuum is applied under the filter mesh to remove filtrate/solvent and air-dry the filter cakes residing in port 1-4. The vacuum pressure can be controlled by the regulator equipped on the vacuum pump. However, the vacuum is established in the filtrate receiver vessel and therefore is not tightly maintained during operation. Then the carousel is rotated one index counter-clockwise i.e. port 1 becomes port 2 for wash, port 2 becomes port 3 etc. Port 5 is equipped with a piston at the top to push the filter cake into the collector vessel at the bottom. EtOH is used for washing and CIP for both model systems in order to lessen or prevent filter mesh fouling. For clear notation in this work, one clock-wise rotation will be referred to as a ‘step’ and a full revolution (i.e. material traveling from port 1 to being pushed out at port 5) will be referred to as a ‘cycle’. The time between each step is determined by the vacuum time set by

the user and the cycle time is the residence time of the continuous filtration process which is approximately four times the vacuum time.

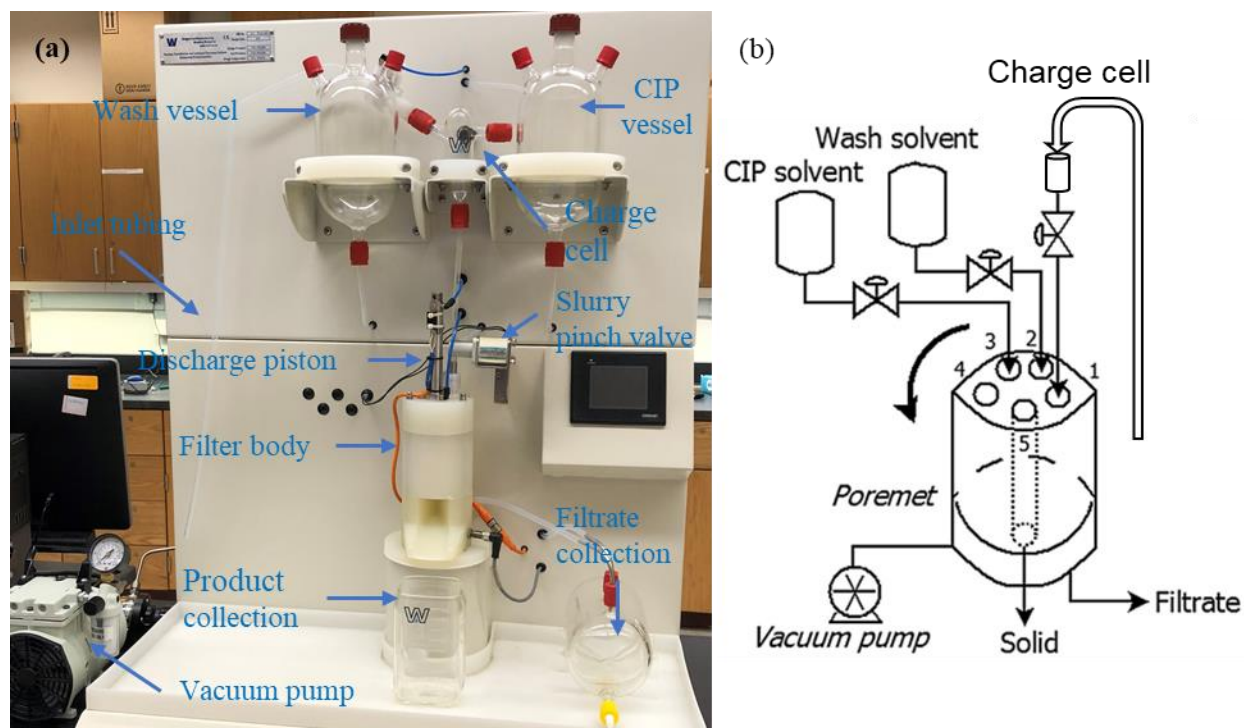


Figure 6-1 (a) A picture and (b) schematics of the continuous filtration carousel (CFC) used in this study manufactured by AWL.

6.2.3 Filtration experimental methods

Six stand-alone filtration experiments using premade slurries were performed to evaluate CFC performance for each model system. The slurries were made via batch crystallization experiments: PCM slurries were produced via unseeded batch cooling crystallization experiments where concentrated solution (240 mg PCM/1 mL EtOH) was cooled from 45°C, its saturation temperature, to 20°C at the cooling rate of 0.3°C/min. All PCM crystals produced in this study are of the stable polymorphic form (form I); BA crystal slurries were obtained via a semi-batch anti-solvent crystallization experiment where antisolvent (water) was added to concentrated BA EtOH solution (360 mg BA/1 mL EtOH) over 90 minutes. At the end of the batch experiment the solvent to anti-

solvent ratio (SASR) which is defined as the volume ratio of EtOH to water, reached 0.23. Solubility data for PCM in EtOH and BA in water-EtOH were obtained from the literature [14], [196], [210]. Vacuum time and wash time were varied to investigate their effects on the properties of the filter cake as shown in Table 6-1. The filtration time was varied between 1 -2 minutes which is consistent with idle time duration of intermittent product removal commonly practiced in continuous crystallization studies.[14] The amount of slurry drawn in each step was determined based on the coupled crystallization experiment flow rate which will be described in section 6.2.4. During each filtration experiment, samples were collected every cycle for moisture content analysis using a Veritas A64M moisture balance. At the end of each experiment, a small sample was drawn from all filtered products collected during the experiment for PSD measurement using dry-dispersion laser diffraction (Malvern Mastersizer 3000 Aero S). The order of experiments was randomized. A bench vacuum filtration of the same slurry was also performed for each experiment using a Synthware Buchner filter funnel (150mL fine) for filter product size comparison.

Table 6-1 Experimental conditions of the stand-alone filtration experiments of PCM and BA systems.

Exp#	Filtration Time (min)	Slurry Drawn per Step (mL)	Wash time (min)
Exp1	1	5.4	0.5
Exp2	1	5.4	1
Exp3	1.5	8.17	0.5
Exp4	1.5	8.17	1
Exp5	2	10.8	0.5
Exp6	2	10.8	1

6.2.4 Integration of crystallization and filtration

The coupling of continuous crystallization and filtration was achieved by connecting the CFC directly to the OBR (described in section 4.2.1) through its overhead port as shown in Figure 6-2. Both PCM and BA model systems were examined with a continuous experiment using the coupled

OBR-CFC system. Both continuous experiments feature continuous feed and intermittent product removal with the CFC. The volume in each experiment was maintained at approximately 245 mL after each removal and the residence time of each experiment was 45 minutes. In the PCM experiment, 240 mg/mL PCM EtOH solution was fed into the vessel at 5.45 mL/min continuously via a peristaltic pump (Cole-Parmer). Feed solution is saturated at 45°C and the OBR is maintained at 18°C during continuous operation which is slightly lower than room temperature to prevent further crystallization in the CFC or in the transfer tubing. An unseeded batch cooling crystallization was carried out as the start-up procedure: 245mL of 240 mg/mL PCM solution was cooled linearly from 45°C to 18°C at 0.3°C/min without seeding. The crystals produced during batch serve as seed for subsequent continuous operation. For BA, the same semi-batch anti-solvent crystallization experiment described in section 6.2.3 was performed as the start-up procedure followed by continuous operation. Concentration BA EtOH (360 mg/mL) and water were fed into the crystallizer at 1.23 mL/min and 4.21 mL/min respectively to achieve the SASR of 0.23 [14].

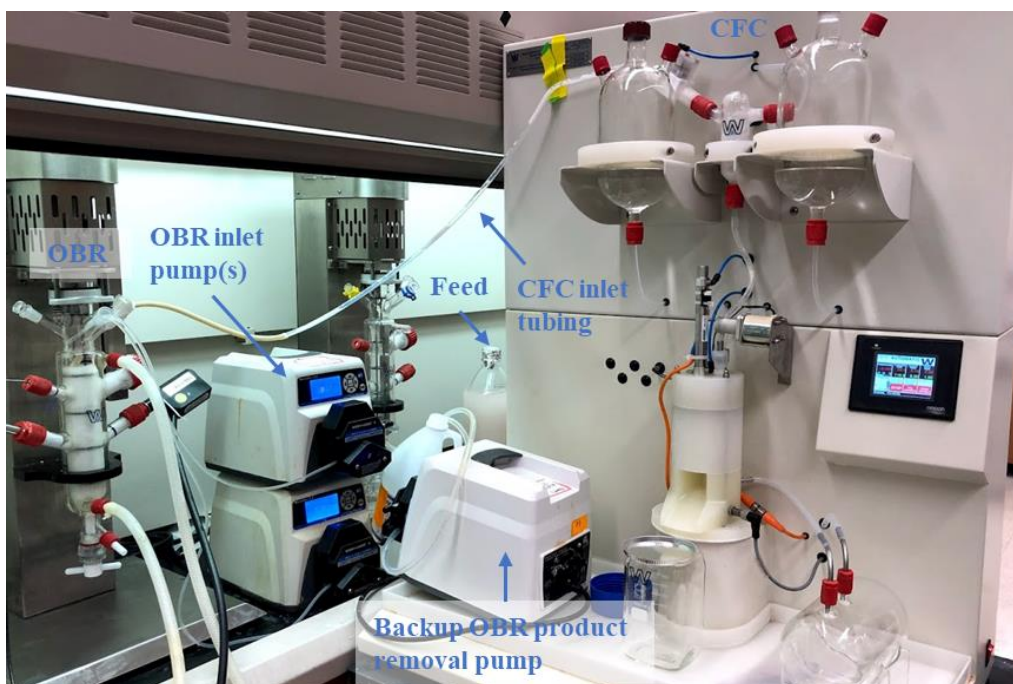


Figure 6-2 Coupled continuous crystallization and filtration system set-up.

For both model systems, crystallization slurry was directly removed by the CFC drawing scheme where a certain amount of slurry was drawn intermittently. The amount of slurry withdrawn in each step was calculated to achieve the optimal filtration time based on the results of the stand-alone filtration experiments which will be discussed in section 6.3.1. An additional peristaltic pump was implemented to remove slurry in the same fashion as the CFC drawing scheme during the first two residence times and during automated CIP when filter fouling is detected as the CFC drawing scheme is disabled during CIP for one full cycle in addition to the CIP time period. At the end of each residence time, a sample is collected at the outlet of CFC for moisture content and PSD analysis. All solid products were collected and dried to calculate yield. A summary of the start-up and continuous operation conditions is listed in Table 6-2.

Table 6-2 Start-up and continuous operation conditions of the coupled crystallization and filtration experiment for PCM and BA systems.

	Compound	PCM	BA
Start-up Conditions	Initial T/SASR	45°C	20°C, ∞
	End T/SASR	18°C	20°C, 0.23
	Cooling/Antisolvent Addition Rate	0.3°C/min	2.26mL/min
	Feed Conc (mg/mL)	0.24	0.36
	Feeding rate (mL/min)	5.34	BA solution: 1.23; water: 4.21
Continuous Operation	Crystallizer volume (mL)	245	245
	Residence time (min)	45	45
	Crystallizer T/SASR	18°C	20°C, 0.23
	CFC slurry drawn per step (mL)	8.17	10.8
	CFC vacuum time per step (min)	1.5	2
	CFC wash time (s)	0.5	1

6.3 Results and Discussion

6.3.1 Filtration experiments

The effect of filtration time and wash time was investigated for both PCM-EtOH and BA-EtOH-water slurries using the experiments summarized in Table 6-1. The moisture content of each

experiment is plotted in Figure 6-3. The moisture content of PCM products were all under 10% which are comparable or less in comparison with experiments carried out in the precedent CFC prototype [15]. Changing the vacuum time did not affect the moisture content significantly. The cake resistance, or the material flux across the filter, is similar if the slurry properties and vacuum pressure are similar (assuming the cake is incompressible) [211] which yields linear proportionality between filtration time and cake height. Therefore, the moisture content was predictably unaffected as slurry drawn per step was proportionally changed with changing vacuum time to match the flow rates of coupled experiments described in section 6.2.4. Increasing the wash time slightly worsen the filter cake moisture content for vacuum time 1-minute and 1.5-minute experiments because more solvent would take longer to dry whereas increasing wash time from 0.5 to 1 second barely affected 2-minute vacuum time experiments likely because such a small increase was insignificant compared to the large filter cake volume.

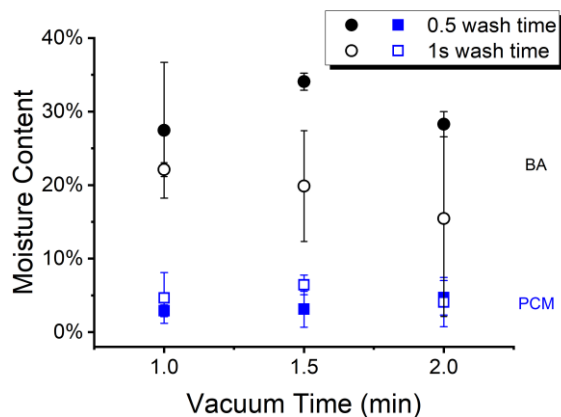


Figure 6-3 Moisture content of the filter product with various vacuum times and wash times for PCM and BA slurries.

On the other hand, BA experiments yielded moisture content between 15% - 35% which are similar or less compared to literature [15], BA products had much higher moisture content than PCM as a result of the added water which is more difficult to dry. Increasing the wash time

significantly improved the moisture content in the filter cakes because EtOH was able to dissolve fines that were fouling and blocking the filter mesh while increasing the overall volatility of the liquid. Changing the vacuum time also did not result in significant changes in moisture content.

Another important factor to consider when evaluation filtration performance is its effect on the product PSD. Because the slurry was produced via crystallization, the resulting crystal size distribution is difficult to measure directly. A typical bench vacuum filtration followed by oven drying was performed with the same slurries of the CFC experiment to obtain isolated crystal products for PSD analysis. The D50 and span comparison between the CFC products and bench filtration products is shown in Table 6-3. Microscopic images are shown in Figure 6-4.

Table 6-3 D50 and span comparison of the CFC and bench vacuum filtration products for both PCM and BA experiments.

		Exp#	Exp1	Exp2	Exp3	Exp4	Exp5	Exp6
		Vacuum Time (min)	1.0	1.0	1.5	1.5	2.0	2.0
		Wash Time (s)	0.5	1.0	0.5	1.0	0.5	1.0
PCM	CFC Product	D50 (µm)	104	105	122	97	126	107.3
		Span	2.10	1.87	1.70	1.90	1.72	1.86
	Bench Product	D50 (µm)	93.0	94.8	93.6	94.8	93.6	95.9
		Span	1.59	1.81	1.74	1.81	1.74	1.66
BA	CFC Product	D50 (µm)	58.4	-	46.1	41.3	53.6	49.7
		Span	1.95	-	2.01	2.68	2.14	1.94
	Bench Product	D50 (µm)	54.5	-	41.2	53.6	54.5	47.3
		Span	1.87	-	1.75	2.14	1.87	1.78

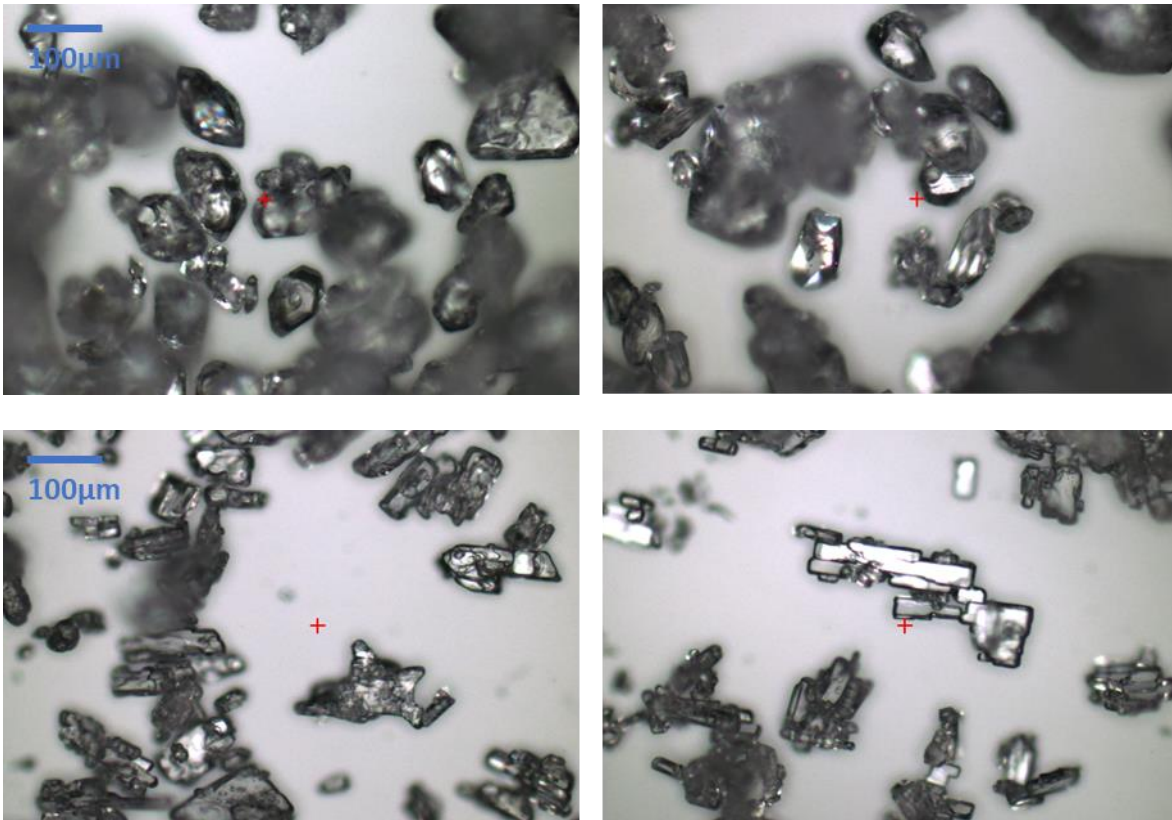


Figure 6-4 Microscopic images of CFC filtered and moisture balance dried PCM crystals (top row) and BA crystals (bottom row).

Compared to bench vacuum filtered products, CFC products generally had larger medium size due to washing. EtOH is a strong solvent for both PCM and BA which dissolved fines during washing and therefore lead to larger PSDs. PCM CFC products yielded comparable uniformity (span) compare to bench products whereas BA CFC products were generally less uniform than bench filtration. Benzoic acid crystals often agglomerate when an anti-solvent like water or toluene is present [94], [135], [212] because of fine particle generation and its elongated particle geometry as observed in Figure 6-4. In addition, the cake in the chamber had limited drying time and was handled with various mechanical force which also promotes agglomeration. Bench vacuum filtration on the other hand allows more area for even drying resulting in less agglomeration. The heavy agglomeration during CFC operation caused wide and even bimodal PSD of BA products.

However, this can be easily improved by implementing a drying step as opposed to fast drying in the moisture balance. PCM on the other hand are more cubic in shape resulting in less agglomeration and moisture detention.

Increasing the washing time from 0.5 to 1 second resulted in smaller, less uniform products for most PCM experiments. During 1 second washing, the washing solvent was not thoroughly drawn through the filter cake. The excess EtOH possibly caused some crystallization by evaporation in addition to washing away fines which led to more fine generation than 0.5 second washing time experiments. PCM CFC experiment 1 and 2 are an exception because the product recovered was of such little amount that Mastersizer laser signal was unstable which is also the case for BA CFC experiment 1 and 2. Therefore a conclusion cannot be drawn with confidence for vacuum time of 1 minute. BA CFC experiment 2 product was of such little amount and so heavily agglomerated that the Mastersizer was not able to obtain a reading. In other BA CFC experiments, the washing time effects on product PSD were not very significant. However, increasing the wash time largely improved filter fouling. During BA experiments 1,3, and 5, filter fouling was detected, and auto-CIP was initiated after about 30-40 minutes of operation whereas auto-CIP was not required during experiments 2,4,6 in the 60-80 minutes operation time tested. The de-fouling effect of washing also explains why increasing wash time resulted in less moisture content for BA experiments. Without periodic washing and solid removal, traditional bench vacuum filtration is much more prone to fouling and process failure. In comparison, no filter fouling incident was observed during PCM experiments. Changing the vacuum time did not have significant effects on product PSDs or moisture content.

Taking both moisture content and product PSD results into consideration, an optimal set of operating conditions can be picked for both PCM and BA systems. PCM experiment 3 (vacuum

time 1.5 minutes, wash time 0.5 second) yielded the most uniform PSD with one of the lowest moisture contents and thus is selected as the optimal condition. In BA experiments, experiment 6 (vacuum time 2 minutes, wash time 1 second) was the best performing experiment. Therefore experiment 3 and 6 were selected for following coupled experiments of PCM and BA systems respectively as indicated by Table 6-2.

6.3.2 Integration with continuous crystallization

A coupled continuous crystallization process in the OBR and continuous filtration in the CFC was demonstrated using the selected conditions from the stand-alone experiments for both PCM and BA crystallization systems. Concentration (in terms of UV peak height at 250 μm), particle count, square-weighted mean chord length (SWMCL) and temperature (T) profiles of PCM experiment are shown in Figure 6-5. ‘Negative’ residence times represent the batch startup procedure and time zero indicates the start of continuous operation. During the first two residence times, peristaltic pumps were used to feed continuously and remove slurry intermittently every 1.5 minutes. Concentration slightly raised at time zero as continuous feed initiated while FBRM count remained relatively constant. As coupled CFC operation started at the beginning of the second residence time, SWMCL sharply decreased as total particle counts increased while concentration remained unaffected. This is likely due to the more effective drawing scheme of the CFC which removed large particles that the peristaltic pump was not removing effectively. Peristaltic pump driven product removal leaves slurries stagnant when idle which burdens the pump during active slurry removal. During coupled OBR-CFC operation, steady state quickly established around 4 residence times with some periodic disturbances on the concentration because of the level oscillation in the OBR. This is caused by the CFC overdrawing at the beginning of each step after which, the slurry falls back into the crystallizer as described in section 6.2.2a. As a result, the level in the OBR fell

and raised in a larger range than the peristaltic pump removal scheme. However, the system operated in a state of control where concentration and particle count was able to recover after each disturbance which is a more appropriate term to describe the steady operation of continuous processes [10], [23], [100].

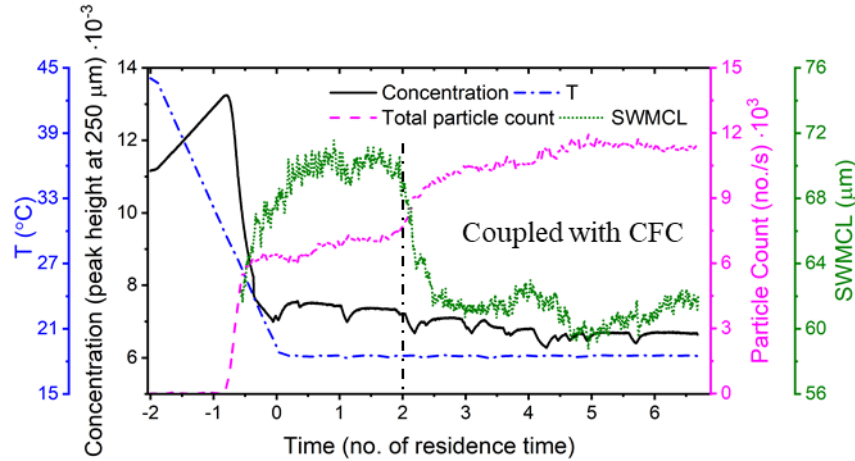


Figure 6-5 Operating profile of continuous crystallization of PCM in the OBR.

Samples are collected at the outlet of the CFC periodically for moisture content and PSD analysis, the results of which are shown in Figure 6-6. Product moisture content, medium size and span stabilized after approximately 4 residence times which is consistent with the process dynamics in the crystallizer. The state-of-control values of product moisture content (~5%), D50 (~170 μm) and PSD span (~1.3) are also comparable with the stand-alone CFC experiment 3. A total of 34.3g of CFC-filtered and oven-dried products was obtained in the last three residence times reaching a ‘steady-state’ yield around 47.6% as defined below

$$\text{yield}\% = \frac{\text{crystal obtained}}{\text{max amount of crystal possible}} \cdot 100 = \frac{m_{\text{collected}} / t_{\text{collection}}}{\dot{Q}_{\text{in}} \cdot (C_f - C_{\text{sat}} @ 18^\circ\text{C})} \quad (6.1)$$

where $m_{\text{collected}}$ stands for the mass of crystal collected (mg) in a period of time during state-of-control operation denoted as $t_{\text{collection}}$ (min), \dot{Q}_{in} represents inlet volumetric flow rate (mL/min), C_f denotes feed concentration (mg PCM/mL solution) and C_{sat} stands for saturation concentration

(mg PCM/mL solution). No filter fouling was detected and thus CIP was not required during operation. Unconsumed supersaturation in the OBR, solid lost in the crevices of the CFC, and solid lost due to human error during sample handling are all possible explanations of yield lost.

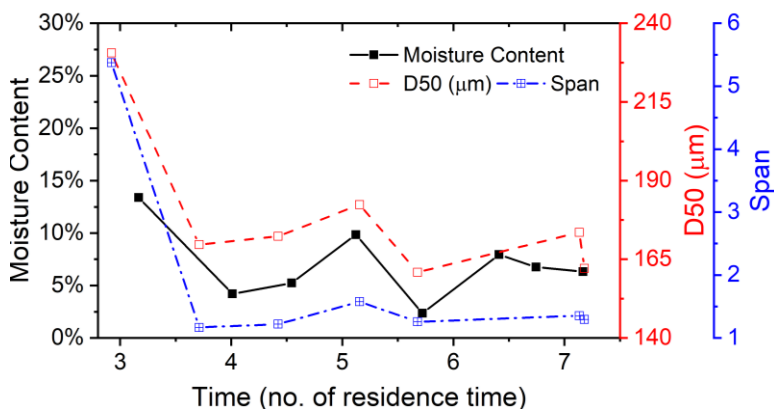


Figure 6-6 Coupled CFC product moisture content, D50 and span of PCM.

Concentration (in terms of UV peak height at 220 μm), particle count, SWMCL and calculated SASR profiles of the BA experiment are shown in Figure 6-7. Samples are collected at the outlet of the CFC periodically for moisture content and PSD analysis, the results of which are shown in Figure 6-8. Similar to the PCM experiment, ‘negative’ resident times represents the semi-batch start-up procedure and at around two residence times, CFC operation was initiated. Because of the strong tendency of BA crystal to agglomerate with water, the peristaltic pump was not able to remove slurries effectively. The idle BA slurries completely blocked the outlet tubing several times and slurry had to be removed manually by releasing the tubing from the pump gear. Once the CFC was coupled, the vacuum driven drawing scheme was able to transfer slurries from the OBR much more efficiently without blockage issue however it caused even larger level variation than the PCM experiment because of the 2-minute vacuum time (10.8 mL/step filtration rate). This caused particle count and SWMCL in the OBR unable to maintain a controlled state. However, concentration, product moisture content and D50 were relatively unaffected after 4 residence times.

The product high moisture content observed in this experiment was also consistent with stand-alone CFC experiments and can be attributed to the difficult particle morphology of BA. Heavy agglomeration, as also observed during stand-alone experiments (Figure 6-4), broadens the product PSD. The low medium product size was consistent with stand-alone experiments and is generally expected in continuous anti-solvent crystallization processes of difficult-to-grow compounds such as BA. A total of 22.5 g of CFC filtered, oven dried BA product was obtained in the last three residence times attaining a yield of 47.0%.

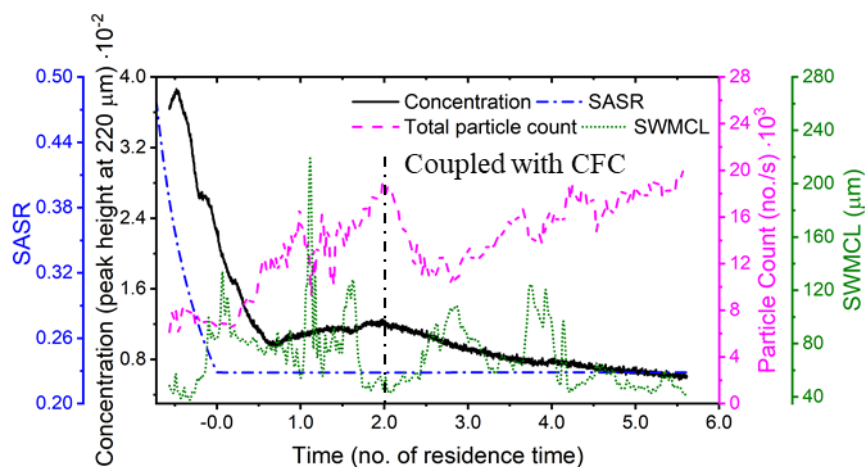


Figure 6-7 Operating profile of continuous anti-solvent crystallization of BA in the OBR.

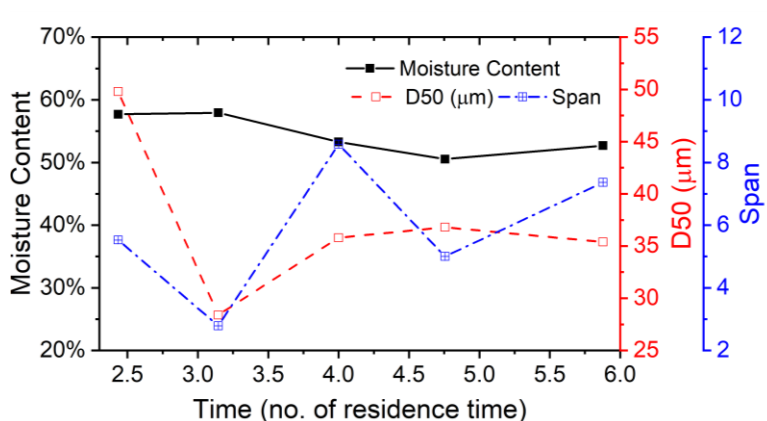


Figure 6-8 Coupled CFC product moisture content, D50 and span of BA.

Filter fouling did not occur during operation on account of periodic washing and solid removal which is a great advantage of the CFC. Similar performance was not seen with bench scale vacuum filtration. After concluding the coupled experiment of BA, the content of the crystallizer was removed with a peristaltic pump in the same intermittent fashion as it did in the first two residence times of the experiment. The outlet of the pump was placed directly onto a bench-scale vacuum set-up filtration (with the same pore size). It was completely fouled in just 10 minutes where liquor could no longer pass through the filter which is a common issue associated with semi-batch filtration set-ups [27], [213].

Coupled CFC-OBR operation to isolate PCM crystals was successful where state-of-control was reached in about four residence times and dry and uniform PCM particles were obtained at a considerable yield. On the other hand, dry and uniformly sized products were not obtained during coupled BA crystallization and filtration. However, implementing a drying mechanism in the CFC carousel can significantly improve the CFC performance with difficult systems such as the BA-EtOH-water system which has been explored with AWL's next generation continuous filtration drying unit [147].

6.3.3 Risk considerations of the CFC

It is valuable, especially for pharmaceutical and food applications, to examine the possible risk factors associated with continuous filtration that may cause process failure. Different processes may have different levels of influence on the overall quality of the product thus process failure may be defined differently in different situations. In this short discussion, process failure is loosely defined as producing possible undesirable product quality attributes or inducing process operation difficulties. An Ishikawa diagram (also known as a fishbone diagram) is constructed in Figure 6-9 to demonstrate potential factors that may lead to process failure. The risks factors are generally

categorized into six general areas. Most factors shown in Figure 6-9 are applicable to any continuous filtration operation while a few factors are unique to the CFC.

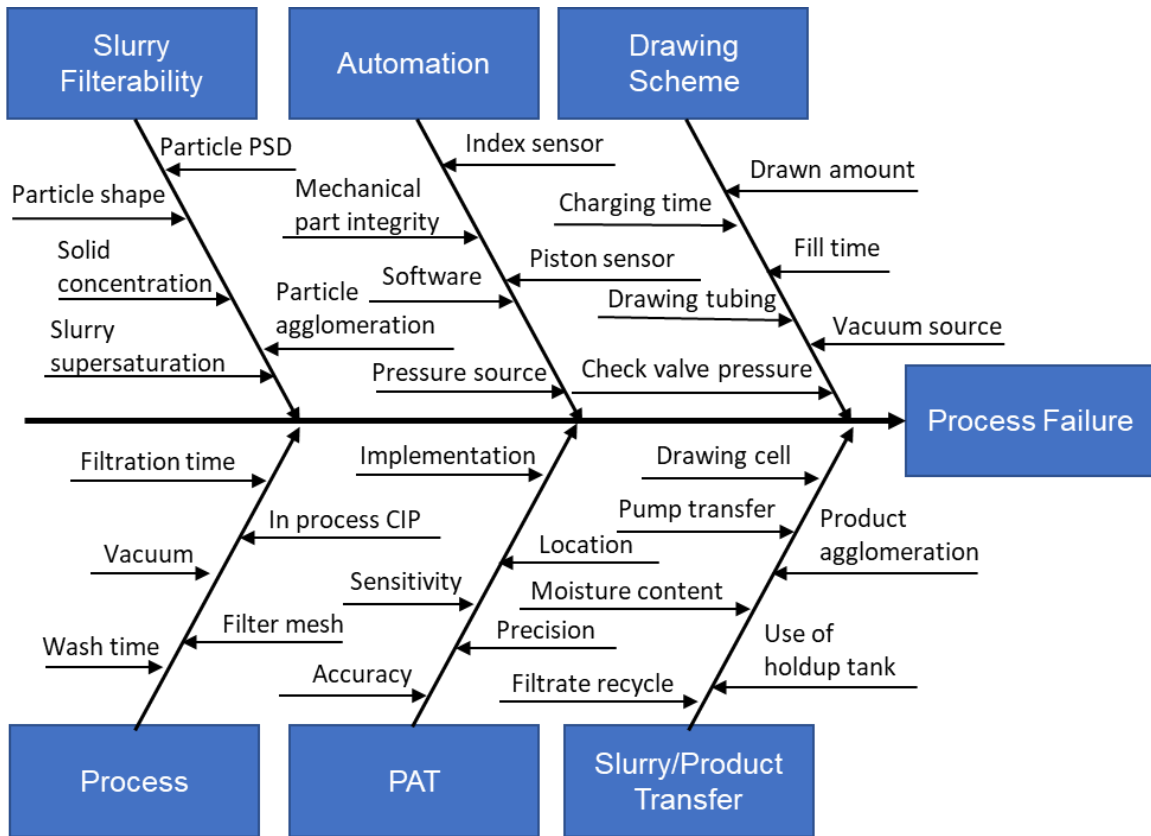


Figure 6-9 Ishikawa diagram showing potential risks of continuous filtration that may lead to process failure.

d. Slurry filterability

Difficult to filter slurries may lead to excessive filter fouling despite washing and cleaning efforts. Adverse material and slurry properties such as needle, plate like particle shapes, heavy particle concentration, excessive fines, and/or wide particle PSDs makes the slurry more difficult to filter. In addition, high supersaturation can cause heavy crystallization on the filter mesh which easily fouls the filter. These risk factors are best mitigated by particle engineering during crystallization or pre-treatment such as washing and solvent swapping before filtration.

e.Process

Process parameters largely determine the end product quality as demonstrated in this study. Filtration time, vacuum pressure, wash time, CIP setting, and filter mesh selection are all parameters that should be optimized to avoid process failure.

f.Automation

The CFC is a highly automated equipment that requires proper communication between the sensors and the software as well as the mechanical parts and the software which is likely the case for any other continuous filtration equipment. As any mechanical parts wears down over time, maintenance and replacement must be scheduled regularly to ensure their integrity. This is especially important because malfunctioning sensors or moving mechanical parts can result in operator injuries or near misses such as body parts or garments getting caught in rotating gears. Pressure source is used by the CFC to enable automation of the piston and the check valve. Maintaining a stable pressure source is essential to the CFC operation.

g.Process analytical technology (PAT)

Process analytical technology is the critical tools to gain mechanistic understanding of the process[11]. On the current CFC configuration, it is difficult to implement online PAT tools which poses a potential risk as online monitoring and control abilities are not possible. Flow cell PAT tools can be implemented to gain more insights into the continuous filtration process dynamics. If PAT tools are implemented and are used for monitoring or control, the sensitivity, precision and accuracy must be tested based on its application to quantify the risks.

h. Drawing scheme

The drawing scheme is a strong advantage of the CFC over a passive continuous filtration unit which may require peristaltic pump facilitated slurry transfer. The fill time (time allowed for slurry to fall from charge cell to the carousel), charging time and vacuum pressure of the CFC should be optimized and controlled for consistent slurry drawing. However, the drawing amount can still be affected by upstream vessel position and level variations which may drive the process away from state-of-control operation. A flowmeter may offer more control over the drawing scheme which is implemented in the next generation CFC [147].

i. Slurry/Product transfer

Slurry transfer has been identified as the most challenging issue associated with continuous two-phase processes such as crystallization and filtration [23], [27], [66], [100]. Insufficient slurry transfer may cause slurry accumulation, vessel overflow and complete blockage of outlet tubing. Direct coupling of continuous crystallization and filtration may be the obvious better choice, but it may be difficult to implement due to scale and scheduling. Using a hold-up tank may be inevitable as a middle step when transferring between the crystallizer and the CFC. If a pump is used to transfer slurries, special attention must be paid to avoid excessive tubing kinks, fittings or pump idle time. The design of the drawing cell is also important to prevent overdrawing of slurries which will spill over the entire carousel when released. The solid product transfer scheme is also important because if solid products were not timely and sufficiently removed from the filter, the 'leftover' solids may cause filter media fouling, corrosion of carousel gears, lowered yield and potential polymorph transformation. Ensuring piston functionality and communication with the software is critical to ensure effective solid product removal.

The factors discussed above will likely not all have detrimental effects on the process. Nevertheless, a combination of a few factors may worsen the effect of each other and easily cause process failure. When such failure happens, it is important to organize and trace the possible causes in the six aspects discussed above to prevent or significantly delay process failures.

6.4 Conclusion

Successful continuous filtration processes have been established in the new CFC for PCM-EtOH and BA-EtOH-water systems. Stand-alone filtration experiments have been carried out to examine the effects of vacuum time (slurry drawing rate) and wash time on product moisture content and PSD. Vacuum time had no significant impacts on the process but wash time was shown to be very influential. A set of CFC operating conditions were chosen based on the stand-alone experiments and true continuous crystallization-filtration was successfully carried out for both PCM and BA model systems without the use of a hold-up tank. For PCM, stable state-of-control operation was established after four residence times and desirable crystal products were produced continuously. A considerable yield of 47.6% was achieved during state-of-control operation. While heavy agglomeration and water entrapment was encountered during BA crystallization-filtration process, CFC still showed great advantages for its sustained operation without complete filter fouling or failure which can be challenging for semi-batch filtration setups. 47% yield was also achieved. The implementation of heated drying in the filtration chambers can largely improve the drying of the filter cake and heavy the agglomeration of BA crystals which is being investigated. In addition, a short discussion has been given on the potential risk factors associated with continuous filtration which can be helpful when conducting risk management analysis in industrial applications.

7. CONCLUSION AND FUTURE DIRECTIONS

7.1 Conclusion

Continuous manufacturing has been identified as an emerging technology in the current movement to modernize pharmaceutical manufacturing. Developing successful continuous crystallization processes may be the key in achieving end-to-end continuous manufacturing. Crystallization is a complex phenomenon that entirely takes place in a metastable thermostatic state where supersaturated molecules come together to form nuclei that then further grow in size. Batch crystallization, while being recipe-based and relatively easy to perform, suffers from batch-to-batch variations often causing discrepancies in downstream processes. Batch processes are also large in size and must go through an elaborate scale-up practice. Batch crystallization scale-up is especially very difficult as the mixing dynamics can significantly change the crystallization kinetics and particle morphology. Scale-up is often considered the most complex and highest failing rate practice during development. Continuous operations on the other hand operates at a state-of-control where consistent products are produced continuously. Pilot plant and even lab hood equipment can satisfy API production target depending on the patient population and the lifespan of the drug potentially eliminating traditional scale-up practices.

MSMPR crystallizers and PFCs have been critically reviewed to discuss their operations, applicability and limitations. Compared to PFCs, MSMPR operations are less complex and able to handle long residence times which is often needed for slow nucleating and/or slow growing compounds. MSMPR operation was studied in this thesis in both a traditional STC and an innovative platform, the OBR. Because the two systems have been developed at different levels in the development stage, the studies in the two systems were aimed differently in this thesis. STC has been relatively well studied as an MSMPR system where risk-based model development is one

of the last missing steps. To demonstrate this, a PBM was developed for the cooling crystallization of CBZ in the STC, the kinetics of which have yet to be studied in current literature. The limitation and applicability of the PBM was then verified and validated systematically based on its risk level and credibility goal according to the referenced guideline suggesting potential use of modeling to determine a design space for crystallization process development. A discussion on the transferability of batch kinetics to continuous operation was given. Because crystallization is highly stochastic, the supersaturation and solid concentration heavily influence nucleation and growth rates. Thus, development experiments must cover the range of supersaturation and solid conditions that might be experienced by the target process.

While STC has been a popular choice for crystallization, there are disadvantages associated with agitational mixing such as poor local mixing and high shear. Oscillatory reactors have been gaining popularity for its gentler, more thorough mixing dynamics. A novel oscillatory baffle reactor was studied in this thesis for the systematic process development of continuous crystallization. The OBR consists of an elongated vessel body and four 'donut' shaped baffles to create oscillations. A continuous OBR platform was established with PAT capabilities. The basis of its use for crystallization was established by studying the RTD for both liquid and solid contents. The results showed that the RTDs were more uniform in the OBR than the STC. The proof-of-concept of continuous crystallization in the OBR was then demonstrated and compared to the STC where the OBR produced less aggregated and more uniform products without severe particle breakage or sedimentation which have been encountered during STC experiments.

Developing appropriate start-up strategies is critical in establishing an efficient and stable continuous crystallization process. However, it is not well studied in the literature. Being used for continuous crystallization for the first time, it is important to investigate different start-up

strategies and their (or lack thereof) effects on product quality attributes in the OBR systematically. Five common start-up strategies were studied: (1) linear cooling batch start-up, (2) optimized batch start-up, (3) direct continuous start-up with clear saturated solution, (4) direct continuous start-up with seeded suspension with pre-sieved raw material and (5) direct continuous start-up with seeded suspension with steady state products from strategy. The five start-up strategies resulted in similar steady states despite major differences in process dynamics likely because the residence time was much longer than PCM crystallization time scale. Batch start-ups and seeded continuous start-up resulted in heavy particle washout and nucleation while start-up (5) yielded stable and smooth concentration, particle count and SWMCL profiles over the duration of the experiment which may be very desirable. Unseeded start-up is not recommended because primary nucleation required higher supersaturation build-up and generated excessive fines. The optimization of batch cooling profile in start-up (2) used kinetic parameters developed via batch crystallization experiments carried out in the OBR. It correctly predicted the washout but underpredicted nucleation during continuous operation. However, it indeed produced the highest yield and most uniform steady state product. It remains debatable whether the cost of long start-up time is worthy of the very small improvement in yield and size uniformity.

While much advances are being made in developing continuous crystallization to catch up with the development in continuous reaction and drug product processes, its inseparable following step, filtration, has only been scarcely investigated in the current literature. Only a handful of publications can be found on the topic of continuous filtration and even fewer focus on the coupling of continuous filtration with continuous crystallization. An innovative CFC was studied in this thesis to address this gap in current development. The proof-of-concept has been studied by colleagues on an earlier iteration of the CFC where a hold-up tank was used in the coupling with

crystallization. The current CFC prototype features a vacuum driven drawing scheme, similar to that of a pressure swing transfer zone commonly used on MSMR systems, allowing direct coupling of continuous filtration and crystallization. A truly continuous drug substance isolation step was developed where supersaturated PCM-EtOH solution and BA-EtOH-water solution were crystallized in the OBR and filtered in the CFC to obtain isolated PCM and BA crystals at the outlet of the CFC continuously. The operating parameters were optimized with systematically designed stand-alone filtration experiments. PCM-EtOH model system exhibited good filterability because of the prism-like crystal shape of the PCM and the volatility of EtOH. Dry (~5% moisture content) PCM solids were collected at the outlet of the CFC continuously ready for further downstream processes. Whereas BA crystals are of elongated plate-like morphology which are prone to agglomeration and moisture entrapment. Wet and agglomerated BA filter cake was obtained at the outlet of the CFC. with the implementation of drying in the CFC chamber, the performance of CFC can be improved significantly. In a semi-batch filtration operation with a bench scale vacuum filter on the other hand, the filter was quickly fouled by fine particles. The periodic washing and solid removal operation in the CFC poses a major advantage lessening filter fouling issues. In hopes of promoting continuous filtration development in the industry, a discussion on its risk considerations was given answering the current paradigm shift to QbD regulatory approach. Risk factors are organized into six categories to construct a fish-bone diagram assisting risk assessment.

Systematically developing a truly continuous drug substance isolation step was demonstrated in this thesis applying innovative technologies and methodologies with the aid of modern PATs and computational techniques. Drug substance isolation marks the end of API manufacturing steps and transitions into drug product processing. Developing a continuous drug substance isolation step can enable end-to-end continuous manufacturing.

7.2 Future directions

With the current research effort in continuous crystallization, only the last few missing pieces need to be addressed:

- Stricter model verification and validation of the PBM for high risk model-based control strategy implementation. Agglomeration was likely present but not taken into consideration in this thesis which should be added to the PBM of CBZ in the STC. The resulting PBM should be able to past stricter verification and validation activities for high-impact control strategies.
- Continuous crystallization of difficult to crystallize compounds in the OBR. Because the OBR promotes nucleation and growth, previously problematic compounds may become available candidates for continuous operation in the OBR. An example compound, Lactose, has been tested preliminarily. Lactose exhibits long nucleation induction time, slow growth rates and brittle crystal structure which is problematic for STC operations. However, it was successfully crystallized in the OBR in our lab in batch mode at lower supersaturation conditions and faster cooling rates that could not result in crystallization in the STC. A continuous crystallization may be possible requiring less concentrated upstream solution at shortened residence times. OBR can be an alternative to STC to enable crystallizations of difficult compounds like lactose.
- Implementation of pressure swing transfer zones to develop multi-stage OBR MSMPR systems. Such an OBR cluster carousel is being constructed with built-in transfer mechanisms by AWL and NiTech. The RTD of such a system would be similar to that of a PFC which makes the transition from batch to continuous much simpler. This OBR cluster carousel can be developed into an advanced system for continuous crystallization.

- Implementation of hot air flow in the CFC chamber to enable drying which improves its performance for difficult to dry cakes. A heating mechanism can be installed to allow port 4 which is currently blanked, to become a drying chamber. Difficult systems such as BA-EtOH-water can be filtered continuously yielding dry and less agglomerated filter cakes.

While my efforts are small in the magnificent wave of continuous manufacturing that is currently sweeping the pharmaceutical industry, I believe my work strengthens the collective understanding of continuous crystallization and filtration process development. My work promotes the modernization of pharmaceutical processes via continuous manufacturing which can be the flexible solution to drug shortages. Even though ambitious and challenging, I believe end-to-end continuous pharmaceutical manufacturing will ‘see its light of day’ in the very near future.

APPENDIX

POPULATION BALANCE MODEL SOLUTION METHODS

Population balance modeling is a common computational technique to describe two-phase processes such as crystallization. Method of moment (MOM) [144] is a common PBM solution method that describes the population distribution by its moments:

$$\mu_j = \int_{L_0}^{\infty} f(t, L) L^j dL \quad (\text{A.1})$$

where μ_j denotes the j th moment of the population distribution f : μ_0 is the total number of particles, μ_1 represents the total length, μ_2 is the total surface, μ_3 is the total particle volume per unit volume of the slurry. The batch population balance Eq(2.8) can then be converted into a series of ordinary differential equation using moments:

$$\begin{aligned} \frac{d\mu_0}{dt} &= B \\ \frac{d\mu_1}{dt} &= G\mu_0 \\ \frac{d\mu_2}{dt} &= 2G\mu_1 \end{aligned} \quad (\text{A.2})$$

Mass and energy balance can be written as:

$$\frac{dC}{dt} = -3\rho_c k_v G \mu_2 \quad (\text{A.3})$$

$$\frac{dT}{dt} = \frac{-hA(T - T_w)}{V\rho_{sol}C_p} - \frac{\Delta H_c 3k_v\rho_c}{V\rho_{sol}C_p} G\mu_2 \quad (\text{A.4})$$

The PBM is now converted as a system of ordinary differential equations which can be easily solved; however, a full PSD cannot be obtained using MOM.

Alternatively, a finite volume method can be applied to numerically solve for the full population distribution, as well as concentration (and temperature) over time. A high-resolution

finite volume method (HRFV) is commonly used to solve PBM for crystallization processes employing the Van Leer flux limiter [29], [214], [215]. HRFV discretizes the population density function f in its internal coordinate L and in time t : denoting with h as the bin size and k the time step. Let f_l^m denote the population density at size step l and time step m ($m \geq 0$, $1 \leq l \leq N$, i. e. mesh size) which can then be approximated as

$$f_l^m \approx \frac{1}{h} \int_{(l-1)h}^{lh} f(L, mk) dL \quad (\text{A.5})$$

Then the population balance Eq(2.8) can be discretized as

$$\begin{aligned} \frac{1}{k}(f_l^{m+1} - f_l^m) = \\ -\frac{1}{h}(G_l f_l^m - G_{l-1} f_{l-1}^m) - \left[\frac{G_l}{2h} \left(1 - \frac{kG_l}{h}\right) (f_{l+1}^m - f_l^m) \phi_l - \frac{G_{l-1}}{2h} \left(1 - \frac{kG_{l-1}}{h}\right) (f_l^m - f_{l-1}^m) \phi_{l-1} \right] + \varepsilon_b \frac{B}{h} \end{aligned} \quad (\text{A.6})$$

where ε_b corresponds to the dirac delta function. In this PBM formulation, $\varepsilon_b = 1$ if $l = 1$ or $\varepsilon_b = 1$ otherwise. Eq(A.6) also applies for dissolution by simply replacing growth with dissolution without nucleation. For high resolution solutions, the Van Leer flux limiter Φ has been demonstrated to yield second-order accuracy without introducing numerical dispersion [215]–[217]:

$$\phi_l = \phi(\theta_l) \equiv \frac{|\theta_l| + \theta_l}{|\theta_l| + 1} \quad (\text{A.7})$$

where

$$\theta_l = \frac{f_l^m - f_{l-1}^m}{f_{l+1}^m - f_l^m} \quad (\text{A.8})$$

Finally, the mass balance Eq(2.10) is an ordinary differential equation (ODE)

$$\frac{dC}{dt} = -3k_v \rho_c \sum_{l=0}^N (G_l f_l [lh]^2) \quad (\text{A.9})$$

REFERENCES

- [1] J. A. DiMasi, R. W. Hansen, and H. G. Grabowski, "The price of innovation: new estimates of drug development costs," *J. Health Econ.*, vol. 22, no. 2, pp. 151–185, Mar. 2003.
- [2] P. Suresh and P. K. Basu, "Improving Pharmaceutical Product Development and Manufacturing: Impact on Cost of Drug Development and Cost of Goods Sold of Pharmaceuticals," *J. Pharm. Innov.*, vol. 3, no. 3, pp. 175–187, Sep. 2008.
- [3] The U.S. Food and Drug Administration, "Pharmaceutical CGMPs for the 21s Century - A risk-based approach." 2004.
- [4] L. X. X. Yu, "Pharmaceutical quality by design: product and process development, understanding, and control.," *Pharm. Res.*, vol. 25, no. 4, pp. 781–91, 2008.
- [5] M. Nasr, "Risk-based CMC review paradigm," in *Advisory committee for pharmaceutical science meeting*.
- [6] U.S. Food and Drug Adminiatration CDER, "Guidance for industry: Immediate release solid oral dosage forms scale-up and postapproval changes: Chemistry, manufacturing, and controls, in vitro dissolution testing, and in vivo bioequivalence documentation." 1995.
- [7] U.S. Food and Drug Adminiatration CDER, "Guidance for industry: Modified release solid oral dosage forms scale-up and postapproval changes: Chemistry, manufacturing, and controls, in vitro dissolution testing, and in vivo bioequivalence documentation." 1997.
- [8] U.S. Food and Drug Adminiatration CDER, "Nonsterile semisolid dosage forms scale-up and postapproval changes: chemistry, manufacturing, and controls, in vitro dissolution testing, and in vivo bioequivalence documentation." 1997.
- [9] U.S. Food and Drug Adminiatration CDER, "Food and Drug Administration CDER. Guidance for industry: Changes to an approved NDA or ANDA (April 2004)." 2004.

- [10] S. L. Lee *et al.*, “Modernizing Pharmaceutical Manufacturing: from Batch to Continuous Production,” *J. Pharm. Innov.*, vol. 10, no. 3, pp. 191–199, Sep. 2015.
- [11] U.S. Food and Drug Administration, “Guidance for industry PAT: a framework for innovative pharmaceutical development, manufacturing, and quality assurance,” 2004.
- [12] U.S. Food and Drug Administration, “Quality Considerations for Continuous Manufacturing Guidance for Industry DRAFT GUIDANCE,” no. February. 2019.
- [13] N. Nishida, G. Stephanopoulos, and A. W. Westerberg, “A review of process synthesis,” *AIChE J.*, vol. 27, no. 3, pp. 321–351, 1981.
- [14] S. Ferguson, G. Morris, H. Hao, M. Barrett, and B. Glennon, “Characterization of the anti-solvent batch, plug flow and MSMPR crystallization of benzoic acid,” *Chem. Eng. Sci.*, vol. 104, pp. 44–54, 2013.
- [15] D. Acevedo, R. Peña, Y. Yang, A. Barton, P. Firth, and Z. K. Nagy, “Evaluation of mixed suspension mixed product removal crystallization processes coupled with a continuous filtration system,” *Chem. Eng. Process. Process Intensif.*, vol. 108, pp. 212–219, Oct. 2016.
- [16] D. Acevedo, V. K. Kamaraju, B. Glennon, and Z. K. Nagy, “Modeling and Characterization of an in Situ Wet Mill Operation,” *Org. Process Res. Dev.*, vol. 21, no. 7, pp. 1069–1079, Jul. 2017.
- [17] Y. Yang and Z. K. Nagy, “Advanced control approaches for combined cooling/antisolvent crystallization in continuous mixed suspension mixed product removal cascade crystallizers,” *Chem. Eng. Sci.*, vol. 127, pp. 362–373, 2015.
- [18] Y. C. Liu *et al.*, “A comparative study of continuous operation between a dynamic baffle crystallizer and a stirred tank crystallizer,” *Chem. Eng. J.*, vol. 367, pp. 278–294, Jul. 2019.
- [19] K. Plumb, “Continuous processing in the pharmaceutical industry: Changing the mind set,”

- Chem. Eng. Res. Des.*, vol. 83, no. 6 A, pp. 730–738, 2005.
- [20] P. McKenzie, S. Kiang, J. Tom, A. E. Rubin, and M. Futran, “Can Pharmaceutical Process Development Become High Tech?,” *AIChE J.*, vol. 52, no. 12, pp. 3990–3994, 2006.
- [21] S. Chatterjee, “FDA Perspective on Continuous Manufacturing,” in *IFPAC Annual Meeting*, 2012.
- [22] J. Woodcock, “Modernizing Pharmaceutical Manufacturing – Continuous Manufacturing as a Key Enabler,” in *MIT-CMAC International Symposium on Continuous Manufacturing of Pharmaceuticals*, 2014.
- [23] X. Yang *et al.*, “Risk Considerations on Developing a Continuous Crystallization System for Carbamazepine,” *Org. Process Res. Dev.*, vol. 21, no. 7, pp. 1021–1033, Jul. 2017.
- [24] K. Plumb, “Continuous Processing in the Pharmaceutical Industry,” *Chem. Eng. Res. Des.*, vol. 83, no. 6, pp. 730–738, Jun. 2005.
- [25] S. D. Schaber, D. I. Gerogiorgis, R. Ramachandran, J. M. B. Evans, P. I. Barton, and B. L. Trout, “Economic Analysis of Integrated Continuous and Batch Pharmaceutical Manufacturing: A Case Study,” *Ind. Eng. Chem. Res.*, vol. 50, no. 17, pp. 10083–10092, 2011.
- [26] Z. K. Nagy, M. Fujiwara, X. Y. Woo, and R. D. Braatz, “Determination of the Kinetic Parameters for the Crystallization of Paracetamol from Water Using Metastable Zone Width Experiments,” *Ind. Eng. Chem. Res.*, vol. 47, no. 4, pp. 1245–1252, Feb. 2008.
- [27] B. Wood, K. P. Girard, C. S. Polster, and D. M. Croker, “Progress to Date in the Design and Operation of Continuous Crystallization Processes for Pharmaceutical Applications,” *Org. Process Res. Dev.*, vol. 23, no. 2, pp. 122–144, Feb. 2019.
- [28] R. Davey and J. Garside, *From Molecules to Crystallizers: An Introduction to*

- Crystallization*. 2000.
- [29] E. Simone, B. Szilagyi, and Z. K. Nagy, “Systematic model identification and optimization-based active polymorphic control of crystallization processes,” *Chem. Eng. Sci.*, vol. 174, pp. 374–386, 2017.
- [30] A. M. Schwartz and A. S. Myerson, “Solutions and Solution Properties,” in *Handbook of industrial crystallization*, Woburn, MA: Butterworth-Heinemann, 2002, p. 16.
- [31] P. Barrett and B. Glennon, “Characterizing the metastable zone width using Lasentec FBRM and PVM,” *Chem. Eng. Res. Des.*, vol. 80, no. 7, pp. 799–805, Oct. 2002.
- [32] A. S. Myerson and R. Ginde, “Crystals, Crystal Growth, and Nucleation,” in *Handbook of Industrial Crystallization*, 2nd ed., 2001, pp. 33–66.
- [33] J. W. Mullin, “Nucleation,” in *Crystallization*, 2001, pp. 181–215.
- [34] G. D. Botsaris, “Secondary Nucleation — A Review,” in *Industrial Crystallization*, Boston, MA: Springer US, 1976, pp. 3–22.
- [35] J. GARSIDE and R. J. DAVEY, “INVITED REVIEW SECONDARY CONTACT NUCLEATION: KINETICS, GROWTH AND SCALE-UP,” *Chem. Eng. Commun.*, vol. 4, no. 4–5, pp. 393–424, Jan. 1980.
- [36] J. Garside, “Industrial crystallization from solution,” *Chem. Eng. Sci.*, vol. 40, no. 1, pp. 3–26, 1985.
- [37] W. L. McCabe and R. P. Stevens, “Rate of growth of crystals in aqueous solutions,” *Chem. Eng. Prog.*, vol. 47, no. 4, pp. 168–174, 1951.
- [38] R. Becker and W. Döring, “Kinetische Behandlung der Keimbildung in übersättigten Dämpfen,” *Ann. Phys.*, vol. 416, no. 8, pp. 719–752, Jan. 1935.
- [39] M. Volmer, *Kinetik der Phasenbildung*. 1939.

- [40] J. W. Gibbs, "The collected works of J. Willard Gibbs." Yale Univ. Press, New Haven, CT, 1948.
- [41] D. Erdemir, A. Y. Lee, and A. S. Myerson, "Nucleation of crystals from solution: classical and two-step models," *Acc. Chem. Res.*, vol. 42, no. 5, pp. 621–629, May 2009.
- [42] D. Chakraborty and G. N. Patey, "Evidence that crystal nucleation in aqueous NaCl solution Occurs by the two-step mechanism," *Chem. Phys. Lett.*, vol. 587, pp. 25–29, 2013.
- [43] R. J. Davey, S. L. M. Schroeder, and J. H. ter Horst, "Nucleation of Organic Crystals-A Molecular Perspective," *Angew. Chemie Int. Ed.*, vol. 52, no. 8, pp. 2166–2179, Feb. 2013.
- [44] H. H. Ting and W. L. McCabe, "Supersaturation and crystal formation in seeded solutions," *Ind. Eng. Chem.*, vol. 26, no. 11, pp. 1201–1207, Nov. 1934.
- [45] R. F. STRICKLAND-CONSTABLE and R. E. A. MASON, "Breeding of Nuclei," *Nature*, vol. 197, no. 4870, pp. 897–898, Mar. 1963.
- [46] R. F. Strickland-Constable, *Kinetics and mechanism of crystallization from the fluid phase and of the condensation and evaporation of liquids*. London, UK: Academic Press, 1968.
- [47] J. W. Mullin, "Crystal Growth," in *Crystallization*, 2001, pp. 216–288.
- [48] Z. K. Nagy, J. W. Chew, M. Fujiwara, and R. D. Braatz, "Comparative performance of concentration and temperature controlled batch crystallizations," *J. Process Control*, vol. 18, no. 3–4, pp. 399–407, Mar. 2008.
- [49] M. Ohara and R. C. Reid, *Modeling Crystal Growth Rates from Solutions*. 1973.
- [50] F. C. Frank, "The influence of dislocations on crystal growth," *Discuss. Faraday Soc.*, vol. 5, no. 0, p. 48, Jan. 1949.
- [51] W. K. Burton, N. Cabrera, and F. C. Frank, "The Growth of Crystals and the Equilibrium Structure of their Surfaces," *Philos. Trans. R. Soc. A Math. Phys. Eng. Sci.*, vol. 243, no.

- 866, pp. 299–358, Jun. 1951.
- [52] R. Ghez and G. H. Gilmer, “An analysis of combined surface and volume diffusion processes in crystal growth,” *J. Cryst. Growth*, vol. 21, no. 1, pp. 93–109, Jan. 1974.
- [53] P. Bennema, “The importance of surface diffusion for crystal growth from solution,” *J. Cryst. Growth*, vol. 5, pp. 29–43, 1969.
- [54] W. R. Wilcox, “Movement of crystal inclusions in a centrifugal field,” *J. Appl. Phys.*, vol. 42, no. 5, pp. 1823–1827, 1971.
- [55] J. Nyvlt, O. Sohnle, M. Matuchaova, and M. Broul, *The Kinetics of Industrial Crystallization*. Elsevier, Amsterdam, 1985.
- [56] J. W. Mullin, “Industrial techniques and equipment,” in *Crystallization*, Butterworth-Heinemann, 2001, pp. 315–402.
- [57] Y. Hu, J. K. Liang, A. S. Myerson, and L. S. Taylor, “Crystallization Monitoring by Raman Spectroscopy: Simultaneous Measurement of Desupersaturation Profile and Polymorphic Form in Flufenamic Acid Systems,” *Ind. Eng. Chem. Res.*, vol. 44, no. 5, pp. 1233–1240, 2005.
- [58] H. Wikström, I. R. Lewis, and L. S. Taylor, “Comparison of sampling techniques for in-line monitoring using Raman spectroscopy,” *Appl. Spectrosc.*, vol. 59, no. 7, pp. 934–941, 2005.
- [59] E. Simone, A. N. Saleemi, and Z. K. Nagy, “Raman, UV, NIR, and Mid-IR Spectroscopy with Focused Beam Reflectance Measurement in Monitoring Polymorphic Transformations,” *Chem. Eng. Technol.*, vol. 37, no. 8, pp. 1305–1313, Aug. 2014.
- [60] E. Kougoulos, A. G. Jones, K. H. Jennings, and M. W. Wood-Kaczmar, “Use of focused beam reflectance measurement (FBRM) and process video imaging (PVI) in a modified mixed suspension mixed product removal (MSMPR) cooling crystallizer,” *J. Cryst. Growth*,

- vol. 273, no. 3–4, pp. 529–534, Jan. 2005.
- [61] J. Schöll, D. Bonalumi, L. Vicum, M. Mazzotti, and M. Müller, “In situ monitoring and modeling of the solvent-mediated polymorphic transformation of L-glutamic acid,” *Cryst. Growth Des.*, 2006.
- [62] G. Morris, G. Power, S. Ferguson, M. Barrett, G. Hou, and B. Glennon, “Estimation of Nucleation and Growth Kinetics of Benzoic Acid by Population Balance Modeling of a Continuous Cooling Mixed Suspension, Mixed Product Removal Crystallizer,” *Org. Process Res. Dev.*, vol. 19, no. 12, pp. 1891–1902, Dec. 2015.
- [63] A. N. Saleemi, C. D. Rielly, and Z. K. Nagy, “Comparative Investigation of Supersaturation and Automated Direct Nucleation Control of Crystal Size Distributions using ATR-UV/vis Spectroscopy and FBRM,” *Cryst. Growth Des.*, vol. 12, no. 4, pp. 1792–1807, Apr. 2012.
- [64] Z. K. Nagy and R. D. Braatz, “Advances and New Directions in Crystallization Control,” *Annu. Rev. Chem. Biomol. Eng.*, vol. 3, no. 1, pp. 55–75, Jul. 2012.
- [65] Y. Yang, L. Song, and Z. K. Nagy, “Automated Direct Nucleation Control in Continuous Mixed Suspension Mixed Product Removal Cooling Crystallization,” *Cryst. Growth Des.*, vol. 15, no. 12, pp. 5839–5848, 2015.
- [66] Z. K. Nagy, G. Fevotte, H. Kramer, and L. L. Simon, “Recent advances in the monitoring, modelling and control of crystallization systems,” *Chem. Eng. Res. Des.*, vol. 91, no. 10, pp. 1903–1922, Oct. 2013.
- [67] D. Acevedo, Y. Yang, D. J. Warnke, and Z. K. Nagy, “Model-Based Evaluation of Direct Nucleation Control Approaches for the Continuous Cooling Crystallization of Paracetamol in a Mixed Suspension Mixed Product Removal System,” *Cryst. Growth Des.*, vol. 17, no. 10, pp. 5377–5383, Oct. 2017.

- [68] Y. Yang, L. Song, Y. Zhang, and Z. K. Nagy, "Application of Wet Milling-Based Automated Direct Nucleation Control in Continuous Cooling Crystallization Processes," *Ind. Eng. Chem. Res.*, vol. 55, no. 17, pp. 4987–4996, May 2016.
- [69] S. Vonhoff, J. Condliffe, and H. Schiffter, "Implementation of an FTIR calibration curve for fast and objective determination of changes in protein secondary structure during formulation development," *J. Pharm. Biomed. Anal.*, vol. 51, no. 1, pp. 39–45, 2010.
- [70] K. Liang, G. White, D. Wilkinson, L. J. Ford, K. J. Roberts, and W. M. L. Wood, "An Examination into the Effect of Stirrer Material and Agitation Rate on the Nucleation of L-Glutamic Acid Batch Crystallized from Supersaturated Aqueous Solutions," 2003.
- [71] M. R. Mackley, K. B. Smith, and N. P. Wise, "The mixing and separation of particle suspensions using oscillatory flow in baffled tubes," *Trans. Inst. Chem. Eng.*, vol. 71, no. Part A, pp. 649–656, 1993.
- [72] N. Gherras, E. Serris, and G. Fevotte, "Monitoring industrial pharmaceutical crystallization processes using acoustic emission in pure and impure media," *Int. J. Pharm.*, vol. 439, no. 1–2, pp. 109–119, 2012.
- [73] G. Hou, G. Power, M. Barrett, B. Glennon, G. Morris, and Y. Zhao, "Development and characterization of a single stage mixed-suspension, mixed-product-removal crystallization process with a novel transfer unit," *Cryst. Growth Des.*, vol. 14, no. 4, pp. 1782–1793, 2014.
- [74] X. Liu, D. Sun, F. Wang, Y. Wu, Y. Chen, and L. Wang, "Monitoring of antisolvent crystallization of sodium scutellarein by combined FBRM-PVM-NIR," *J. Pharm. Sci.*, vol. 100, no. 6, pp. 2452–2459, 2011.
- [75] L. L. Simon, Z. K. Nagy, and K. Hungerbuhler, "Endoscopy-based in situ bulk video imaging of batch crystallization processes," *Org. Process Res. Dev.*, vol. 13, no. 6, pp.

- 1254–1261, 2009.
- [76] Á. Borsos, B. Szilágyi, P. Ş. Agachi, and Z. K. Nagy, “Real-Time Image Processing Based Online Feedback Control System for Cooling Batch Crystallization,” *Org. Process Res. Dev.*, vol. 21, no. 4, pp. 511–519, 2017.
- [77] Y. Zhou, R. Srinivasan, and S. Lakshminarayanan, “Critical evaluation of image processing approaches for real-time crystal size measurements,” *Comput. Chem. Eng.*, vol. 33, no. 5, pp. 1022–1035, 2009.
- [78] D. Acevedo *et al.*, “Raman Spectroscopy for Monitoring the Continuous Crystallization of Carbamazepine,” *Org. Process Res. Dev.*, vol. 22, pp. 156–165, 2018.
- [79] E. Simone, A. N. Saleemi, N. Tonnon, and Z. K. Nagy, “Active Polymorphic Feedback Control of Crystallization Processes Using a Combined Raman and ATR-UV/Vis Spectroscopy Approach,” *Cryst. Growth Des.*, vol. 14, no. 4, pp. 1839–1850, Apr. 2014.
- [80] Y. Yang *et al.*, “Application of Ultra-Performance Liquid Chromatography as an Online Process Analytical Technology Tool in Pharmaceutical Crystallization,” *Cryst. Growth Des.*, vol. 16, no. 12, pp. 7074–7082, 2016.
- [81] Y. Yang *et al.*, “Application of feedback control and in situ milling to improve particle size and shape in the crystallization of a slow growing needle-like active pharmaceutical ingredient,” *Int. J. Pharm.*, vol. 533, no. 1, pp. 49–61, Nov. 2017.
- [82] P. Kolář, J. W. Shen, A. Tsuboi, and T. Ishikawa, “Solvent selection for pharmaceuticals,” *Fluid Phase Equilib.*, vol. 194–197, pp. 771–782, 2002.
- [83] A. T. Karunanithi, L. E. K. Achenie, and R. Gani, “A computer-aided molecular design framework for crystallization solvent design,” *Chem. Eng. Sci.*, vol. 61, no. 4, pp. 1247–1260, 2006.

- [84] C. H. Gu, H. Li, R. B. Gandhi, and K. Raghavan, "Grouping solvents by statistical analysis of solvent property parameters: Implication to polymorph screening," *Int. J. Pharm.*, vol. 283, no. 1–2, pp. 117–125, 2004.
- [85] A. S. Myerson, S. E. Decker, and W. Fan, "Solvent selection and batch crystallization," *Ind. Eng. Chem. Process Des. Dev.*, vol. 25, no. 4, pp. 925–929, Oct. 1986.
- [86] J. S. Wey and P. H. Karpinski, "Batch Crystallization," in *Handbook of industrial crystallization*, Elsevier Science & Technology, 2001.
- [87] E. Aamir, Z. K. Nagy, and C. D. Rielly, "Evaluation of the Effect of Seed Preparation Method on the Product Crystal Size Distribution for Batch Cooling Crystallization Processes," *Cryst. Growth Des.*, vol. 10, no. 11, pp. 4728–4740, Nov. 2010.
- [88] A. Mersmann and F. W. Rennie, "Seeding," in *Crystallization Technology Handbook*, 1970, pp. 401–482.
- [89] Y. Cao, D. Acevedo, Z. K. Nagy, and C. D. Laird, "Real-time feasible multi-objective optimization based nonlinear model predictive control of particle size and shape in a batch crystallization process," *Control Eng. Pract.*, vol. 69, pp. 1–8, Dec. 2017.
- [90] R. Peña, C. L. Burcham, D. J. Jarmer, D. Ramkrishna, and Z. K. Nagy, "Modeling and optimization of spherical agglomeration in suspension through a coupled population balance model," *Chem. Eng. Sci.*, vol. 167, pp. 66–77, Aug. 2017.
- [91] S. H. Chung, D. L. Ma, and R. D. Braatz, "Optimal seeding in batch crystallization," *Can. J. Chem. Eng.*, vol. 77, no. 3, pp. 590–596, Jun. 1999.
- [92] F. Puel, G. Févotte, and J. P. Klein, "Simulation and analysis of industrial crystallization processes through multidimensional population balance equations. Part 1: a resolution algorithm based on the method of classes," *Chem. Eng. Sci.*, vol. 58, no. 16, pp. 3715–3727,

- Aug. 2003.
- [93] L. Feng and K. A. Berglund, “ATR-FTIR for Determining Optimal Cooling Curves for Batch Crystallization of Succinic Acid,” *Cryst. Growth Des.*, vol. 2, no. 5, pp. 449–452, Sep. 2002.
- [94] R. Peña and Z. K. Nagy, “Process Intensification through Continuous Spherical Crystallization Using a Two-Stage Mixed Suspension Mixed Product Removal (MSMPR) System,” *Cryst. Growth Des.*, vol. 15, no. 9, pp. 4225–4236, Sep. 2015.
- [95] Q. Su *et al.*, “A perspective on Quality-by-Control (QbC) in pharmaceutical continuous manufacturing,” *Comput. Chem. Eng.*, vol. 125, pp. 216–231, 2019.
- [96] D. Green and A. S. Myerson, “Crystallizer Mixing: Understanding and Modeling Crystallizer Mixing and Suspension Flow,” in *Handbook of Industrial Crystallization*, 2001, pp. 182–199.
- [97] Z. K. Nagy and E. Aamir, “Systematic design of supersaturation controlled crystallization processes for shaping the crystal size distribution using an analytical estimator,” *Chem. Eng. Sci.*, vol. 84, pp. 656–670, 2012.
- [98] T. Wang *et al.*, “Recent progress of continuous crystallization,” *J. Ind. Eng. Chem.*, vol. 54, pp. 14–29, 2017.
- [99] D. Zhang, S. Xu, S. Du, J. Wang, and J. Gong, “Progress of Pharmaceutical Continuous Crystallization,” *Engineering*, vol. 3, no. 3, pp. 354–364, Jun. 2017.
- [100] D. Acevedo *et al.*, “Encrustation in Continuous Pharmaceutical Crystallization Processes—A Review,” *Org. Process Res. Dev.*, vol. 23, no. 6, pp. 1134–1142, Jun. 2019.
- [101] H. S. Fogler, “Distributions of residence times for chemical reactors,” in *Elements of Chemical Reaction Engineering*, 2006, p. 869.

- [102] T. N. Zwietering, “Suspending of solid particles in liquid by agitators,” *Chem. Eng. Sci.*, vol. 8, no. 3–4, pp. 244–253, Jun. 1958.
- [103] C. Engineering and L. Sapienza, “Abrasion and Breakage Phenomena,” vol. 47, pp. 3105–3111, 1992.
- [104] B. Biscans, “Impact attrition in crystallization processes. Analysis of repeated impacts events of individual crystals,” *Powder Technol.*, vol. 143–144, pp. 264–272, 2004.
- [105] Q. Su, Z. K. Nagy, and C. D. Rielly, “Pharmaceutical crystallisation processes from batch to continuous operation using MSMPR stages: Modelling, design, and control,” *Chem. Eng. Process. Process Intensif.*, vol. 89, pp. 41–53, Mar. 2015.
- [106] G. Power, G. Hou, V. K. Kamaraju, G. Morris, Y. Zhao, and B. Glennon, “Design and optimization of a multistage continuous cooling mixed suspension, mixed product removal crystallizer,” *Chem. Eng. Sci.*, vol. 133, pp. 125–139, 2015.
- [107] J. Garside and M. B. Shah, “Crystallization Kinetics from MSMPR Crystallizers,” *Ind. Eng. Chem. Process Des. Dev.*, vol. 19, no. 4, pp. 509–514, Oct. 1980.
- [108] J. Garside and N. S. Tavaré, “Mixing, Reaction and Precipitation: Limits of Micromixing in an MSMPR Crystallizer,” *Chem. Eng. Sci.*, vol. 40, no. 8, pp. 1485–1493, 1985.
- [109] C. S. Polster *et al.*, “Pilot-scale continuous production of LY2886721: amide formation and reactive crystallization,” *Org. Process Res. Dev.*, vol. 18, no. 11, pp. 1295–1309, Nov. 2014.
- [110] K. P. Cole *et al.*, “Kilogram-scale prexasertib monolactate monohydrate synthesis under continuous-flow CGMP conditions,” *Science (80-.)*, vol. 356, no. 6343, pp. 1144–1150, Jun. 2017.
- [111] I. R. Baxendale *et al.*, “Achieving Continuous Manufacturing: Technologies and Approaches for Synthesis, Workup, and Isolation of Drug Substance May 20–21, 2014

- Continuous Manufacturing Symposium,” *J. Pharm. Sci.*, vol. 104, no. 3, pp. 781–791, Mar. 2015.
- [112] J. Chen, B. Sarma, J. M. B. Evans, and A. S. Myerson, “Pharmaceutical Crystallization,” *Cryst. Growth Des.*, vol. 11, no. 4, pp. 887–895, Apr. 2011.
- [113] Y. Cui, M. O’Mahony, J. J. Jaramillo, T. Stelzer, and A. S. Myerson, “Custom-Built Miniature Continuous Crystallization System with Pressure-Driven Suspension Transfer,” *Org. Process Res. Dev.*, vol. 20, no. 7, pp. 1276–1282, Jul. 2016.
- [114] J. Li, B. L. Trout, and A. S. Myerson, “Multistage Continuous Mixed-Suspension, Mixed-Product Removal (MSMPR) Crystallization with Solids Recycle,” *Org. Process Res. Dev.*, vol. 20, no. 2, pp. 510–516, Feb. 2016.
- [115] H. Zhang *et al.*, “Application of Continuous Crystallization in an Integrated Continuous Pharmaceutical Pilot Plant,” *Cryst. Growth Des.*, vol. 14, no. 5, pp. 2148–2157, May 2014.
- [116] M. D. Johnson *et al.*, “Development and Scale-Up of a Continuous, High-Pressure, Asymmetric Hydrogenation Reaction, Workup, and Isolation,” *Org. Process Res. Dev.*, vol. 16, no. 5, pp. 1017–1038, May 2012.
- [117] Q. Su, C. D. Rielly, K. A. Powell, and Z. K. Nagy, “Mathematical modelling and experimental validation of a novel periodic flow crystallization using MSMPR crystallizers,” *AIChE J.*, vol. 63, no. 4, pp. 1313–1327, Apr. 2017.
- [118] K. A. Powell, A. N. Saleemi, C. D. Rielly, and Z. K. Nagy, “Monitoring Continuous Crystallization of Paracetamol in the Presence of an Additive Using an Integrated PAT Array and Multivariate Methods,” *Org. Process Res. Dev.*, vol. 20, no. 3, pp. 626–636, Mar. 2016.
- [119] A. J. Alvarez, A. Singh, A. S. Myerson, and N. L. 64849, “Crystallization of Cyclosporine

- in a Multistage Continuous MSMPR Crystallizer,” *Growth Des.*, vol. 11, no. 10, pp. 4392–4400, Oct. 2011.
- [120] A. Rashid, E. White, T. Howes, J. Litster, and I. Marziano, “From Raw Data to Process: The Path to a Batch or a Continuous Crystallizer Design for Ibuprofen,” *Org. Process Res. Dev.*, vol. 21, no. 2, pp. 187–194, Feb. 2017.
- [121] J. L. Quon, H. Zhang, A. Alvarez, J. Evans, A. S. Myerson, and B. L. Trout, “Continuous Crystallization of Aliskiren Hemifumarate,” *Cryst. Growth Des.*, vol. 12, no. 6, pp. 3036–3044, Jun. 2012.
- [122] Y. Yang, L. Song, T. Gao, and Z. K. Nagy, “Integrated Upstream and Downstream Application of Wet Milling with Continuous Mixed Suspension Mixed Product Removal Crystallization,” *Cryst. Growth Des.*, vol. 15, no. 12, pp. 5879–5885, Dec. 2015.
- [123] O. Narducci, A. G. Jones, and E. Kougoulos, “Continuous crystallization of adipic acid with ultrasound,” *Chem. Eng. Sci.*, vol. 66, no. 6, pp. 1069–1076, 2011.
- [124] B. Wierzbowska, K. Piotrowski, J. Koralewska, A. Matynia, N. Hutnik, and K. Wawrzyniecki, “Crystallization of vitamin C in a continuous DT MSMPR crystallizer – Size independent growth kinetic model approach,” *Cryst. Res. Technol.*, vol. 43, no. 4, pp. 381–389, Apr. 2008.
- [125] T.-T. T. C. Lai, J. Cornevin, S. Ferguson, N. Li, B. L. Trout, and A. S. Myerson, “Control of Polymorphism in Continuous Crystallization via Mixed Suspension Mixed Product Removal Systems Cascade Design,” *Cryst. Growth Des.*, vol. 15, no. 7, pp. 3374–3382, Jul. 2015.
- [126] R. R. E. Steendam and J. H. ter Horst, “Continuous Total Spontaneous Resolution,” *Cryst. Growth Des.*, vol. 17, no. 8, pp. 4428–4436, Aug. 2017.

- [127] J. Lu, J. D. Litster, and Z. K. Nagy, “Nucleation Studies of Active Pharmaceutical Ingredients in an Air-Segmented Microfluidic Drop-Based Crystallizer,” *Cryst. Growth Des.*, vol. 15, no. 8, pp. 3645–3651, 2015.
- [128] M. Jiang *et al.*, “Continuous-Flow Tubular Crystallization in Slugs Spontaneously Induced by Hydrodynamics,” *Cryst. Growth Des.*, vol. 14, no. 2, pp. 851–860, Feb. 2014.
- [129] R. J. P. Eder *et al.*, “Continuously seeded, continuously operated tubular crystallizer for the production of active pharmaceutical ingredients,” *Cryst. Growth Des.*, vol. 10, no. 5, pp. 2247–2257, May 2010.
- [130] R. D. Dombrowski, J. D. Litster, N. J. Wagner, and Y. He, “Crystallization of alpha-lactose monohydrate in a drop-based microfluidic crystallizer,” *Chem. Eng. Sci.*, vol. 62, no. 17, pp. 4802–4810, Sep. 2007.
- [131] A. J. Alvarez and A. S. Myerson, “Continuous Plug Flow Crystallization of Pharmaceutical Compounds,” *Cryst. Growth Des.*, vol. 10, no. 5, pp. 2219–2228, May 2010.
- [132] H. Siddique, C. J. Brown, I. Houson, and A. J. Florence, “Establishment of a Continuous Sonocrystallization Process for Lactose in an Oscillatory Baffled Crystallizer,” *Org. Process Res. Dev.*, vol. 19, no. 12, pp. 1871–1881, Dec. 2015.
- [133] S. Lawton, G. Steele, P. Shering, L. Zhao, I. Laird, and X.-W. Ni, “Continuous Crystallization of Pharmaceuticals Using a Continuous Oscillatory Baffled Crystallizer,” *Org. Process Res. Dev.*, vol. 13, no. 6, pp. 1357–1363, Nov. 2009.
- [134] C. J. Brown and X.-W. Ni, “Determination of metastable zone width, mean particle size and detectable number density using video imaging in an oscillatory baffled crystallizer,” *CrystEngComm*, vol. 14, no. 8, p. 2944, 2012.
- [135] R. Peña, J. A. Oliva, C. L. Burcham, D. J. Jarmer, and Z. K. Nagy, “Process Intensification

- through Continuous Spherical Crystallization Using an Oscillatory Flow Baffled Crystallizer,” *Cryst. Growth Des.*, vol. 17, no. 9, pp. 4776–4784, Sep. 2017.
- [136] X. Ni, A. Valentine, A. Liao, S. B. C. Sermage, G. B. Thomson, and K. J. Roberts, “On the Crystal Polymorphic Forms of *l*-Glutamic Acid Following Temperature Programmed Crystallization in a Batch Oscillatory Baffled Crystallizer,” *Cryst. Growth Des.*, vol. 4, no. 6, pp. 1129–1135, Nov. 2004.
- [137] X. Ni and A. Liao, “Effects of mixing, seeding, material of baffles and final temperature on solution crystallization of *l*-glutamic acid in an oscillatory baffled crystallizer,” *Chem. Eng. J.*, vol. 156, no. 1, pp. 226–233, Jan. 2010.
- [138] C. J. Brown and X.-W. Ni, “Evaluation of Growth Kinetics of Antisolvent Crystallization of Paracetamol in an Oscillatory Baffled Crystallizer Utilizing Video Imaging,” *Cryst. Growth Des.*, vol. 11, no. 9, pp. 3994–4000, Sep. 2011.
- [139] R. Kacker, S. I. Regensburg, and H. J. M. Kramer, “Residence time distribution of dispersed liquid and solid phase in a continuous oscillatory flow baffled crystallizer,” *Chem. Eng. J.*, vol. 317, pp. 413–423, Jun. 2017.
- [140] T. McGlone, N. E. B. Briggs, C. A. Clark, C. J. Brown, J. Sefcik, and A. J. Florence, “Oscillatory Flow Reactors (OFRs) for Continuous Manufacturing and Crystallization,” *Org. Process Res. Dev.*, vol. 19, no. 9, pp. 1186–1202, Sep. 2015.
- [141] D. Ramkrishna, “Chapter 2 - The Framework of Population Balance,” *Popul. Balanc.*, pp. 7–45, 2000.
- [142] J. Litster, *Design and Processing of Particulate Products*. Cambridge, United Kingdom, United Kingdom: Cambridge University Press, 2016.
- [143] D. Ramkrishna, “CHAPTER 3 Birth and Death Functions,” *Popul. Balanc. theory Appl. to*

Part. Syst. Eng., 2000.

- [144] K. A. Berglund, “Analysis and measurement of crystallization utilizing the population balance,” in *Handbook of Industrial Crystallization*, Butterworth-Heinemann, 2002, pp. 101–113.
- [145] N. A. F. A. Samad, R. Singh, G. Sin, K. V. Gernaey, and R. Gani, “A generic multi-dimensional model-based system for batch cooling crystallization processes,” *Comput. Chem. Eng.*, vol. 35, no. 5, pp. 828–843, 2011.
- [146] D. Fysikopoulos, B. Benyahia, A. Borsos, Z. K. Nagy, and C. D. Rielly, “A framework for model reliability and estimability analysis of crystallization processes with multi-impurity multi-dimensional population balance models,” *Comput. Chem. Eng.*, vol. 122, pp. 275–292, 2019.
- [147] S. Ottoboni *et al.*, “Development of a Novel Continuous Filtration Unit for Pharmaceutical Process Development and Manufacturing,” *J. Pharm. Sci.*, vol. 108, no. 1, pp. 372–381, Jan. 2019.
- [148] The U.S. Food and Drug Administration, “Guidance for Industry Q8 pharmaceutical development,” no. May. 2009.
- [149] T. Ono, H. J. M. Kramer, J. H. Ter Horst, and P. J. Jansens, “Process modeling of the polymorphic transformation of L-glutamic acid,” *Cryst. Growth Des.*, 2004.
- [150] M. W. Hermanto, R. D. Braatz, and M. Sen Chiu, “High-order simulation of polymorphic crystallization using weighted essentially nonoscillatory methods,” *AIChE J.*, 2009.
- [151] S. Qamar, S. Noor, and A. Seidel-Morgenstern, “An efficient numerical method for solving a model describing crystallization of polymorphs,” *Ind. Eng. Chem. Res.*, 2010.
- [152] N. C. S. Kee, P. D. Arendt, L. May Goh, R. B. H. Tan, and R. D. Braatz, “Nucleation and

- growth kinetics estimation for l-phenylalanine hydrate and anhydrate crystallization,” *CrystEngComm*, 2011.
- [153] N. A. Mitchell, C. T. Ó’Ciardhá, and P. J. Frawley, “Estimation of the growth kinetics for the cooling crystallisation of paracetamol and ethanol solutions,” *J. Cryst. Growth*, vol. 328, no. 1, pp. 39–49, Aug. 2011.
- [154] E. Aamir, Z. Nagy, and C. Rielly, “Combined quadrature method of moments and method of characteristics approach for efficient solution of population balance models for dynamic modeling and,” *Ind. Eng. Chem. Res.*, pp. 8575–8584, 2009.
- [155] D. Acevedo and Z. K. Nagy, “Systematic classification of unseeded batch crystallization systems for achievable shape and size analysis,” *J. Cryst. Growth*, vol. 394, pp. 97–105, May 2014.
- [156] Y. Yang and Z. K. Nagy, “Combined cooling and antisolvent crystallization in continuous mixed suspension, mixed product removal cascade crystallizers: Steady-state and startup optimization,” *Ind. Eng. Chem. Res.*, vol. 54, no. 21, pp. 5673–5682, May 2015.
- [157] T. Vetter, C. L. Burcham, and M. F. Doherty, “Regions of attainable particle sizes in continuous and batch crystallization processes,” *Chem. Eng. Sci.*, vol. 106, pp. 167–180, 2014.
- [158] A. L. Grzesiak, M. Lang, K. Kim, and A. J. Matzger, “Comparison of the four anhydrous polymorphs of carbamazepine and the crystal structure of form I,” *J. Pharm. Innov.*, vol. 92, no. 11, pp. 2260–2271, 2003.
- [159] W. Czernicki and M. Baranska, “Carbamazepine polymorphs: Theoretical and experimental vibrational spectroscopy studies,” *Vib. Spectrosc.*, vol. 65, pp. 12–23, 2013.
- [160] J. B. Arlin, L. S. Price, S. L. Price, and A. J. Florence, “A strategy for producing predicted

- polymorphs: Catemeric carbamazepine form v,” *Chem. Commun.*, vol. 47, no. 25, pp. 7074–7076, 2011.
- [161] A. Getsoian, R. M. Lodaya, and A. C. Blackburn, “One-solvent polymorph screen of carbamazepine,” *Int. J. Pharm.*, vol. 348, no. 1–2, pp. 3–9, 2008.
- [162] B. H. Chen, S. Bermingham, A. H. Neumann, H. J. M. Kramer, and S. P. Asprey, “On the Design of Optimally Informative Experiments for Dynamic Crystallization Process Modeling,” *Ind. Eng. Chem. Res.*, vol. 43, no. 16, pp. 4889–4902, Aug. 2004.
- [163] B. H. Chen and S. P. Asprey, “On the design of optimally informative dynamic experiments for model discrimination in multiresponse nonlinear situations,” *Ind. Eng. Chem. Res.*, vol. 42, no. 7, pp. 1379–1390, 2003.
- [164] J. F. Pérez-Calvo, S. S. Kadam, and H. J. M. Kramer, “Determination of kinetics in batch cooling crystallization processes—A sequential parameter estimation approach,” *AIChE J.*, 2016.
- [165] The American Society of Mechanical Engineers, *Assessing Credibility of Computational Modeling and Simulation Results through Verification and Validation: Application to Medical Devices*. 2018.
- [166] L. F. Shampine and M. W. Reichelt, “The MATLAB ODE Suite,” *SIAM J. Sci. Comput.*, vol. 18, no. 1, pp. 1–22, 2003.
- [167] M. Bohlin and Å. C. Rasmuson, “Application of controlled cooling and seeding in batch crystallization,” *Can. J. Chem. Eng.*, vol. 70, no. 1, pp. 120–126, Feb. 1992.
- [168] N. Kubota, N. Doki, M. Yokota, and A. Sato, “Seeding policy in batch cooling crystallization,” *Powder Technol.*, vol. 121, no. 1, pp. 31–38, Nov. 2001.
- [169] G. A. Hareland, “Evaluation of flour particle size distribution by laser diffraction, sieve

- analysis and near-infrared reflectance spectroscopy,” *J. Cereal Sci.*, vol. 21, pp. 183–190, 1993.
- [170] J. -L LOIZEAU, D. ARBOUILLE, S. SANTIAGO, and J. -P VERNET, “Evaluation of a wide range laser diffraction grain size analyser for use with sediments,” *Sedimentology*, 1994.
- [171] D. L. Black, M. Q. McQuay, and M. P. Bonin, “Laser-based techniques for particle-size measurement: A review of sizing methods and their industrial applications,” *Prog. Energy Combust. Sci.*, vol. 22, no. 3, pp. 267–306, 1996.
- [172] S. J. Blott and K. Pye, “Particle size distribution analysis of sand-sized particles by laser diffraction: An experimental investigation of instrument sensitivity and the effects of particle shape,” *Sedimentology*, 2006.
- [173] G. Eshel, G. J. Levy, U. Mingelgrin, and M. J. Singer, “Critical Evaluation of the Use of Laser Diffraction for Particle-Size Distribution Analysis,” *Soil Sci. Soc. Am. J.*, vol. 68, no. 3, p. 736, 2014.
- [174] A. Mersmann, “Crystallization and precipitation,” *Chem. Eng. Process. Process Intensif.*, vol. 38, no. 4–6, pp. 345–353, Sep. 1999.
- [175] S. Kaneko, Y. Yamagami, H. Tochiara, and I. Hirasawa, “Effect of supersaturation on crystal size and number of crystals produced in antisolvent crystallization,” *J. Chem. Eng. JAPAN*, vol. 35, no. 11, pp. 1219–1223, 2002.
- [176] N. Kubota, “An interpretation of the metastable zone width concerning primary nucleation in anti-solvent crystallization,” *J. Cryst. Growth*, vol. 310, no. 22, pp. 4647–4651, 2008.
- [177] A. W. Dickens, M. R. Mackley, and H. R. Williams, “Experimental residence time distribution measurements for unsteady flow in baffled tubes,” *Chem. Eng. Sci.*, vol. 44, no.

- 7, pp. 1471–1479, 1989.
- [178] M. R. Mackley, G. M. Tweddle, and I. D. Wyatt, “Experimental heat transfer measurements for pulsatile flow in baffled tubes,” *Chem. Eng. Sci.*, vol. 45, no. 5, pp. 1237–1242, 1990.
- [179] M. R. Mackley and P. Stonestreet, “Heat transfer and associated energy dissipation for oscillatory flow in baffled tubes,” *Chem. Eng. Sci.*, vol. 50, no. 14, pp. 2211–2224, Jul. 1995.
- [180] X. Ni, S. Gao, and D. W. Pritchard, “A study of mass transfer in yeast in a pulsed baffled bioreactor,” *Biotechnol. Bioeng.*, vol. 45, no. 2, pp. 165–175, Jan. 1995.
- [181] X. Ni, S. Gao, and L. Santangeli, “On the Effect of Surfactant on Mass Transfer to Water-Glycerol Solutions in a Pulsed Baffled Reactor,” *J. Chem. Technol. Biotechnol.*, vol. 69, no. 2, pp. 247–253, Jun. 1997.
- [182] X. Ni and S. Gao, “Scale-up correlation for mass transfer coefficients in pulsed baffled reactors,” *Chem. Eng. J. Biochem. Eng. J.*, vol. 63, no. 3, pp. 157–166, Sep. 1996.
- [183] X. Ni and P. Gough, “On the discussion of the dimensionless groups governing oscillatory flow in a baffled tube,” *Chem. Eng. Sci.*, vol. 52, no. 18, pp. 3209–3212, Sep. 1997.
- [184] A. Fitch, “On the determination of axial dispersion coefficient in a batch oscillatory baffled column using laser induced fluorescence,” *Chem. Eng. J.*, vol. 92, no. 1–3, pp. 243–253, Apr. 2003.
- [185] M. R. Mackley and X. Ni, “Mixing and dispersion in a baffled tube for steady laminar and pulsatile flow,” *Chem. Eng. Sci.*, vol. 46, no. 12, pp. 3139–3151, 1991.
- [186] C. M. Chew and R. I. Ristic, “Crystallization by oscillatory and conventional mixing at constant power density,” *AIChE J.*, vol. 51, no. 5, pp. 1576–1579, May 2005.
- [187] M. R. Hewgill, M. R. Mackley, A. B. Pandit, and S. S. Pannu, “Enhancement of gas-liquid mass transfer using oscillatory flow in a baffled tube,” *Chem. Eng. Sci.*, vol. 48, no. 4, pp.

- 799–809, Feb. 1993.
- [188] X. Ni and M. R. Mackley, “Chemical reaction in batch pulsatile flow and stirred tank reactors,” *Chem. Eng. J.*, vol. 52, no. 3, pp. 107–114, 1993.
- [189] X. Ni, S. Gao, R. H. Cumming, and D. W. Pritchard, “A comparative study of mass transfer in yeast for a batch pulsed baffled bioreactor and a stirred tank fermenter,” *Chem. Eng. Sci.*, vol. 50, no. 13, pp. 2127–2136, Jul. 1995.
- [190] R. I. Ristic, “Oscillatory mixing for crystallization of high crystal perfection pharmaceuticals,” *Chem. Eng. Res. Des.*, vol. 85, no. 7, pp. 937–944, 2007.
- [191] C. R. Brunold, J. C. B. Hunns, M. R. Mackley, and J. W. Thompson, “Experimental observations on flow patterns and energy losses for oscillatory flow in ducts containing sharp edges,” *Chem. Eng. Sci.*, vol. 44, no. 5, pp. 1227–1244, 1989.
- [192] X. Ni, M. R. Mackley, A. P. Harvey, P. Stonestreet, M. H. I. Baird, and N. V. Rama Rao, “Mixing Through Oscillations and Pulsations—A Guide to Achieving Process Enhancements in the Chemical and Process Industries,” *Chem. Eng. Res. Des.*, vol. 81, no. 3, pp. 373–383, Mar. 2003.
- [193] X. Ni, G. Nelson, and I. Mustafa, “Flow patterns and oil-water dispersion in a 0.38 m diameter oscillatory baffled column,” *Can. J. Chem. Eng.*, vol. 78, no. 1, pp. 211–220, Feb. 2000.
- [194] J. Y. Oldshue, *Fluid Mixing Technology*. New York: McGraw-Hill, 1983.
- [195] E. B. Burgina, V. P. Baltakhinov, E. V. Boldyreva, and T. P. Shakhtschneider, “IR spectra of paracetamol and phenacetin,” *J. Struct. Chem.*, vol. 45, no. 1, pp. 64–73, 2004.
- [196] J. Worlitschek and M. Mazzotti, “Model-based optimization of particle size distribution in batch-cooling crystallization of paracetamol,” in *Crystal Growth and Design*, 2004, vol. 4,

- no. 5, pp. 891–903.
- [197] M. N. Kashid, A. Renken, and L. Kiwi-Minsker, “Real Reactors and Residence Time Distribution (RTD),” in *Microstructured Devices for Chemical Processing*, Wiley-VCH Verlag GmbH & Co. KGaA, 2015, pp. 89–128.
- [198] A. S. Myerson, “Nucleation Kinetics,” in *Handbook of Industrial Crystallization*, 2nd ed., Elsevier Science, 2002, pp. 50–52.
- [199] A. T.-C. Mak, “Solid–liquid mixing In Mechanically Agitated Vessels,” 1992.
- [200] X. Ni, J. . Cosgrove, A. . Arnott, C. . Greated, and R. . Cumming, “On the measurement of strain rate in an oscillatory baffled column using particle image velocimetry,” *Chem. Eng. Sci.*, vol. 55, no. 16, pp. 3195–3208, Aug. 2000.
- [201] T. T. C. Lai, S. Ferguson, L. Palmer, B. L. Trout, and A. S. Myerson, “Continuous crystallization and polymorph dynamics in the l -glutamic acid system,” *Org. Process Res. Dev.*, vol. 18, no. 11, pp. 1382–1390, 2014.
- [202] N. A. Mitchell, P. J. Frawley, and C. T. Ó’Ciardhá, “Nucleation kinetics of paracetamol–ethanol solutions from induction time experiments using Lasentec FBRM®,” *J. Cryst. Growth*, vol. 321, no. 1, pp. 91–99, Apr. 2011.
- [203] C. Tien, R. Bai, and B. V. Ramarao, “Analysis of Cake Growth in Cake Filtration: Effect of Fine Particle Retention,” *AIChE J.*, 1997.
- [204] J. More, M. Bulmer, M. Boychyn, M. Hoare, T. Reynolds, and T. Sanderson, “Scale-down of continuous filtration for rapid bioprocess design: Recovery and dewatering of protein precipitate suspensions,” *Biotechnol. Bioeng.*, vol. 83, no. 4, pp. 454–464, 2003.
- [205] M. T. Kuo and E. C. Barrett, “Continuous filter cake washing performance,” *AIChE J.*, vol. 16, no. 4, pp. 633–638, 1970.

- [206] F. Ruslim, H. Nirschl, W. Stahl, and P. Carvin, "Optimization of the wash liquor flow rate to improve washing of pre-deliquored filter cakes," *Chem. Eng. Sci.*, vol. 62, no. 15, pp. 3951–3961, 2007.
- [207] R. Wakeman, "The influence of particle properties on filtration," *Sep. Purif. Technol.*, vol. 58, no. 2, pp. 234–241, 2007.
- [208] J. Gursch *et al.*, "Continuous Processing of Active Pharmaceutical Ingredients Suspensions via Dynamic Cross-Flow Filtration," *J. Pharm. Sci.*, vol. 104, no. 10, pp. 3481–3489, 2015.
- [209] J. Gursch *et al.*, "Dynamic cross-flow filtration: enhanced continuous small-scale solid-liquid separation," *Drug Dev. Ind. Pharm.*, vol. 42, no. 6, pp. 977–984, Jun. 2016.
- [210] D. O'Grady, "Multiscale characterisation of anti-solvent crystallization," University College Dublin, Ireland, 2007.
- [211] A. Rushton, A. S. Ward, and R. G. Holdich, "Filtration Process Equipment and Calculations," in *Solid-Liquid Filtration and Separation Technology*, VCH, 1996, pp. 397–480.
- [212] J. Katta, "Spherical crystallization of benzoic acid," vol. 348, pp. 61–69, 2008.
- [213] M. E. Laska, R. P. Brooks, M. Gayton, and N. S. Pujar, "Robust scale-up of dead end filtration: Impact of filter fouling mechanisms and flow distribution," *Biotechnol. Bioeng.*, vol. 92, no. 3, pp. 308–320, 2005.
- [214] S. Kumar and D. Ramkrishna, "On the solution of population balance equations by discretization—I. A fixed pivot technique," *Chem. Eng. Sci.*, vol. 51, no. 8, pp. 1311–1332, Apr. 1996.
- [215] R. Gunawan, I. Fusman, and R. D. Braatz, "High resolution algorithms for multidimensional population balance equations," *AIChE J.*, vol. 50, no. 11, pp. 2738–2749, Nov. 2004.

- [216] B. van Leer, “Towards the ultimate conservative difference scheme. II. Monotonicity and conservation combined in a second-order scheme,” *J. Comput. Phys.*, vol. 14, no. 4, pp. 361–370, 1974.
- [217] R. J. LeVeque, D. Mihalas, E. A. Dorfi, and E. Muller, *Computational Methods for Astrophysical Fluid Flow*. 1998.

VITA

Yiqing Liu, who goes by Claire, was born in a ‘small’ steel town called Anshan in northeastern China to a family of engineers in 1991. With strong influences from her parents, Claire became interested in engineering and mathematics at a young age. At the age of 15, an English-as-a-second-language summer camp exposed her to American culture and she decided to come to the United States for her higher education. Claire attended the University of Wisconsin – Madison where she double majored in chemical engineering and mathematics. Upon graduating from college, Claire decided to join the Davidson School of Chemical Engineering at Purdue University to pursue her doctorate degree under Prof. Zoltan K. Nagy. While in graduate school, she engaged in leadership positions in the departmental graduate student organization (GSO) and graduate women’s group (GWG) where she initiated and led the volunteering program at a local animal shelter (Almost Home Humane Society). In the third year of her Ph.D. program, she went to the U.S. Food and Drug Administration at Silver Spring, MD for an industrial internship. Upon receiving her doctorate degree, Claire will be joining Pfizer as a Process Modeling Engineer.

PUBLICATIONS

- Y. C. Liu**, D. Dunn, M. Lipari, A. Barton, P. Firth, J. Speed, D. Wood, Z. K. Nagy, “A comparative study of continuous operation between a dynamic baffle crystallizer and a stirred tank crystallizer,” *Chem. Eng. J.*, vol. 367, pp. 278–294, Jul. 2019.
- Y. C. Liu**, D. Acevedo, X. Yang, S. Naimi, W. Wu, N. Pavurala, Z. K. Nagy, C. N. Cruz, T. F. O’Connor, “Population balance model development verification and validation of cooling crystallization of carbamazepine,” (awaiting clearance).
- Y. C. Liu**, A. Domokos, S. Coleman, P. Firth, Z. K. Nagy, “Development of continuous filtration in a novel continuous filtration carousel integrated with continuous crystallization,” *Org. Process Res. Dev.* (accepted after modifications).
- Y. C. Liu**, Z. K. Nagy, “Continuous crystallization: equipment and operation,” book chapter (submitted to editor).
- D. Acevedo, X. Yang, **Y. C. Liu**, T. F. O’Connor, A. Koswara, M. Rapti, C. N. Cruz, “Encrustation in Continuous Pharmaceutical Crystallization Processes—A Review,” *Org. Process Res. Dev.*, vol. 23, no. 6, pp. 1134–1142, Jun. 2019.
- T. F. O’Connor, D. Acevedo, X. Yang, **Y. C. Liu**, C. N. Cruz, “Continuous Crystallization: Quality Considerations,” *AAPS PharmSciTech.* (Submitted).
- J. Zhang, **Y. C. Liu**, S. Mazumder, D. Acevedo, X. Yang, S. Naimi, W. Wu, N. Pavurala, Z. K. Nagy, C. N. Cruz, T. F. O’Connor, “Risk considerations for continuous cooling crystallization of carbamazepine in a plug flow oscillatory baffled crystallizer,” (in preparation)